AD NUMBER
AD339905
CLASSIFICATION CHANGES
TO: unclassified
FROM: secret
LIMITATION CHANGES
TO: Approved for public release, distribution unlimited
FROM: Distribution authorized to U.S. Gov't. agencies and their contractors; Administrative/Operational Use; 08 JUL 1959. Other requests shall be referred to Defense Atomic Support Agency, Washington, DC. Restricted Data.
AUTHORITY
dna ltr, 6 jun 1980; dna ltr, 6 jun 1980

AD 339905L

USING RESTRICTED DATA

SECRET

WT-1146

This document consists of 96 page

No. 108 of 195 copies, Series A

Operation TEAPOT

NEVADA TEST SITE

February – May 1955

Project 8.4b

BASIC THERMAL–RADIATION MEASUREMENTS (U)

Issuance Date: July 8, 1959

RESTRICTED DATA

This document contains restricted data as defined in the Atomic Energy Act of 1954. Its transmittal or the disclosure of its contents in any manner to an unauthorized person is prohibited.

HEADQUARTERS FIELD COMMAND, DEFENSE ATOMIC SUPPORT AGENCY
SANDIA BASE, ALBUQUERQUE, NEW MEXICO

SECRET

RESTRICTED DATA

Inquiries relative to this report may be made to

Chief, Defense Atomic Support Agency
Washington 25, D. C.

When no longer required, this document may be destroyed in accordance with applicable security regulations.

DO NOT RETURN THIS DOCUMENT

AEC Technical Information Service Extension
Oak Ridge, Tennessee

SECRET

RESTRICTED DATA

WT-1146

OPERATION TEAPOT—PROJECT 8.4b

BASIC THERMAL-RADIATION MEASUREMENTS (U)

R.W. Hillendahl
F.I. Laughridge

U.S. Naval Radiological Defense Laboratory
San Francisco 24, California

SECRET
RESTRICTED DATA

FOREWORD

This report presents the final results of one of the 56 projects comprising the Military-Effects Program of Operation Teapot, which included 14 test detonations at the Nevada Test Site in 1955.

For overall Teapot military-effects information, the reader is referred to "Summary Report of the Technical Director, Military Effects Program," WT-1153, which includes the following: (1) a description of each detonation including yield, zero-point environment, type of device, ambient atmospheric conditions, etc.; (2) a discussion of project results; (3) a summary of the objectives and results of each project; and (4) a listing of project reports for the Military Effects Program.

ABSTRACT

Basic thermal-radiation measurements, comprising total and broad-band spectral distribution of radiant energy, radiant energy as a function of field of view of the measuring instrument, and total radiant power versus time, are reported for the second thermal pulse of Shots 1, 2, 3, 5, 6, 9, and 10. All data were taken from ground stations at ranges as close as feasible to the detonations.

The data is reported and analyzed to obtain the total thermal energy, the total thermal emission per unit of time, fireball sizes and geometries, and color and power temperatures, all as a function of time.

New methods of analysis are used that show promise of correlating the thermal characteristics of the fireball with burst parameters. The new methods result in significantly higher thermal yields in all cases.

Significant differences are shown in the thermal properties of tower and air bursts. The air bursts have higher thermal yields, higher peak irradiances, higher peak temperatures, and different pulse shapes than tower bursts.

The thermal properties of an air burst are shown to vary with altitude. The higher the altitude, the shorter the time scale, the larger the fireball, and the lower the total thermal energy. The peak temperature is little changed.

More-specialized measurements are reported for several shots. Goniometric measurements of the thermal radiation received under the smoke layer during Shot 5 were successfully completed. Indications are that the results are consistent with predictions. Measurements at extremely close ranges were attempted during Shot 12, but with very little success, primarily due to recording difficulties.

Applicable data were obtained for all of the specified objectives, but additional data is needed to complete the study of the thermal radiation from nuclear detonations. Recommendations are made as to what measurements are required.

PREFACE

The methods of data interpretation, the scaling relationships, and conclusions reached in Chapters 4 and 5 of this report, represent the state of the art as of about the end of 1957. As of that time, only the thermal data from Operation Teapot had been analyzed in detail. The data quoted from other field tests had not been subjected to detailed treatment and hence must be considered preliminary in nature.

In the interval between the initial submission of this manuscript and its final publication, the detailed analysis of thermal data from all field tests has been completed and submitted as a summary report (Reference 18). The conclusions and scaling laws for air and tower bursts, as presented in this report of wider scope, are more extensive and complete, and supersede those presented in this text.

ACKNOWLEDGMENTS

The successful completion of Project 8.4b was due to the cooperation and unstinted efforts of many individuals.

A number of the members of the Thermal Radiation Branch, Naval Radiological Defense Laboratory, contributed in one way or another to this project. Dr. W. B. Plum helped with his able administration. R. L. Hopton and S. Martin were especially helpful in the construction of instrumentation. R. P. Day and R. J. Jenkins helped in the calibration of many and varied instruments used. J. R. Nichols, AFC, USN, provided photographic support. Dr. M. G. Gibbons helped in atmospheric attenuation studies.

In addition to the above personnel, the assistance of the numerous individuals assigned to the Procurement Liaison and Materials Control Division and the Engineering Division, Naval Radiological Defense Laboratory, many of whom helped both at the laboratory and in the field, is gratefully acknowledge.

Lt. Col. W. B. Pohlman, USA, and Capt. C. S. Adler, USA, of the Weapons Effects Test Group were extremely helpful.

Last, but not least, it is a pleasure to acknowledge the assistance and encouragement of Dr. A. Guthrie, Head of the Nucleonics Division, Naval Radiological Defense Laboratory.

CONTENTS

FOREWORD ---- 4

ABSTRACT ---- 5

PREFACE ---- 6

ACKNOWLEDGMENTS ---- 7

CHAPTER 1 INTRODUCTION ---- 13
1.1 Objectives ---- 13
1.2 Background and Theory ---- 13

CHAPTER 2 INSTRUMENTATION ---- 17
2.1 Experimental Design ---- 17
2.2 Description of Instrumentation ---- 19

CHAPTER 3 RESULTS ---- 22
3.1 Standard Thermal Energy ---- 22
3.2 High-Altitude Burst ---- 22
3.3 Smoke-Screen Experiment ---- 29
3.4 Plots of Surface Specimens ---- 29
3.5 Thermal Radiant Power Versus Time ---- 31
3.6 Fireball Photography ---- 31

CHAPTER 4 DISCUSSION ---- 66
4.1 Calorimeter Data ---- 67
4.2 Thermal Yield ---- 70
4.3 Broad-Band Spectral Distribution ---- 73
4.4 Irradiance Versus Time ---- 73
4.5 Atmospheric Attenuation ---- 74
4.6 Color Temperatures ---- 77
4.7 Size and Geometry of the Fireball ---- 78
4.8 Power Temperatures ---- 81
4.9 Thermal Measurements at Extremely Close Ranges ---- 82
4.10 Thermal Input to Shot 12 Material Plots ---- 83
4.11 Effects of Burst Altitude ---- 83
4.12 Scaling Laws ---- 86
4.13 Evaluation of the Difference Between Tower and Air Bursts ---- 87
4.14 Effects of Device Type on Thermal Characteristics ---- 88
4.15 Tests of New Instrumentation ---- 88

CHAPTER 5 CONCLUSIONS AND RECOMMENDATIONS ---- 90
5.1 Conclusions ---- 90

5.2 Recommendations ---------- 90

REFERENCES ---------- 92

APPENDIX STATION AND BURST COORDINATES ---------- 94

FIGURES

3.1 Thermal irradiance versus time, Shot 1 ---------- 31
3.2 Thermal irradiance versus time, Shot 2 ---------- 31
3.3 Thermal irradiance versus time, Shot 3 ---------- 32
3.4 Thermal irradiance versus time, Shot 5 ---------- 32
3.5 Thermal irradiance versus time, Shot 6 ---------- 32
3.6 Thermal irradiance versus time, Shot 9 ---------- 32
3.7 Thermal irradiance versus time, Shot 10 ---------- 33
3.8 Shot 1, Film 306; Frames 1 and 2 ---------- 36
3.9 Shot 1, Film 306; Frames 3 and 4 ---------- 36
3.10 Shot 1, Film 306; Frames 5 and 6 ---------- 37
3.11 Shot 1, Film 306; Frames 8 and 12 ---------- 37
3.12 Shot 1, Film 306; Frames 19 and 31 ---------- 38
3.13 Shot 1, Film 306; Frame 55 ---------- 38
3.14 Shot 2, Film 311; Frames 1 and 2 ---------- 39
3.15 Shot 2, Film 311; Frames 3 and 4 ---------- 39
3.16 Shot 2, Film 311; Frames 5 and 7 ---------- 40
3.17 Shot 2, Film 311; Frames 11 and 17 ---------- 41
3.18 Shot 2, Film 311; Frames 27 and 44 ---------- 42
3.19 Shot 2, Film 311; Frame 78 ---------- 43
3.20 Shot 2, Film 313; Frames 1 and 2 ---------- 43
3.21 Shot 2, Film 313; Frames 3 and 4 ---------- 44
3.22 Shot 2, Film 313; Frames 5 and 7 ---------- 45
3.23 Shot 2, Film 313; Frames 11 and 17 ---------- 46
3.24 Shot 2, Film 313; Frames 27 and 44 ---------- 47
3.25 Shot 2, Film 313; Frame 78 ---------- 48
3.26 Shot 3, Film 322; Frames 1 and 3 ---------- 48
3.27 Shot 3, Film 322; Frames 4 and 5 ---------- 49
3.28 Shot 3, Film 322; Frames 7 and 9 ---------- 50
3.29 Shot 3, Film 322; Frames 14 and 22 ---------- 51
3.30 Shot 3, Film 322; Frames 34 and 55 ---------- 52
3.31 Shot 3, Film 322; Frame 98 ---------- 53
3.32 Shot 6, Film 392; Frames 1 and 3 ---------- 53
3.33 Shot 6, Film 392; Frames 5 and 6 ---------- 54
3.34 Shot 6, Film 392; Frames 8 and 11 ---------- 55
3.35 Shot 6, Film 392; Frames 16 and 25 ---------- 56
3.36 Shot 6, Film 392; Frames 40 and 66 ---------- 57
3.37 Shot 6, Film 392; Frame 116 ---------- 58
3.38 Shot 6, Film 393; Frames 1 and 3 ---------- 58
3.39 Shot 6, Film 393; Frames 5 and 6 ---------- 59
3.40 Shot 6, Film 393; Frames 8 and 11 ---------- 60
3.41 Shot 6, Film 393; Frames 16 and 25 ---------- 61
3.42 Shot 6, Film 393; Frames 40 and 66 ---------- 62
3.43 Shot 6, Film 393; Frame 116 ---------- 63
3.44 Fireball radius versus time, Shot 1 ---------- 63
3.45 Fireball radius versus time, Shot 2 ---------- 64
3.46 Fireball radius versus time, Shot 3 ---------- 64
3.47 Fireball radius versus time, Shot 6 ---------- 64

4.1 Time intervals used in data correlation ---------- 69
4.2 Transmission of filters ---------- 71
4.3 Normalized thermal emission versus scaled time ---------- 75
4.4 Predicted ratios of energies received from a Planckian radiator through various filters under a specific set of atmospheric conditions ---- 78
4.5 Temperature versus time, Shot 1 ---------- 79
4.6 Temperature versus time, Shot 2 ---------- 79
4.7 Temperature versus time, Shot 3 ---------- 79
4.8 Temperature versus time, Shot 5 ---------- 80
4.9 Temperature versus time, Shot 6 (Station 220) ---------- 80
4.10 Temperature versus time, Shot 6 (Station 221) ---------- 80
4.11 Temperature versus time, Shot 9 (Station 220) ---------- 81
4.12 Temperature versus time, Shot 9 (Station 221) ---------- 81
4.13 Plot of total yield of a number of shots as a function of time to second maximum ---------- 88

TABLES

2.1 Instrumentation Layout for Standard Thermal Measurements ---------- 18
2.2 Instrument Layout for Shot 10 ---------- 18
2.3 Thermal Instrumentation for Shot 12 Material Plots ---------- 18
2.4 Instrumentation under Smoke Layer on Shot 5 ---------- 19
3.1 Calorimeter Results, Shot 1 ---------- 23
3.2 Calorimeter Results, Shot 2 ---------- 23
3.3 Calorimeter Results, Shot 3 ---------- 24
3.4 Calorimeter Results, Shot 5 ---------- 24
3.5 Calorimeter Results, Shot 6 ---------- 25
3.6 Calorimeter Results, Shot 6 ---------- 26
3.7 Calorimeter Results, Shot 9 ---------- 26
3.8 Calorimeter Results, Shot 9 ---------- 27
3.9 Calorimeter Results, Shot 10 ---------- 27
3.10 Uncorrected Calorimeter Results, Shot 10 ---------- 28
3.11 Thermal Energy under Smoke, Shot 5 ---------- 28
3.12 Thermal Energy under Smoke, Shot 5 ---------- 29
3.13 Thermal Energy under Smoke, Shot 5 ---------- 30
3.14 Results of Thermal Measurements on Shot 12 Plots ---------- 30
3.15 Thermal Radiant Power ---------- 33
3.16 Fireball Motion-Picture Films ---------- 33
3.17 Late Time Fireball Data, Shot 1 ---------- 34
3.18 Late Time Fireball Data, Shot 2 ---------- 34
3.19 Late Time Fireball Data, Shot 3 ---------- 34
3.20 Late Time Fireball Data, Shot 6 ---------- 35
4.1 Boundaries of Time Intervals used in Reduction of Calorimeter Data ---------- 69
4.2 Thermal Yield ---------- 72
4.3 Average Total Thermal Emission versus Time, kt/sec ---------- 74
4.4 Typical Transmission Calculations ---------- 77
4.5 Extremely Close Range Measurements ---------- 83
4.6 Total Energy Data, Shot 10 ---------- 84
4.7 Power Temperature versus Time, Shot 10 ---------- 85
4.8 Thermal Partition for Shots 9 and 10 ---------- 86
4.9 Times to Second Maximum versus Yield ---------- 87

Chapter I
INTRODUCTION

1.1 OBJECTIVES

The objective of Project 8.4b was to determine the physical characteristics of the thermal radiation from nuclear devices detonated during Operation Teapot at ranges where the thermal radiation causes damage to military targets.

More specifically, the objectives were to: (1) accumulate basic thermal data, such as total thermal energy, broadband spectral distribution of the thermal energy, and the thermal irradiance, for weapon sizes for which these data were not available; (2) check the existing thermal scaling laws and to modify and extend them to include a wider range of weapon sizes; (3) attempt thermal measurements, at extremely close ranges and high energies where there were no experimental data available; (4) determine the relative differences in thermal energy received from tower and air bursts and to compute the thermal yields for both cases; (5) see if a correlation exists between weapon characteristics and the characteristics of the thermal radiations; (6) determine the effects of burst altitude upon the pulse shape and other characteristics of the thermal radiations; (7) assist the Army Chemical Corps in the evaluation of the effectiveness of an oil-fog smoke screen as an attenuator of thermal radiations; (8) attempt a determination of thermal input to various material plots placed at close ranges and the correlation of the data with air temperature, sound velocity, gas sampling, and photographic measurements; (9) obtain additional data relative to the atmospheric attenuation of thermal radiations; (10) determine the effective color temperature of the fireball as viewed from close range; (11) determine the apparent geometry and size of the fireball at times of significant thermal emission; (12) determine the minimum power temperature of the fireball as a function of time; and (13) test new thermal instrumentation designed to measure in energy ranges higher and lower than those measured in previous operations.

1.2 BACKGROUND AND THEORY

Thermal radiation is one of the more important parameters that must be measured in the evaluation of a nuclear device and its effects. In addition to providing a method for determining the characteristics of the device itself, thermal-radiation produces gross effects in target materials and is a complicating factor that must be taken into account in conducting experiments at close ranges to detonations.

Some of the more important effects caused by the thermal radiation are: ignition of materials, burning of humans, modification of the shock wave, modification of the fallout pattern of the nuclear debris,[1] and weakening of structural materials, such as aircraft skins, so that

[1] The effects of fire storm on atmospheric circulation have not been fully investigated. Fallout patterns from bombs detonated over inflammable targets may differ significantly from results obtained at test sites where inflammable materials are absent. A burning city may afford some measure of self-protection from fallout.

they become more vulnerable to shock damage.

The interpretation of measurements of thermal radiation is a rather complex problem. In addition to the thermal pulse being a transient phenomenon requiring high-time-response instrumentation, the experiments are usually complicated by the complex geometries of the field test situations. As a result, the so-called standard thermal measurements are of two basic types: (1) the determination of the input to a specific target at a specific location and (2) the determination of the characteristics of the particular nuclear device to make it possible to scale the phenomena to other devices, weapons, and other situations. Standard thermal measurements include total radiant energy, thermal radiant power versus time, broad-band spectral distribution, and field-of-view measurements.

Prior to Teapot, the thermal data for devices of yields of less than 10 kt was extremely limited. The only devices for which data of reasonable accuracy were available were the first and second shots of Operation Tumbler-Snapper. The data from these shots (Reference 1) did not give satisfactory agreement with the accepted scaling laws (Reference 2), which were evidently satisfactory for larger yields.

While the data for total radiant energy did give relatively good agreement with the scaling laws, the data for times to second maximum gave a poor fit. It was believed that this discrepancy was due to the use of a large case to enclose a relatively small nuclear device.

The relatively poor fit using the times to second maximum was of concern because measurements of total radiant energy are, at times, either impossible to obtain or are extremely complex, while the time to second maximum is relatively simple to measure with sufficient accuracy. Operation Teapot provided an opportunity to attempt to resolve these difficulties and to gain additional basic thermal data using existing instrumentation.

Before Teapot there had been relatively little interest shown in thermal measurements at distances where the total radiant energy was more than about 100 cal/cm^2, since total blast destruction usually occurred at these close ranges. Thus, no measurements had been made for these high thermal inputs and the only means of prediction of energy values was by extrapolation. The process of extrapolation was extremely dangerous in this case, because the shock wave arrived during the delivery of a significant portion of the thermal pulse, and it was not known as to what extent the post-shock dust would obscure the target and effectively cut off the thermal input. If the shock wave were to exhibit such an exposure-limiting action, then the thermal energy predicted up to time of shock arrival would have a maximum value at some distance from the device, rather than at ground zero. Such a phenomenon would add further complications to the interpretation of test results.

There were also some questions as to the geometrical and optical properties of the fireball when viewed from close distances. The field of view of the receiving surface, the radiating characteristics of the fireball surface, and asymmetries in the shape of the fireball become increasingly important. The thermal energy received at close distances may also be dependent upon selective spectral absorption of the atmosphere. While it is well known that gaseous absorption of radiation plays a major role in the formation of the fireball proper, little is known at present of the absorption of radiation in the first few hundreds of feet outside the surface of the fireball.

The measurements being made by this project are not intended to provide detailed answers to all of these close-range energy problems, but only to reveal any gross effects that may be present. Thus, if future measurements are required, data will be available to give some insight into the instrumentation problems.

Early in the history of thermal measurements at close distances, it had been determined (Reference 3) that the thermal energy received from a tower burst would be less than that received from an air burst of equivalent yield. Time and opportunity, however, had not made it possible to make any measurements in an effort to determine typical reduction factors. Since the "schedule" of Teapot intermixed tower and air bursts, it was decided to use existing

towers and instrumentation to make measurements, not otherwise required, on certain tower bursts.

Some of the more interesting unknowns concerning the formation of the fireball are the effect of the size and style of the case used to enclose the device and the assembly used in the device itself. It is believed that all or some of these variables could be of considerable importance in determining the shape of the thermal pulse, particularly for the smaller devices. Operation Teapot provided a large selection of these smaller devices, and the data gained should give some insight into the effects of these parameters.

The effect of burst altitude on the formation of the fireball is of both military and scientific interest. The effectiveness of nuclear devices used to counter ballistic missiles and used as anti-aircraft shells is dependent upon the thermal and nuclear radiations emitted, as well as the shock front established at the reduced air densities encountered at high altitudes. Since thermal radiation is a major factor in the destruction of aircraft at lower altitudes, it is important to know if there is a significant change in the thermal characteristics of devices when detonated at high altitudes. The scientific interest in a high-altitude detonation is stimulated by the opportunity to verify the existing theories concerning the effect of variation of air density on the formation of the fireball. For these reasons, thermal measurements of the high-altitude detonation (Shot 10) were made by this project from a location near ground zero. Due to the small yield of the device and the large distance involved, it was necessary to employ new instrumentation designed specifically for this application.

During Operation Upshot-Knothole, the U.S. Naval Radiological Defense Laboratory was again asked to assist the Army Chemical Corps in the determination of the attenuation of an oil-fog smoke screen. The previous results (Reference 4) and a theoretical study made by the University of Michigan (Reference 5) provided sufficient data so that the area to be screened could be efficiently instrumented with the available equipment. While the thermal-radiation measurements themselves are reported herein, details of the smoke screen and its effective attenuation can be found in the report for Project 8.3 (Reference 6).

The interaction of thermal radiation with the exposed surface areas in the vicinity of a nuclear detonation causes major modification of the atmosphere through which the expanding shock front must travel. Differences in the temperature or the composition of the propagating media can cause major changes in the shape of the pressure versus time profile. The air-temperature measurements during Operation Tumbler-Snapper showed that very-high temperatures existed over desert sand prior to shock arrival (Reference 7). The sound-velocity measurements during Operation Upshot-Knothole showed pronounced increases in the sound velocity over fir boughs, as compared with the velocity over desert sand. The increased velocity was believed due to a combination of increased temperature due to combustion and a change of chemical composition of the media over the surface of the plot (Reference 8).

In order to attempt an explanation of the phenomena, plots containing eight different materials were exposed during Operation Teapot. Project 8.4b provided thermal instruments in these plots so as to measure the thermal input up until the time of shock arrival. Both the total radiant energy and shape of the thermal pulse were measured with instruments at, or immediately above, the surface of each plot. Additional measurements were also made at a 10-foot elevation over some of these plots. A complete description of the plots, their associated instrumentation, and the measured inputs can be found in the report for Project 8.4e (Reference 9). Only those measurements deemed to be of interest as basic thermal data are listed in the present report.

The prediction of thermal energies at large distances from the point of detonation is dependent upon the attenuation of the atmosphere. Although the energy as a function of distance for Nevada tests is fairly well known (Reference 4), these data cannot be applied to other atmospheres of interest until scattering and absorption effects are better known. The broad-band spectral-distribution measurements and the field-of-view measurements made by Project 8.4b should prove useful for determining the magnitudes of these effects.

The broad-band spectral measurements should also provide an indication of the effective color temperature of the fireball as seen from distances where the energy ranges are such that the thermal radiation is capable of doing damage to physical objects. By combining the

color-temperature measurements with photographic measurements of the fireball radius versus time, an effective emissivity can be determined for the fireball surface. Should the values for total energy received, spectral distribution of the energy, and the fireball size give consistent results, our knowledge of the fireball and its mechanisms would be substantially increased.

Operation Teapot also provided an opportunity to field test instrumentation planned for use during future operations. Such an opportunity is always welcomed, as it provides some assurance of favorable results where the data are urgently required.

Chapter 2

INSTRUMENTATION

2.1 EXPERIMENTAL DESIGN

Standard basic thermal-radiation measurements were made during six shots from ground installations relatively close to ground zero. The measurements consisted of determinations of the total radiant energy (TE), of the broad-band spectral distribution (SP), of the total radiant energy density as a function of the field of view of measuring instrument (FV), and of the total thermal irradiance versus time (RD). The types and locations of the measurements made during each shot are given in Table 2.1.

Column 3 lists the number of total-radiant-energy measurements made at each location using standard Mark 6F integrating calorimeters. These instruments had quartz filters and a field of view of 90 degrees. Column 4 lists the number of broad-band spectral measurements made at each location. These instruments were identical to those used for the measurements listed in Column 3, except that Corning glass filters were used in place of quartz. Column 5 lists the number of measurements of total radiant energy using instruments with fields of view different from those listed in Column 3. The fields of view chosen were 180, 45, 22, and 11 degrees. The angles refer to the included angle of the cone from which the instruments received energy. The angles used at each station are given in Chapter 3. Column 6 lists the number of irradiance-versus-time measurements made at each station using standard Mark 6F radiometers. These instruments all had quartz filters and a 90-degree field of view.

In some cases, additional measurements were made during these shots with photronic cells, whenever spare recorder channels were available. These cells were used primarily to mark zero time and have limited additional value. A more-complete description of the instrumentation is given in Section 2.2. Further details of the layout of instrumentation are given in Chapter 3 for easier reference and interpretation of data.

In addition to the standard thermal measurements, several types of specialized measurements were made. In particular, measurements were made at extremely low energy ranges of the high-altitude burst (Shot 10), at extremely high energy ranges and over various material plots during Shot 12, and under the smoke layer during Shot 5. The instrumentation for Shot 10 is given in Table 2.2.

The abbreviations used are the same as those for Table 2.1, except that "PC" is used to denote the number of photronic-cell measurements. The numbers and types of instruments used were limited by the preparation time available.

The extremely high energy-range measurements made during Shot 12 consisted of determinations of the thermal input at grade level on the various plots of materials and a limited number of measurements at an elevation of 10 feet. These measurements are listed in Table 2.3.

The abbreviations used to head columns have the same significance as those used for Tables 2.1 and 2.2. The measurements listed in Columns 3 through 7 were made at either the 0-foot or the 10-foot elevation, as indicated. Those at 0 feet were intended to give an estimate of the thermal energy reaching the plot surface and those at 10 feet to indicate the energy received at early times above the smoke and dust layer. Further details of Shot 12 instrumentation are given in References 9 and 17.

The measurements made under the smoke layer during Shot 5 were made in support of

TABLE 2.1 INSTRUMENTATION LAYOUT FOR STANDARD THERMAL MEASUREMENTS*

1 Shot	2 Ground Distance	3 TE	4 SP	5 FV	6 RD
	ft				
1	1,500	2	4	4	2
1	3,000	2	4	4	2
2	2,750	2	4	4	2
2	4,950	2	4	4	2
3	4,550	2	4	4	1
3	5,410	2	4	4	1
5	4,950	2	4	4	1
6	5,200	2	4	4	2
6	6,600	2	4	4	2
9	1,500	2	4	4	2
9	3,000	2	4	4	2

* Standard thermal measurements are those made with NRDL Mark 6F calorimeters and radiometers.

TABLE 2.2 INSTRUMENT LAYOUT FOR SHOT 10

1 Station	2 Distance to Ground Zero	3 TE	4 SP	5 PC
	ft			
8.4b-3	2,000, east	5	4	6
410	34,216, south	1	—	—

TABLE 2.3 THERMAL INSTRUMENTATION FOR SHOT 12 MATERIAL PLOTS

1 Distance to Ground Zero	2 Material in Plot	3 RD at 0 ft	4 TE at 0 ft	5 TE at 10 ft	6 FV at 10 ft	7 RD at 10 ft
ft						
1,000	Water	—	1	1	1	1
2,500	Water	—	—	1	1	—
1,000	Asphalt	1	1	1	1	—
2,000	Asphalt	1	1	1	1	—
1,000	Desert	1	1	1	1	—
200	Desert	1	1	1	1	—
2,000	Concrete	—	1	—	—	—
2,000	Fir Boughs	1	1	—	—	—
2,000	Ivy	1	1	—	—	—
2,000	Painted Wood	1	1	—	—	—
2,000	Soil	1	1	—	—	—

Project 8.3, Army Chemical Corps. These measurements are outlined in Table 2.4. Further details of Shot 5 instrumentation can be found in Reference 6.

The headings of Columns 2 through 5 list the function and field of view of the instruments. All instruments, except the goniometric measurements (GM, listed in Column 4, Table 2.4) were aimed at air zero.

In addition to the measurements listed in Table 2.4, Project 8.4b provided thermal instruments and technical assistance to several other projects. Standard Mark 6F calorimeters and radiometers were supplied to Project 5.1 for use in measuring the thermal input to an airplane parked relatively close to ground zero. Standard instruments were also supplied to Project 5.5 for use in measuring the thermal input to aircraft components positioned at close range. Special calorimeters and radiometers for extremely high energy ranges were supplied to Project 5.4 for use in the determination of the thermal input to specimens of interest in the design of ballistic missiles. A total of more than 300 individual thermal instruments, constructed and calibrated by the Thermal Radiation Branch, Naval Radiological Defense Laboratory, were supplied to the various participating agencies.

2.2 DESCRIPTION OF INSTRUMENTATION

The Mark 6F instrumentation was similar to that used during Operation Upshot-Knothole and is described in detail in the basic thermal report for that operation (References 4 and 18). The detecting instruments used were the Mark 6F calorimeters and radiometers, the signals from which were recorded on oscillographic recorders.

The Mark 6F calorimeter is essentially a blackened copper disk with a thermocouple, either silver-soldered on the back face or embedded in the geometrical center of the disk. The detecting disk receives energy from a field of view of 90 degrees total angle and is covered with a quartz window. The output signal is carried to the recorder over a pair of twisted and shielded wires. The recorder used is a recording oscillograph employing d'Arsonval galvanometers and a moving strip of photosensitive paper. Proper series and shunt resistors are used to adjust the level of the signal and to provide the correct damping for the galvanometers.

TABLE 2.4 INSTRUMENTATION UNDER SMOKE LAYER ON SHOT 5

1	2	3	4	5
Distance to Ground Zero	TE	TE	GM	SP
	Field of View			
	90 deg	180 deg	180 deg	90 deg
ft				
1,000	2	2	8	—
1,400	2	—	6	4
1,900	2	2	8	—

The Mark 6F radiometer consists of a thin, blackened silver foil mounted over a hole in a massive copper block. Constantan wires attached to the center of the foil and to the edge of the hole provide two thermocouples, which permit measurement of the temperature difference from the center of the foil to its edge. The field of view, filter, and recording system are similar to those used with the Mark 6F calorimeter.

The special instrumentation used for Shot 10 consisted of both commercial detectors and the Mark 7F calorimeter, which was designed specifically for this purpose. The commercial instruments used consisted of ten-junction thermopiles available from the Minneapolis-

Honeywell Company and have been described in detail by Harrison and Wannamaker (Reference 10). This instrument was lacking in some of the characteristics desirable in measuring a transient pulse of the type observed from a nuclear detonation, but had the advantage of being available in the limited time in which the instrumentation was assembled. The thermopiles were given an added coating of a diffuse black to increase their absorptivity and make the receiving surface diffuse. Special adaptors were then used to enable the thermopiles to be mounted in a case similar to that used for the Mark 6F instruments.

The principal disadvantage of the thermopiles was their high rate of heat loss. The thermopile loses heat too slowly to record the thermal radiant power versus time, and loses heat too rapidly to properly record the integrated energy, with the realization that large corrections would be necessary to obtain the final energy values. To avoid full reliance upon these corrections, these instruments were used primarily to obtain the broad-band spectral distribution, where to a first approximation, only the comparative readings between instruments are important. The absolute radiant energy was measured with the newly designed Mark 7F calorimeter.

The Mark 7F calorimeter was designed on the same theoretical basis as the Mark 6F instruments, i.e., a receiver thickness small enough to give 20 msec or better time response and great enough to keep the rate of heat loss low enough so that the corrections to be applied to the recorded deflection would be a small percentage of that deflection. The additional design features involved were extension of the sensitivity to low-energy regions without an increase in the rate of heat loss and simplification in the arrangement for mounting the receiver disks.

The extension to low-energy ranges was achieved by the use of a large number of individual disks, each disk being essentially a Mark 6F calorimeter in itself. If the disks are carefully constructed, the net result is simply a multiplication of the output signal by the number of disks used. By combining 20 identical disks, each having an output of 1 mvolt/(cal/cm^2) and a heat loss of 5 pct/sec the resultant instrument has an output of 1 mvolt per $\frac{1}{20}$ cal/cm^2, but maintains a heat loss of 5 pct/sec. Further design makes it possible to make the resistance of the instrument exactly the value required for the proper damping of the galvanometer used in the recorder, thus achieving the maximum possible deflection while still maintaining proper damping.

The mounting of the individual disks was simplified because of the relatively small temperature rise, of the order of a few degrees, as contrasted with the several-hundred-degree temperature rise sometimes encountered with the Mark 6F instruments. While the higher temperature required an invariable, nonconducting, mechanical mount, it was possible to use lucite cementing techniques in the case of the lower temperatures. It was also possible to use dead-air spaces of the proper proportions so as to minimize the convective losses of the disks and thus balance out the added conductive losses caused by the larger area of support in the cementing method. Only the preparation time available limited the number of these instruments used. The signals from both the ten-junction thermopiles and the Mark 7F calorimeters were recorded in a manner similar to that used for the Mark 6F calorimeters.

The instrumentation required for Shot 12 was for use at energy ranges higher by a factor of ten than the energy ranges for which the Mark 6F instruments were designed. The instruments designed for this purpose, designated the Mark 8F calorimeters and radiometers, were again a modification of the Mark 6F design. The diffuse black surface of platinum black was replaced by a diffuse white surface of magnesium oxide. The absorptivity of the receiving element was thus lowered by a factor of about seven without changing the other characteristics of the instruments. This procedure permitted use of the Mark 8F instruments and thus provided a simplification of the field instrumentation.

The instrumentation used under smoke on Shot 5, at some locations on Shot 12, and in the field-of-view measurements on other shots, required the use of the Mark 6F instruments with a 180-degree field of view rather than the standard 90-degree field of view. A dome filter was designed and fabricated from quartz for this purpose. Under the conditions that the radius of the dome be large and the wall section thin, the rounded cover causes little or no error to be introduced. In fabrication, however, it was not possible (due to the short time available) to form the quartz domes completely free from defects. As a result, the domes had a small

imperfection directly normal to the receiving surface. This imperfection had the same effect as a small convex lens. In selecting the domes for use, an attempt was made to select domes in which this "lens" had a focal length of greater than half the distance to the receiving disk. For this situation, no energy is added to or subtracted from the amount the disk would receive if the lens effect were not present.

Several variations of the standard Mark 6F instruments were also used for various shots. The broad-band spectral distribution was measured by replacing the quartz windows of the 90-degree instruments with Corning glass filters of suitable transmission characteristics. The details of these filters are given in Chapter 4 to avoid repetition. The filters used were similar to those used during previous operations. The fields-of-view measurements were made by extending the length of the calorimeter cases so that the front of the case limited the field of view to the desired total angle. All other details of these instruments were identical to the standard instruments.

The instrumentation provided for other projects was all of the standard Mark 6F variety, with the exception of that provided for Projects 5.4 and 5.5; this nonstandard instrumentation was designed and constructed in a fashion similar to that used for the Project 8.4b high-energy-range measurements during Shot 12. Standardization of instrument characteristics and recording techniques was carried out wherever possible, because of the extremely large number of measurements employed.

Chapter 3
RESULTS

Standard thermal measurements were made during Shots 1, 2, 3, 5, 6, and 9. In several cases data were lost at one of the two stations on these shots, but in all cases data are available from a second station. The loss of data was due to failure of the paper drive mechanism in the recorders, caused by swelling of the photographic paper due to excess moisture in the recording shelters. Since elimination of the moisture is not always feasible, a special type of film, also less sensitive to gamma radiation, has since been used to replace the paper. No recorder failures have been reported since the new film has been in use.

Satisfactory thermal measurements were made during Shot 10 from a station 2,000 feet east of ground zero. Results were obtained under the smoke screen during Shot 5 up to the time of shock arrival at each of the three stations. The results at the material plots for Shot 12 were poor. Approximately half of the data were lost due to some type of recorder failure never before experienced, and as yet unexplained.

3.1 STANDARD THERMAL ENERGY

Integrated values of the thermal energy (cal/cm^2) arriving at the detecting units of Mark 6F calorimeters are given in Tables 3.1 through 3.8. Energy values are reported in tabular form from time zero to twelve specified times of interest. The significance of these particular times is discussed in Chapter 4. The energy values listed in these tables represent the energy transmitted by the filters used on each instrument and must be corrected for filter transmission to obtain the energy incident at the measuring station. Transmission curves for all filters and methods of correction are given in Chapter 4. The column headings list the various types of measurements made at each location, and have the following meanings:

FV 180: A black receiver protected by a thin quartz dome. Included angle of field of view is 180 degrees (2π steradians).

FV 90: A black receiver protected by a flat quartz filter. Included angle of field of view is 90 degrees.

FV 45: Same as FV 90 except that included angle is 45 degrees.

FV 22: Same as FV 90 except that included angle is 22 degrees.

FV 11: Same as FV 90 except that included angle is 11 degrees.

SP 052: A black receiver protected by a flat Corning 0-52 filter. Included angle of field of view is 90 degrees (Reference 11).

SP 369: Same as SP 052, but with Corning 3-69 filter.

SP 258: Same as SP 052, but with Corning 2-58 filter.

SP 756: Same as SP 052, but with Corning 7-56 filter.

Although the energy values are given to as many as four significant figures, the accuracy is not of this order of magnitude. The accuracy of the data is discussed in Section 4.2.

3.2 HIGH-ALTITUDE BURST

Shot 10 was a high-altitude shot of low yield, so that the energy incident at the ground-zero station was two orders of magnitude lower than that generally measured with the standard

TABLE 3.1 CALORIMETER RESULTS, SHOT 1*

Station 220, slant range 2,428 ft.

Time	Type of Measurement								
	FV180	FV180	FV90	FV45	(FV22)†	SP052	SP369	SP258	SP756
sec	cal/cm²	cal/cm²	cal/cm²	cal/cm²	cal/cm²	cal/cm²	cal/cm²	cal/cm²	cal/cm²
0.000	0.000	0.000	0.000	0.000	0.000	0.000	0.000	0.000	0.000
0.024	0.245	0.115	0.126	0.117	0.064	0.126	0.102	0.066	0.017
0.043	0.979	0.577	0.654	0.586	0.128	0.692	0.441	0.298	0.104
0.053	1.406	0.922	1.079	0.936	0.193	1.130	0.644	0.431	0.155
0.067	1.954	1.381	1.654	1.286	0.193	1.694	0.914	0.596	0.241
0.086	2.501	1.897	2.287	1.636	0.193	2.318	1.184	0.776	0.344
0.125	3.107	2.470	2.998	2.044	0.257	3.002	1.521	0.992	0.464
0.192	3.590	2.982	3.565	2.433	0.449	3.622	1.851	1.222	0.584
0.288	4.077	3.556	4.203	2.859	0.514	4.248	2.228	1.487	0.722
0.480	4.503	4.072	4.774	3.270	0.643	4.812	2.602	1.786	0.878
0.768	4.872	4.535	5.281	3.681	0.709	5.319	2.978	2.088	1.071
1.440	5.316	5.121	5.901	4.221	0.842	5.907	3.440	2.466	1.323
—	6.076	6.098	6.834	4.862	0.975	6.827	4.208	3.081	1.798
Accuracy†	RU 0.063	RU 0.058	RU 0.063	RU 0.061	RU 0.064	RU 0.063	RU 0.033	RU 0.032	RU 0.017

* These data must be corrected, before use, as described in Chapter 4.

† See Section 4.2 concerning accuracy of results.

TABLE 3.2 CALORIMETER RESULTS, SHOT 2*

Station 8.4b-1, slant range 5,005 ft.

Time	Type of Measurement								
	(FV180)†	FV180	FV90	FV45	FV11	SP052	SP369	SP258	SP756
sec	cal/cm²	cal/cm²	cal/cm²	cal/cm²	cal/cm²	cal/cm²	cal/cm²	cal/cm²	cal/cm²
0.000	0.000	0.000	0.000	0.000	0.000	0.000	0.000	0.000	0.000
0.034	0.087	0.072	0.093	0.096	0.084	0.094	0.064	0.044	0.026
0.061	0.314	0.255	0.286	0.290	0.265	0.284	0.200	0.133	0.052
0.075	0.437	0.387	0.409	0.412	0.384	0.406	0.280	0.189	0.078
0.095	0.575	0.538	0.571	0.556	0.539	0.568	0.392	0.267	0.104
0.122	0.782	0.720	0.763	0.748	0.720	0.762	0.532	0.366	0.142
0.177	1.058	1.002	1.046	1.023	0.987	1.049	0.757	0.522	0.208
0.272	1.387	1.343	1.388	1.347	1.303	1.393	1.010	0.723	0.311
0.408	1.597	1.578	1.605	1.556	1.501	1.605	1.199	0.869	0.404
0.680	1.785	1.756	1.803	1.753	1.649	1.794	1.370	1.021	0.510
1.088	1.851	1.889	1.916	1.871	1.718	1.898	1.467	1.105	0.581
2.040	1.893	1.953	1.993	1.957	1.750	1.970	1.532	1.160	0.643
—	(2.00)	(2.02)	(2.05)			(2.02)	(1.57)	(1.19)	(0.694)
Accuracy†	RU 0.018	RU 0.010	RU 0.010	RU 0.012	RU 0.012	RU 0.012	RU 0.013	RU 0.011	RU 0.012

* These data must be corrected, before use, as described in Chapter 4.

† See Section 4.2 concerning accuracy of results.

TABLE 3.3 CALORIMETER RESULTS, SHOT 3*

Station 8.4b-2, slant range 4,960 ft.

Time	Type of Measurement								
	(FV180)†	FV180	FV90	FV45	FV11	SP052	SP369	SP258	SP756
sec	cal/cm²	cal/cm²	cal/cm²	cal/cm²	cal/cm²	cal/cm²	cal/cm²	cal/cm²	cal/cm²
0.000	0.000	0.000	0.000	0.000	0.000	0.000	0.000	0.000	0.000
0.043	0.216	0.186	0.206	0.199	0.180	0.209	0.162	0.103	0.040
0.077	0.629	0.586	0.616	0.605	0.515	0.610	0.446	0.308	0.118
0.094	0.859	0.800	0.839	0.826	0.704	0.839	0.607	0.422	0.156
0.119	1.177	1.122	1.162	1.142	0.988	1.158	0.835	0.581	0.222
0.153	1.581	1.512	1.562	1.541	1.352	1.563	1.153	0.808	0.312
0.221	2.226	2.139	2.196	2.163	1.912	2.186	1.669	1.201	0.480
0.340	3.054	2.956	3.031	2.974	2.549	3.001	2.365	1.759	0.765
0.510	3.648	3.547	3.634	3.554	2.978	3.585	2.907	2.200	1.025
0.850	4.193	4.085	4.180	4.058	3.298	4.113	3.424	2.657	1.328
1.360	4.481	4.368	4.475	4.328	3.460	4.399	3.704	2.922	1.534
2.550	4.650	4.548	4.668	4.484	3.551	4.579	3.863	3.084	1.699
—	4.723	4.696	4.837	4.606	3.600	4.704	3.950	3.152	1.791
Accuracy†	RU 0.019	RU 0.010	RU 0.010	RU 0.012	RU 0.012	RU 0.011	RU 0.014	RU 0.011	RU 0.013

* These data must be corrected, before use, as described in Chapter 4.

† See Section 4.2 concerning accuracy of results.

TABLE 3.4 CALORIMETER RESULTS, SHOT 5*

Station 8.4b-1, slant range 4,676 ft.

Time	Type of Measurement								
	(FV180)†	FV180	FV90	FV45	FV11	SP052	SP369	SP258	SP756
sec	cal/cm²	cal/cm²	cal/cm²	cal/cm²	cal/cm²	cal/cm²	cal/cm²	cal/cm²	cal/cm²
0.000	0.000	0.000	0.000	0.000	0.000	0.000	0.000	0.000	0.000
0.036	0.134	0.107	0.126	0.128	0.112	0.127	0.100	0.060	0.026
0.064	0.402	0.332	0.364	0.368	0.322	0.366	0.264	0.179	0.067
0.078	0.549	0.470	0.517	0.520	0.459	0.516	0.364	0.239	0.093
0.099	0.766	0.682	0.730	0.726	0.655	0.728	0.514	0.334	0.132
0.128	1.020	0.925	0.986	0.985	0.888	0.988	0.701	0.464	0.180
0.185	1.428	1.325	1.392	1.397	1.253	1.395	1.002	0.691	0.278
0.284	1.882	1,785	1.860	1.844	1.657	1.861	1.384	0.973	0.411
0.426	2.325	2.206	2.298	2.271	2.003	2.285	1.745	1.260	0.570
0.710	2.677	2.529	2.647	2.605	2.243	2.626	2.050	1.518	0.732
1.136	2.927	2.775	2.904	2.841	2.399	2.870	2.262	1.719	0.914
2.130	3.085	2.943	3.080	3.001	2.493	3.031	2.403	1.847	1.051
—	3.127	3.073	3.214	3.124	2.512	3.150	2.472	1.933	1.150
Accuracy†	RU 0.012	RU 0.010	RU 0.011	RU 0.012	RU 0.012	RU 0.011	RU 0.012	RU 0.012	RU 0.014

* These data must be corrected, before use, as described in Chapter 4.

† See Section 4.2 concerning accuracy of results.

TABLE 3.5 CALORIMETER RESULTS, SHOT 6*

Station 220, slant range 5,270 ft.

Time	Type of Measurement									
	(FV180)†	(FV180)†	TE90	FV90	(FV45)†	FV11	SP052	SP369	SP258	SP756
sec	cal/cm^2	cal/cm^2	cal/cm^2	cal/cm^2	cal/cm^2	cal/cm^2	cal/cm^2	cal/cm^2	cal/cm^2	cal/cm^2
0.000	0.000	0.000	0.000	0.000	0.000	0.000	0.000	0.000	0.000	0.000
0.051	0.113	0.333	0.172	0.185	0.172	0.136	0.160	0 133	0.111	0.044
0.091	0.450	1.027	0.686	0.708	0.688	0.575	0.677	0.500	0.364	0.133
0.111	0.674	1.448	1.028	1.047	1.030	0.846	1.034	0.732	0.522	0.191
0.141	1.010	1.987	1.512	1.535	1.523	1.249	1.508	1.031	0.758	0.279
0.182	1.458	2.612	2.078	2.112	2.086	1.685	2.099	1.428	1.040	0.395
0.263	2.154	3.443	2.814	2.838	2.798	2.286	2.803	1.956	1.447	0.557
0.404	2.909	4.241	3.547	3.590	3.541	2.827	3.546	2.584	1.948	0.776
0.606	3.503	4.834	4.113	4.168	4.119	3.202	4.099	3.091	2.389	0.995
1.010	4.039	5.379	4.638	4.697	4.612	3.492	4.626	3.590	2.815	1.265
1.616	4.332	5.804	5.045	5.097	4.986	3.602	4.994	3.955	3.146	1.514
3.030	4.564	6.124	5.356	5.405	5.224	3.672	5.296	4.213	3.371	1.742
—	4.679	6.288	5.526	5.567	5.326	3.720	5.430	4.308	3.452	1.852
Accuracy†	RU 0.028	RU 0.030	RU 0.028	RU 0.031	RU 0.034	RU 0.034	RU 0.040	RU 0.033	RU 0.016	RU 0.014

* These data must be corrected, before use, as described in Chapter 4.

† See Section 4.2 concerning accuracy of results.

TABLE 3.6 CALORIMETER RESULTS, SHOT 6*

Station 221, slant range 6,698 ft.

Time	Type of Measurement								
	FV180	(FV180)†	FV90	FV45	FV11	SP052	SP369	SP258	SP756
sec	cal/cm^2	cal/cm^2	cal/cm^2	cal/cm^2	cal/cm^2	cal/cm^2	cal/cm^2	cal/cm^2	cal/cm^2
0.000	0.000	0.000	0.000	0.000	0.000	0.000	0.000	0.000	0.000
0.051	0.132	0.098	0.107	0.107	0.109	0.102	0.083	0.066	0.028
0.091	0.477	0.365	0.398	0.390	0.381	0.391	0.289	0.212	0.088
0.111	0.706	0.543	0.596	0.585	0.579	0.595	0.427	0.316	0.127
0.141	1.031	0.821	0.885	0.884	0.885	0.882	0.632	0.461	0.181
0.182	1.437	1.149	1.219	1.218	1.208	1.219	0.878	0.644	0.250
0.263	1.972	1.651	1.657	1.656	1.657	1.653	1.217	0.919	0.347
0.404	2.520	2.236	2.097	2.091	2.086	2.088	1.584	1.234	0.500
0.606	2.930	2.664	2.437	2.430	2.425	2.415	1.882	1.500	0.654
1.010	3.328	3.013	2.765	2.750	2.726	2.720	2.172	1.764	0.830
1.616	3.554	3.242	3.014	3.001	2.934	2.962	2.395	1.980	0.997
3.030	3.695	3.410	3.196	3.179	3.018	3.123	2.540	2.113	1.141
—	3.738	3.502	3.294	3.272	3.028	3.208	2.597	2.161	1.214
Accuracy†	RU 0.016	RU 0.016	RU 0.015	RU 0.018	RU 0.018	RU 0.017	RU 0.013	RU 0.013	RU 0.014

* These data must be corrected, before use, as described in Chapter 4.
† See Section 4.2 concerning accuracy of results.

TABLE 3.7 CALORIMETER RESULTS, SHOT 9*

Station 220, slant range 2,397 ft.

Time	Type of Measurement								
	FV180	(FV180)†	FV90	FV45	(FV22)†	SP052	SP369	SP258	SP756
sec	cal/cm^2	cal/cm^2	cal/cm^2	cal/cm^2	cal/cm^2	cal/cm^2	cal/cm^2	cal/cm^2	cal/cm^2
0.000	0.000	0.000	0.000	0.000	0.000	0.000	0.000	0.000	0.000
0.037	0.721	0.605	0.504	0.451	0.374	0.462	0.274	0.192	0.073
0.066	2.990	3.221	2.339	2.077	1.865	2.306	1.360	0.893	0.323
0.080	4.357	4.789	3.500	3.080	2.816	3.452	1.990	1.338	0.465
0.102	6.175	7.036	5.137	4.521	4.129	5.044	2.883	1.969	0.676
0.131	7.693	8.944	6.716	5.892	5.386	6.568	3.741	2.565	0.888
0.190	9.030	10.681	8.241	7.265	6.587	8.079	4.651	3.194	1.099
0.292	10.356	12.404	9.807	8.634	7.833	9.589	5.616	3.879	1.347
0.438	11.346	13.815	11.110	9.789	8.871	10.877	6.495	4.570	1.578
0.730	12.235	15.229	12.483	10.999	9.917	12.224	7.472	5.296	1.924
1.168	13.078	16.359	13.597	11.976	10.618	13.311	8.277	5.971	2.240
2.190	14.446	17.986	15.217	13.300	11.126	14.823	9.545	7.060	2.806
—	16.386	20.079	17.325	14.983	11.516	16.735	11.260	8.706	4.091
Accuracy†	RU 0.060	RU 0.055	RU 0.056	RU 0.056	RU 0.053	RU 0.057	RU 0.030	RU 0.032	RU 0.019

* These data must be corrected, before use, as described in Chapter 4.
† See Section 4.2 concerning accuracy of results.

Mark 6F instrumentation. Satisfactory total-energy results were obtained with the Mark 7F calorimeter designed for this purpose. Only one such instrument was used, however, at the ground-zero station. Preparation time permitted the construction of only three such instruments, which were used in the airborne station (Reference 12), Station 410, and the ground-zero station

TABLE 3.8 CALORIMETER RESULTS, SHOT 9*

Station 221, slant range 3,808 ft.

Time	Type of Measurement								
	FV180	FV180	FV90	FV45	FV11	SP052	SP369	SP258	SP756
sec	cal/cm^2	cal/cm^2	cal/cm^2	cal/cm^2	cal/cm^2	cal/cm^2	cal/cm^2	cal/cm^2	cal/cm^2
0.000	0.000	0.000	0.000	0.000	0.000	0.000	0.000	0.000	0.000
0.037	0.530	0.193	0.188	0.196	0.187	0.196	0.119	0.091	0.027
0.066	1.761	0.914	0.897	0.900	0.839	0.905	0.536	0.363	0.120
0.080	2.225	1.391	1.351	1.356	1.209	1.353	0.788	0.544	0.173
0.102	2.804	2.020	1.967	1.961	1.687	1.955	1.127	0.777	0.252
0.131	3.326	2.646	2.578	2.532	2.143	2.554	1.466	1.008	0.331
0.190	3.865	3.249	3.167	3.077	2.579	3.118	1.803	1.251	0.411
0.292	4.471	3.870	3.774	3.643	3.035	3.712	2.185	1.522	0.505
0.438	4.969	4.374	4.272	4.109	3.387	4.201	2.525	1.782	0.599
0.730	5.512	4.915	4.810	4.612	3.739	4.724	2.906	2.065	0.723
1.168	5.947	5.351	5.235	4.998	3.882	5.122	3.200	2.310	0.839
2.190	6.574	5.961	5.847	5.570	4.059	5.668	3.669	2.703	1.052
—	7.404	6.785	6.663	6.335	4.137	6.367	4.291	3.248	1.532
Accuracy†	RU 0.016	RU 0.016	RU 0.017	RU 0.018	RU 0.019	RU 0.016	RU 0.015	RU 0.013	RU 0.013

* These data must be corrected, before use, as described in Chapter 4.

† See Section 4.2 concerning accuracy of results.

(8.4b-3). The thermal energy (cal/cm^2) arriving at the detector of the instrument at ground zero is given in Table 3.9. These values must be corrected for filter transmission to obtain the energy incident at the station, as described in Chapter 4.

Additional measurements were completed using commercially available instrumentation (see Chapter 2 and Reference 10); but due to lack of time and manpower, a satisfactory method of

TABLE 3.9 CALORIMETER RESULTS, SHOT 10*

Station 8.4b-3†, slant range 32,565 ft.

Time	Energy	Time	Energy
sec	cal/cm^2	sec	cal/cm^2
0.000	0.0000	0.172	0.0442
0.005	0.0005	0.190	0.0454
0.022	0.0025	0.258	0.0491
0.037	0.0092	0.292	0.0502
0.039	0.0104	0.430	0.0535
0.047	0.0152	0.438	0.0537
0.060	0.0225	0.688	0.0550
0.066	0.0256	0.730	0.0551
0.077	0.0299	1.168	0.0554
0.080	0.0308	1.290	0.0555
0.102	0.0360	2.190	0.0558
0.112	0.0376	Inf	0.0558
0.131	0.0400	—	—

* This data must be corrected before use as described in Chapter 4.

† Instruments had 90 degree field of view.

data reduction has not yet been developed. The instruments in question exhibit variable heat losses and variable zero drift, both of which are dependent upon the shape of the input pulse. Extensive experimental work would be necessary to handle these corrections analytically. The improvement in results would not justify the expenditure of the necessary manpower, since it

TABLE 3.10 UNCORRECTED CALORIMETER RESULTS, SHOT 10*
Station 8.4b-3†, slant range 32,565 ft.

Time	Q	Q	Q	Q	3-69	2-86	7-56
sec	cal/cm^2	cal/cm^2	cal/cm^2	cal/cm^2	cal/cm^2	cal/cm^2	cal/cm^2
0.000	0.0000	0.0000	0.0000	0.0000	0.0000	0.0000	0.0000
0.005	0.0005	0.0005	0.0005	0.0005	0.0001	0.0000	0.0001
0.010	0.0008	0.0008	0.0008	0.0008	0.0004	0.0002	0.0002
0.015	0.0012	0.0014	0.0013	0.0013	0.0007	0.0004	0.0003
0.020	0.0021	0.0022	0.0021	0.0022	0.0013	0.0007	0.0004
0.025	0.0035	0.0037	0.0035	0.0038	0.0021	0.0011	0.0005
0.030	0.0051	0.0054	0.0052	0.0053	0.0029	0.0016	0.0007
0.035	0.0070	0.0075	0.0071	0 0077	0.0040	0.0021	0.0009
0.040	0.0089	0.0097	0.0093	0.0097	0.0051	0.0027	0.0011
0.045	0.0109	0.0117	0.0112	0.0118	0.0061	0.0033	0.0012

* See Chapter 4 regarding corrections which must be applied to this data before use.
† Instruments had 90 degree field of view.

TABLE 3.11 THERMAL ENERGY UNDER SMOKE, SHOT 5*
Station II, slant range 1,048 ft.

Orientation	Filter	Field of View	Energy to 0.1 sec	Energy to 0.2 sec	Energy to † 0.3 sec
		deg	cal/cm^2	cal/cm^2	cal/cm^2
Air zero	Quartz	180	2.39	6.35	9.39
Up 30 deg	Quartz	180	2.44	6.93	10.52
Up 60 deg	Quartz	180	3.20	8.86	13.47
Up 90 deg	Quartz	180	2.09	5.50	8.15
Up 120 deg	Quartz	180	1.58	3.97	5.72
Up 150 deg	Quartz	180	1.56	3.77	5.14
Vertical	Quartz	180	2.54	6.86	10.32
Air zero	Quartz	180	1.86	5.70	9.21
Up 90 deg	Quartz	90	2.16	5.48	7.92
Up 90 deg	Quartz	90	2.04	5.08	7.23
Up 180 deg	Quartz	180	1.11	2.91	4.19
Left 90 deg	Quartz	180	1.79	4.46	6.33

* See Section 3.4 for explanation of notation and data.
† Shock arrival at approximately 0.3 sec.

is known from other results that the variation of radiation parameters was small for the limited variation in altitude for Shot 10, and since a shot having larger altitude variation is planned. The results of these measurements, covering the interval from zero time until just past the second maximum are given in Table 3.10. These results have not been corrected for heat losses during the exposure, nor for zero drift. Both of these corrections increase with time; the total

TABLE 3.12 THERMAL ENERGY UNDER SMOKE, SHOT 5*
Station III, slant range, 1,436 ft.

Orientation	Filter	Field of View	Energy to 0.1 sec	Energy to 0.2 sec	Energy to 0.3 sec	Energy to † 0.5 sec
		deg	cal/cm^2	cal/cm^2	cal/cm^2	cal/cm^2
Air zero	Quartz	90	1.79	4.27	6.46	9.40
Air zero	Quartz	90	1.63	4.00	6.12	9.07
Air zero	0-52	90	1.54	3.88	5.98	8.90
Air zero	3-69	90	1.13	2.99	4.80	7.39
Air zero	2-58	90	1.04	2.69	4.32	6.69
Air zero	7-56	90	0.64	1.65	2.71	4.42
Vertical	Quartz	180	1.56	3.74	5.48	7.66
Air zero	Quartz	180	2.04	5.03	7.68	11.13
Up 30 deg	Quartz	180	2.02	5.05	7.73	11.38
Up 90 deg	Quartz	180	1.56	3.57	5.12	6.89
Up 120 deg	Quartz	180	0.95	2.30	3.32	4 39
Up 180 deg	Quartz	180	0.73	1.74	2.53	3.44

* See Section 3.4 for explanation of notation and data.
† Shock arrival at approximately 0.5 sec.

correction amounts to about 20 percent by the time of second maximum. The column headings indicate the filters used on the various instruments, Q indicates a fused quartz filter (four instruments), and the other numbers refer to Corning glass filters. All instruments at the ground zero station had a field of view whose included angle was 90 degrees. The only instrumental failure was the instrument using the Corning 0-52 filter, which gave no deflection whatever. The choice of times used in Tables 3.9 and 3.10 is discussed in Chapter 4.

3.3 SMOKE-SCREEN EXPERIMENT

The total thermal energy (cal/cm^2) received under the smoke screen is given, for various times up to shock arrival at each station, in Tables 3.11, 3.12, and 3.13. The data has been corrected for filter losses and represents the energy incident at the measurement station. The orientations listed refer to the orientation of the axis of the instrument. All instruments, except the one labeled "Left 90 degrees," are oriented in a plane that includes air zero, ground zero, and the zenith. The angles listed refer to the angle between air zero and the optical axis of the instrument. The instrument labeled "Left 90 degrees" is directed horizontally and at 90 degrees to the left of ground zero. The instrument labeled "vertical" points to the zenith. The fields of view listed are the total included angles of the acceptance cones of the instruments. The filter designations are Q for fuzed quartz, and 0-52, 3-69, 2-58 and 7-56, for the respective Corning glass filters.

3.4 PLOTS OF SURFACE SPECIMENS

The Shot 12 thermal measurements gave satisfactory results for the asphalt, concrete, and fir plots at 2,000 feet and for the basic thermal data at 2,500 feet over the desert. The results for the desert, ivy, soil, and wood plots at 2,000 feet, as well as for the plots at 1,000 feet, were lost due to unexplained failures of the recording systems. All of the instrumentation had

TABLE 3.13 THERMAL ENERGY UNDER SMOKE, SHOT 5*

Station IV, slant range 1,925 ft.

Orientation	Filter	Field of View	Energy to 0.1 sec	Energy to 0.2 sec	Energy to 0.3 sec	Energy to 0.5 sec	Energy to † 1.0 sec
		deg	cal/cm^2	cal/cm^2	cal/cm^2	cal/cm^2	cal/cm^2
Air zero	Quartz	180	0.35	0.81	1.22	1.78	2.30
Up 30 deg	Quartz	180	0.36	0.85	1.26	1.82	2.37
Up 60 deg	Quartz	180	0.33	0.85	1.26	1.80	2.25
Up 90 deg	Quartz	180	0.30	0.69	1.03	1.46	1.78
Up 120 deg	Quartz	180	0.24	0.60	0.84	1.15	1.35
Up 150 deg	Quartz	180	0.19	0.48	0.71	0.98	1.13
Vertical	Quartz	180	0.31	0.73	1.05	1.48	1.89
Air zero	Quartz	180	0.29	0.74	1.12	1.66	2.16
Air zero	Quartz	90	0.25	0.59	0.87	1.33	1.77
Air zero	Quartz	90	0.20	0.50	0.79	1.20	1.70
Up 180 deg	Quartz	180	0.33	0.54	0.68	0.89	1.11
Left 90 deg	Quartz	180	0.22	0.49	0.71	0.98	1.30

* See Section 3.4 for explanation of notation and data.

† Shock arrival at approximately 1.0 sec.

TABLE 3.14 RESULTS OF THERMAL MEASUREMENTS ON SHOT 12 PLOTS*

Quantity Measured	Surface Measurements			12-Foot Elevation Measurements	
	Asphalt 2,000 ft	Concrete 2,000 ft	Fir Boughs 2,000 ft	Asphalt 2,000 ft	Desert 2,500 ft
Time to first obscuration of instrument, sec	0.04	0.05	0.09	0.22	1.01
Maximum irradiance to instrument, (cal/cm^2)/sec	90	234	184	—	—
Time to maximum irradiance, sec	0.06	0.11	0.10	0.20	0.17
Time of shock arrival, sec	0.45	0.51	0.51	0.45	1.01
Total radiant energy received to time of first obscuration, cal/cm^2	0.9 to 2.0	4.9	6.5	117	—
Radiant energy to time of shock arrival, cal/cm^2	6.1	42	41	Off scale	85
Radiant energy to surface until time of obscuration of instrument at 12-ft elevation, cal/cm^2	—	—	—	5.0	—

* See Section 3.5 and Table 2.3 for explanation of data.

quartz filters. The available data are given in Table 3.14. All values quoted have been corrected for filter losses.

3.5 THERMAL RADIANT POWER VERSUS TIME

Measurements of the shape of the second thermal pulse were made, using Mark 6F radiometers, for Shots 1, 2, 3. 5, 6, and 9 (Figures 3.1 through 3.6). Considerable difficulty has been experienced in obtaining reproducible thermal calibration factors for these instruments,

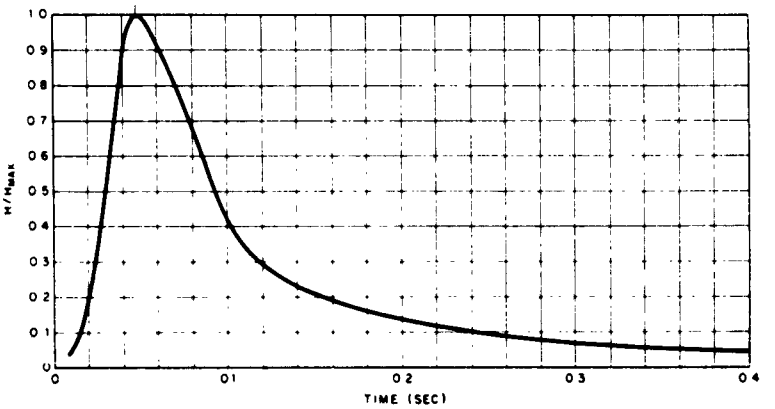

Figure 3.1 Thermal irradiance versus time, Shot 1.

so the curves are not given in absolute form. The time response of these instruments was too slow to resolve the first thermal pulse. The times to second maximum, and the best value of maximum irradiance at each station, as indicated by these instruments, are given in Table 3.15.

Information on thermal radiant power was obtained for Shot 10 by differentiation of the Mark

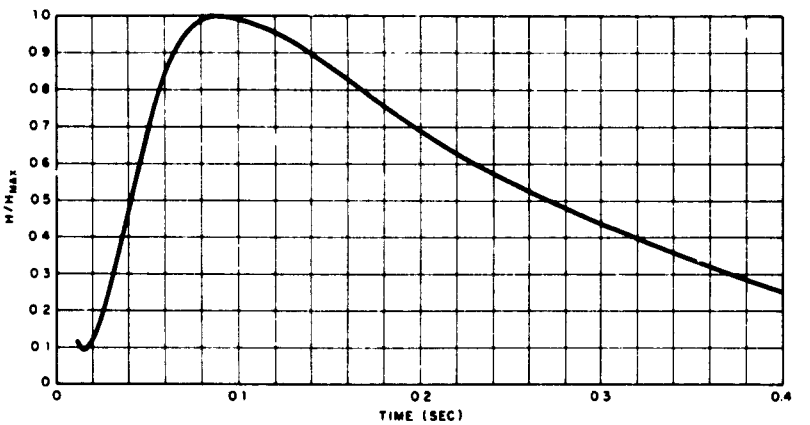

Figure 3.2 Thermal irradiance versus time, Shot 2.

7F calorimeter data and is shown in Figure 3.7. The time to second maximum, estimated from all the Shot 10 data, is given in Table 3.15.

3.6 FIREBALL PHOTOGRAPHY

The cameras operated successfully during Shots 1, 2, 3, 6, 10, and under the smoke for

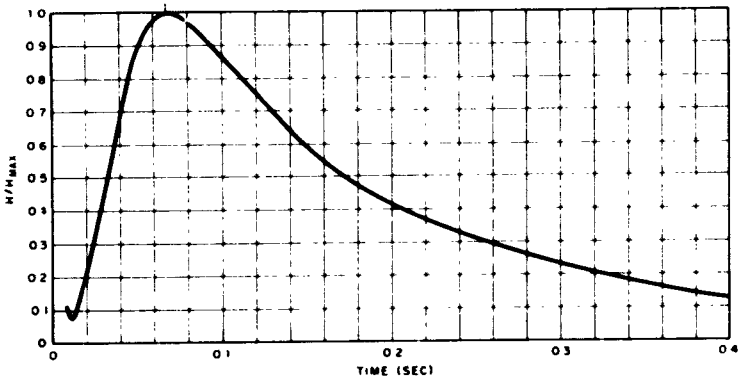

Figure 3.3 Thermal irradiance versus time, Shot 3.

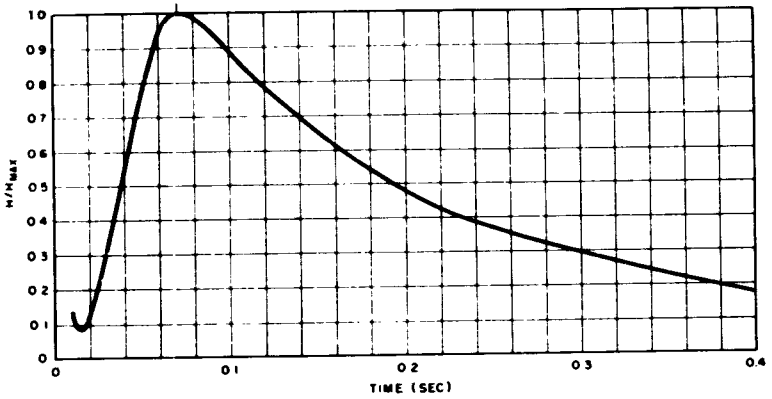

Figure 3.4 Thermal irradiance versus time, Shot 5.

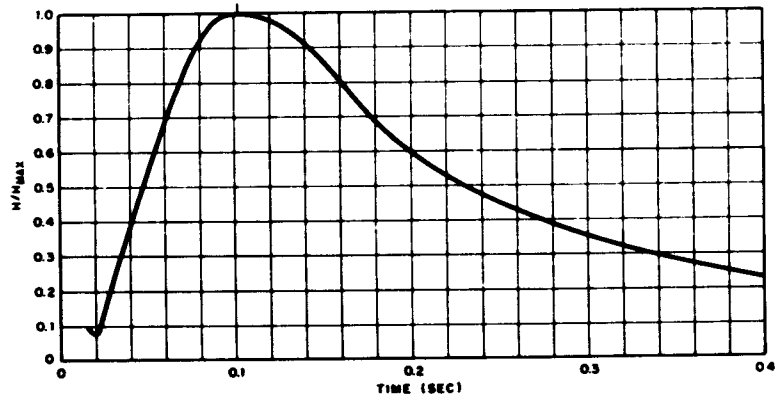

Figure 3.5 Thermal irradiance versus time, Shot 6.

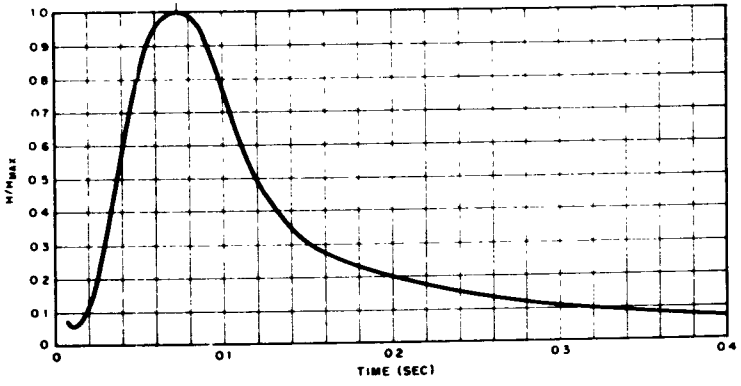

Figure 3.6 Thermal irradiance versus time, Shot 9.

Shot 5. The cameras failed during Shot 9 and in the clear area during Shot 5. While the primary purposes of the motion pictures were to determine the aiming errors for calorimetric instrumentation and the extent of local dust obscuration, usable data concerning late time fireball sizes and geometries can also be obtained from the films. The correction for aiming

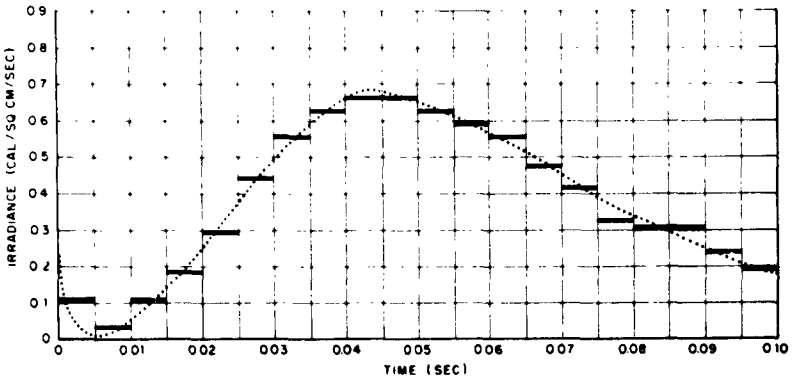

Figure 3.7 Thermal irradiance versus time, Shot 10.

errors was less than 1 percent in every case and was ignored.

The cameras used were 16-mm-gun-sight-aiming-point (GSAP) cameras, which have the single virtue of being inexpensive. They were set to run at 64 frames/sec with standard 120-degree shutter openings. These cameras usually run between 50 and 60 frames/sec. Exposures were varied by the selection of appropriate lens stops and neutral density filters.

The film used was a special Microfile (Emulsion SO-1112) which was obtained through the courtesy of Edgerton, Germeshausen and Grier, Inc. (EG&G). When properly exposed and developed, this film exhibits an extremely wide exposure latitude that is more than capable

TABLE 3.15 THERMAL RADIANT POWER

Shot	Slant Range	Time to Second Maximum	Irradiance at Second Maximum
	ft	sec	$(cal/cm^2)/sec$
1	2,330	0.047	48
1	2,330	0.049	57
2	5,005	0.068	10
2	5,005	0.068	10
3	4,960	0.085	16
5	4,676	0.061	—
5	4,676	0.071	13
6	5,270	0.100	18
6	5,270	0.103	20
6	6,698	0.101	12
6	6,698	0.129	14
9	2,428	0.073	109
9	3,781	0.073	38
9	3,781	0.087	48
10	32,565	(0.043)	0.66

TABLE 3.16 FIREBALL MOTION-PICTURE FILMS

Shot	Slant Range	Film Identification
	ft	
1	3,950	NRDL t/p 306
2	5,005	NRDL t/p 311
2	5,005	NRDL t/p 313
3	4,960	NRDL t/p 322
6	5,270	NRDL t/p 392
6	6,698	NRDL t/p 393

TABLE 3.17 LATE TIME FIREBALL DATA, SHOT 1

Frame	Max Radius	Equiv Radius	Equiv Surface Area	Equiv Volume	Equiv Flat Area	Figure Number
	meters	meters	$cm^2 \cdot 10^8$	$cm^3 \times 10^{12}$	$cm^2 \times 10^8$	
Film 306:						
1	19.0	19.0	0.45	0.03	0.11	3.8
2	49.3	49.3	3.05	0.50	0.76	3.8
3	58.7	58.7	4.34	0.85	1.08	3.9
4	65.5	62.2	4.87	1.01	1.21	3.9
5	67.8	62.8	4.95	1.04	1.21	3.10
6	74.2	62.6	4.93	1.03	1.25	3.10
8	82.0	69.0	5.98	1.38	1.45	3.11
12	93.8	75.9	7.24	1.83	—	3.11
19	100.2	78.8	7.81	2.05	—	3.12
31	101.1	79.9	8.02	2.14	—	3.12

TABLE 3.18 LATE TIME FIREBALL DATA, SHOT 2

Frame	Max Radius	Equiv Radius	Equiv Surface Area	Equiv Volume	Equiv Flat Area	Figure Number
	meters	meters	$cm^2 \times 10^8$	$cm^3 \times 10^{12}$	$cm^2 \times 10^8$	
Film 311:						
1	54.7	54.7	3.76	0.69	0.94	3.14
2	66.5	66.5	5.56	1.23	1.39	3.14
3	72.8	72.8	6.66	1.62	1.68	3.15
4	78.4	78.4	7.73	2.02	1.95	3.15
5	85.8	80.6	8.14	2.14	2.06	3.16
7	95.6	90.5	9.47	2.48	2.02	3.16
11	116.1	104.3	11.21	2.91	2.02	3.17
Film 313:						
1	41.1	41.1	2.12	0.29	0.53	3.20
2	60.0	60.0	4.53	0.91	1.13	3.20
3	69.4	69.4	60.7	1.40	1.50	3.21
4	74.5	74.5	6.98	1.73	1.74	3.21
5	78.4	78.4	7.79	2.01	1.91	3.22
7	91.9	87.8	9.42	2.51	2.00	3.22
11	108.8	102.6	10.73	2.72	—	3.23
17	129.4	119.5	14.47	3.81	—	3.23

TABLE 3.19 LATE TIME FIREBALL DATA, SHOT 3

Frame	Max Radius	Equiv Radius	Equiv Surface Area	Equiv Volume	Equiv Flat Area	Figure Number
	meters	meters	$cm^2 \times 10^8$	$cm^3 \times 10^{12}$	$cm^2 \times 10^8$	
Film 322:						
1	41.4	41.4	2.16	0.30	0.55	3.26
2	87.8	87.8	9.57	2.75	2.33	3.26
4	104.1	99.3	12.0	3.83	3.82	3.27
5	113.9	108.4	13.8	4.52	2.97	3.27
7	127.3	120.1	16.3	5.56	3.36	3.28
9	141.2	134.0	18.7	6.27	3.42	3.28
14	156.7	149.1	31.4	8.36	4.09	3.29

of accommodating the extreme variations in illumination encountered in fireball motion-picture photography. This film is a fine-grain variety and can be used at high levels of nuclear radiation without the necessity for lead shielding.

The films usable for fireball studies are summarized in Table 3.16.

Films from Shot 10 were not used in fireball studies, because the extreme slant range and

TABLE 3.20 LATE TIME FIREBALL DATA, SHOT 6

Frame	Max Radius	Equiv Radius	Equiv Surface Area	Equiv Volume	Equiv Flat Area	Figure Number
	meters	meters	$cm^2 \times 10^8$	$cm^3 \times 10^{12}$	$cm^2 \times 10^8$	
Film 392:						
1	67.6	67.6	5.74	1.29	1.30	3.32
3	102.8	102.8	13.3	4.55	3.03	3.32
5	119.5	119.5	17.7	7.01	4.06	3.33
6	129.7	124.1	19.3	7.84	4.24	3.33
8	132.3	130.0	21.4	9.12	4.74	3.34
11	140.0	139.5	23.2	10.1	4.78	3.34
16	164.4	156.2	27.1	11.6	4.92	3.35
Film 393:						
1	80.6	80.6	8.17	2.20	1.27	3.38
3	110.1	110.1	15.2	5.59	2.37	3.38
5	131.1	127.8	20.5	8.57	3.10	3.39
6	137.6	129.4	20.9	8.96	3.19	3.39
8	143.2	139.6	23.9	10.8	3.48	3.40
11	154.7	150.7	26.6	11.4	3.60	3.40

short focal length made the image too small. These films served their primary purpose of determining the calorimeter alignment error, which proved negligible. The films from Shot 5, under the smoke, show that the stations were covered with smoke at least until the time at which the cameras were destroyed by flying debris in the shock wave.

Particular frames from the films of Table 3.16 were enlarged and are shown in Figures 3.8 through 3.43. The enlargement was held constant throughout, so that relative measurements can be made from these figures. An absolute scale can be determined for each film from the known tower heights, except for Shot 1. For Film 306, the effective focal length of the camera-enlarger system can be found from the five remaining films, and thus an absolute scale determined.

Timing markers were not used on these films. The time scale was based on an alignment of the first frame to coincide with the EG&G data prior to breakaway, and the assumption that the camera speeds were between 50 and 60 frames/sec.

Data from these films is presented in Tables 3.17 through 3.20 and is plotted in Figures 3.44 through 3.47. The horizontal lines represent the uncertainty in the time of each frame for the assumed range of camera speed. At early times the fireball is spherical and is well-defined. At later times its edges become ragged and prominences appear. The term "maximum radius" is used to denote the maximum distance from the fireball center to tip of the furthest prominence. Conduction down tower cables and prominences obviously due to reflected shock were excluded.

The term "equivalent radius" is used to denote the radius of the sphere (or partial sphere)

(Text continued on Page 65)

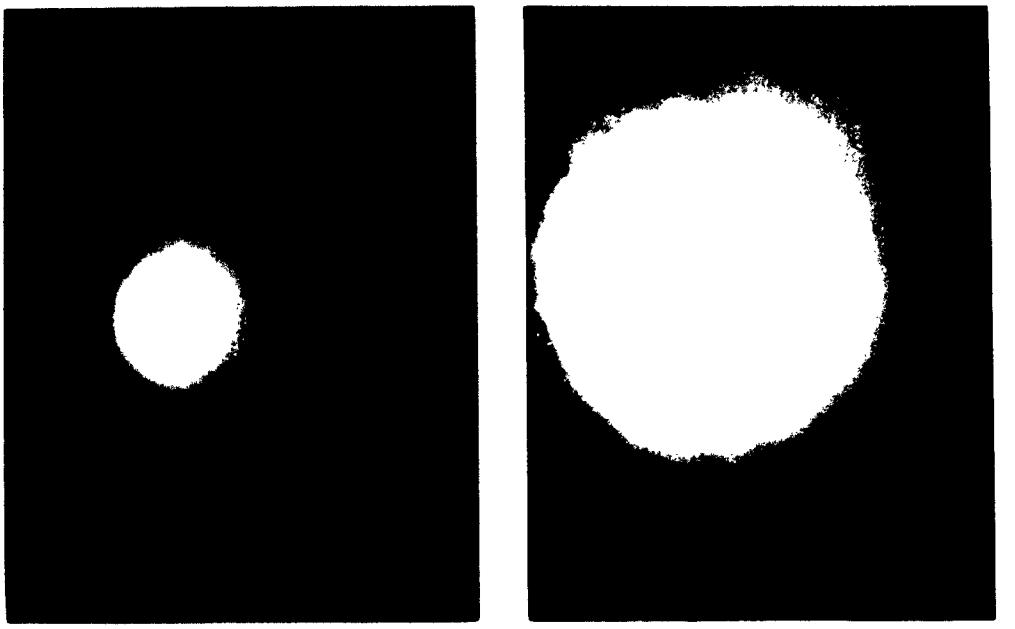

Frame 1 Frame 2

Figure 3.8 Shot 1, Film 306.

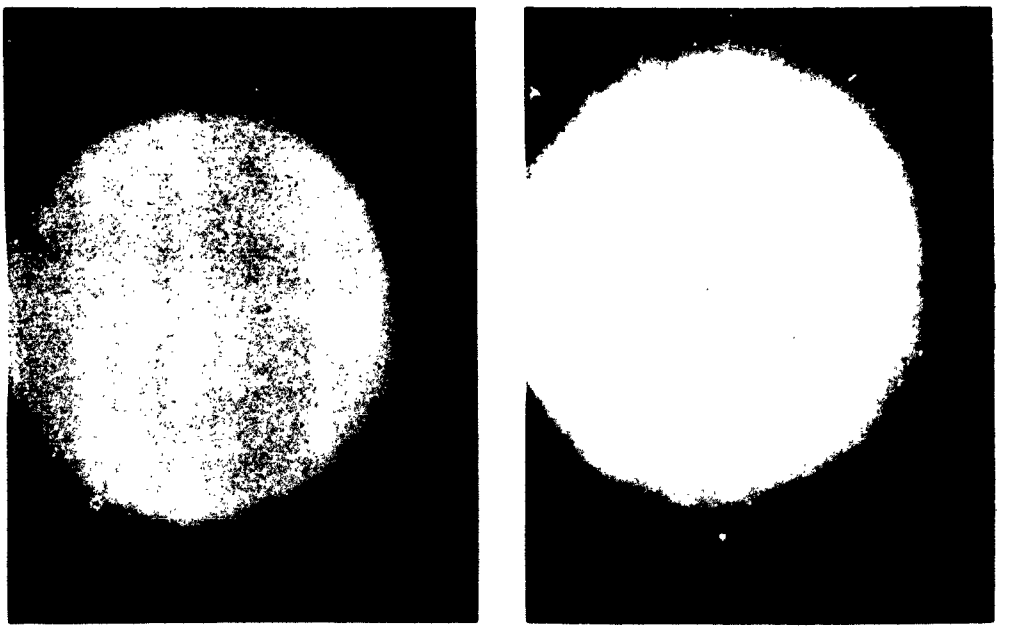

Frame 3 Frame 4

Figure 3.9 Shot 1, Film 306.

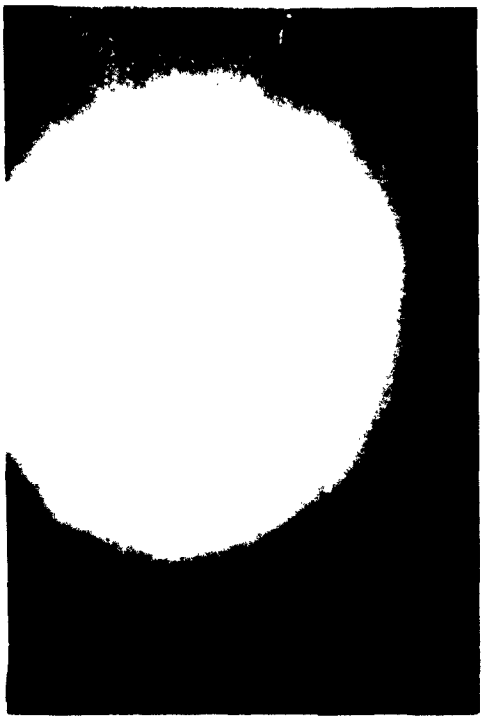

Frame 5

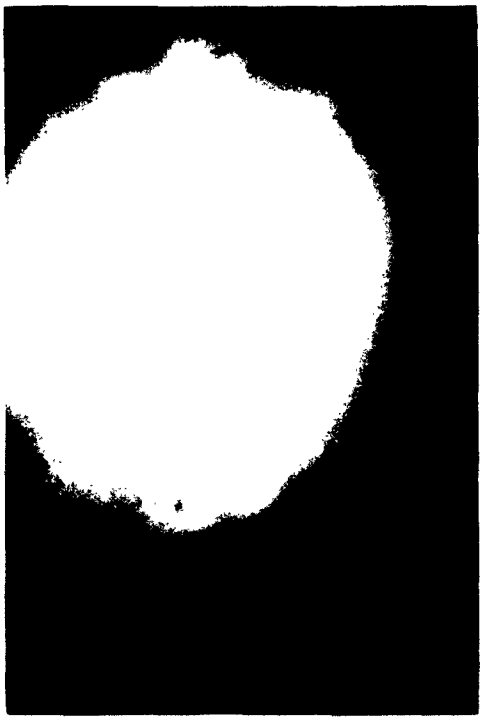

Frame 6

Figure 3.10 Shot 1, Film 306.

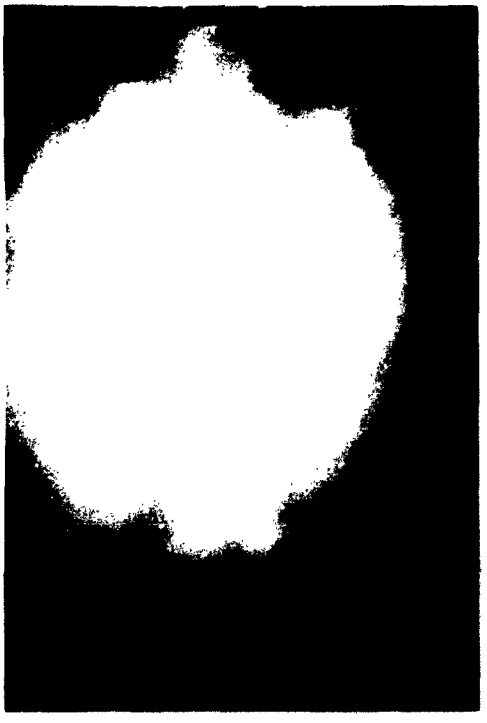

Frame 8

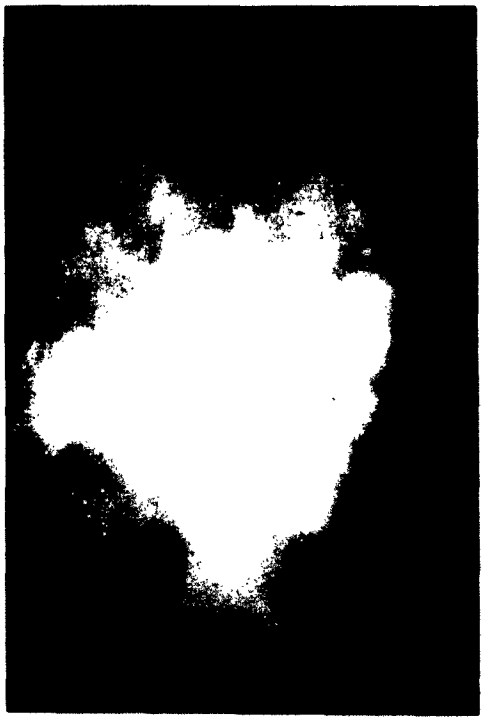

Frame 12

Figure 3.11 Shot 1, Film 306.

Frame 19

Figure 3.12 Shot 1, Film 306.

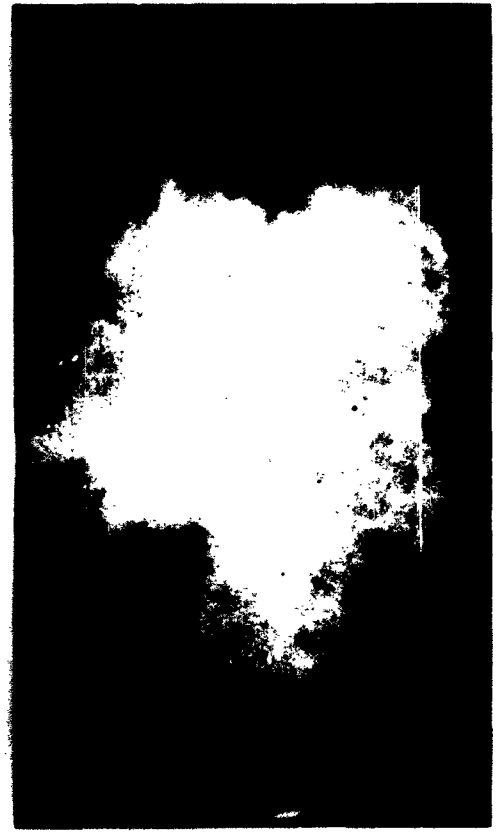

Frame 31

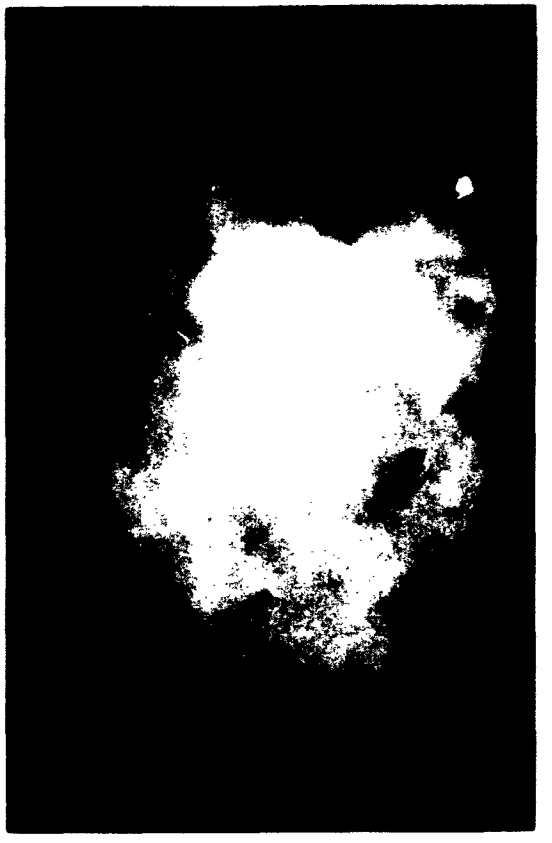

Frame 55

Figure 3.13 Shot 1, Film 306.

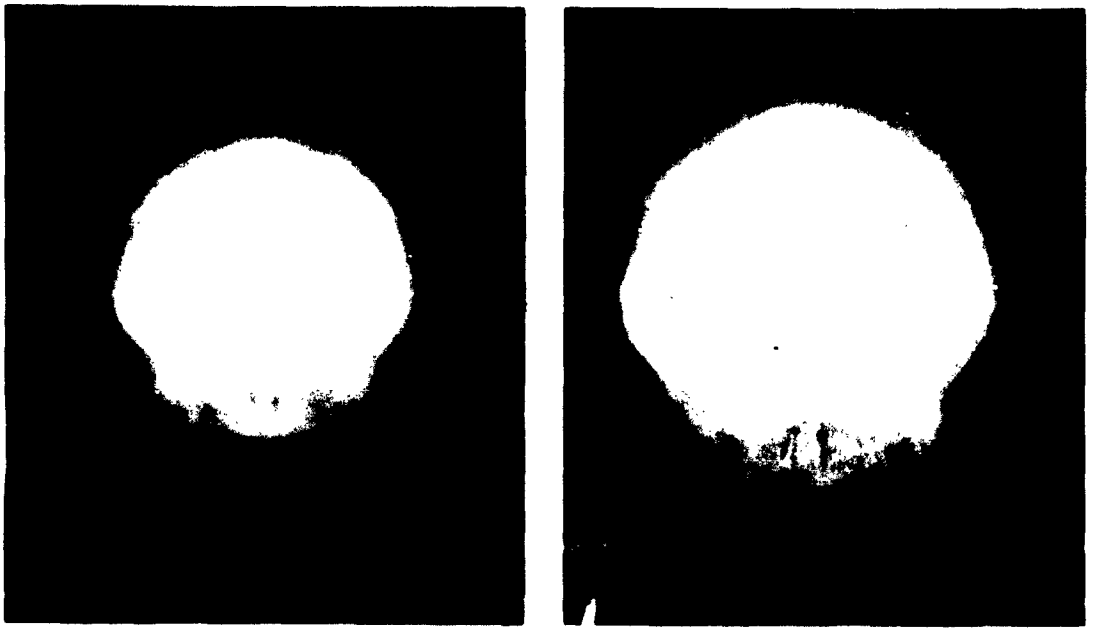

Frame 1 Frame 2

Figure 3.14 Shot 2, Film 311.

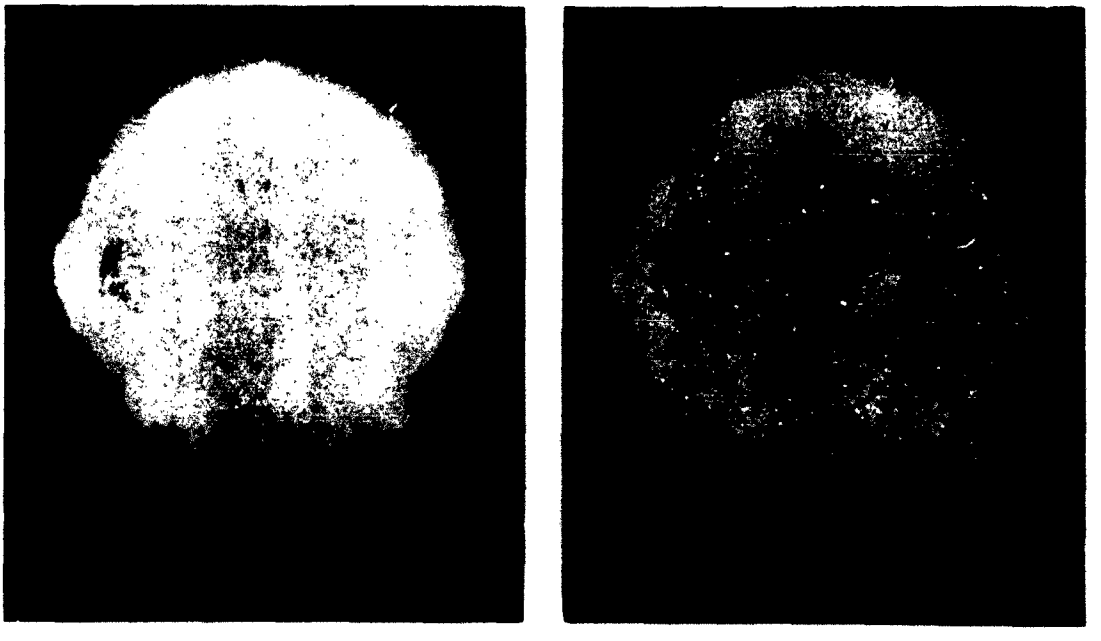

Frame 3 Frame 4

Figure 3.15 Shot 2, Film 311.

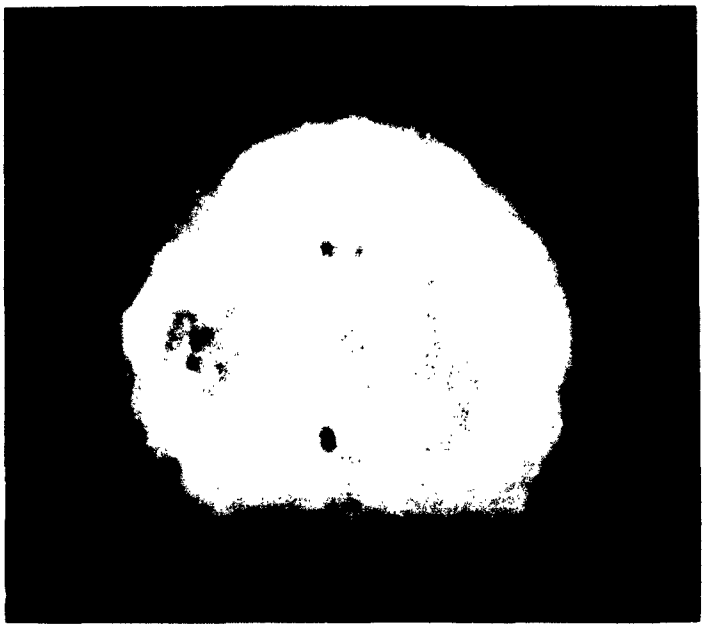

Frame 5

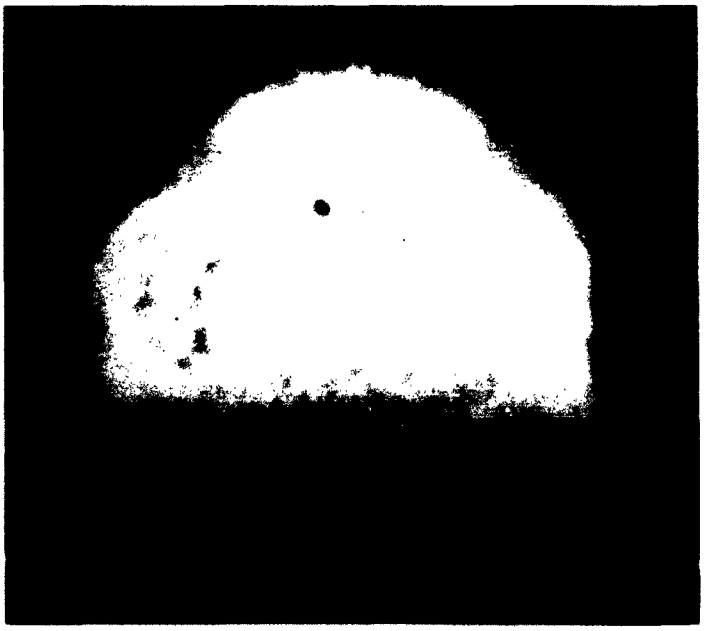

Frame 7

Figure 3.16 Shot 2, Film 311.

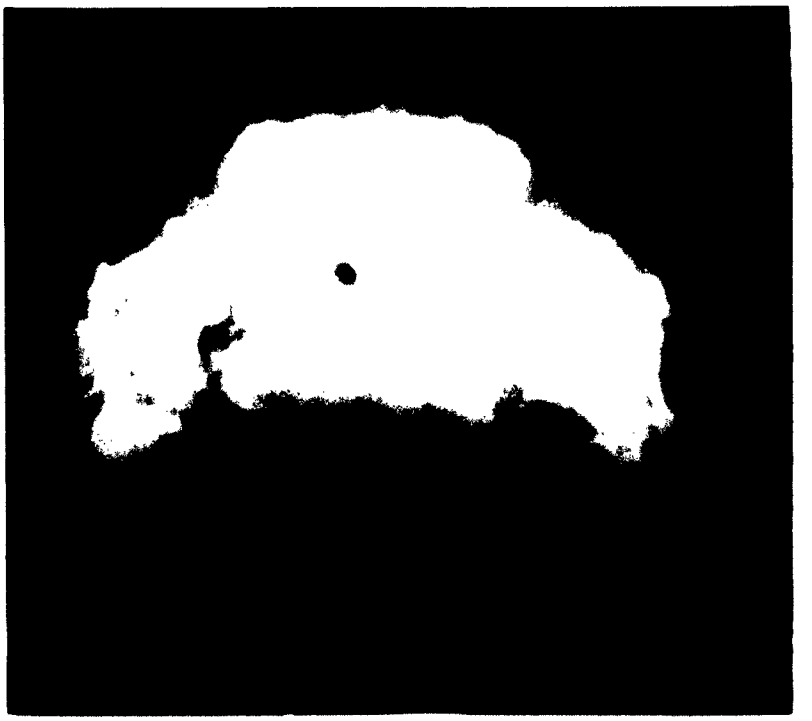

Frame 11

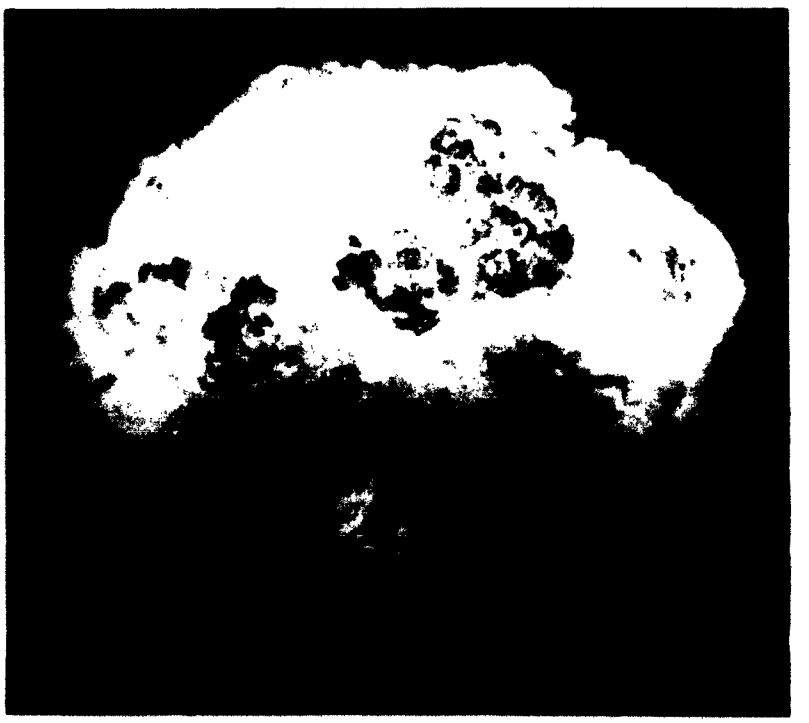

Frame 17

Figure 3.17 Shot 2, Film 311.

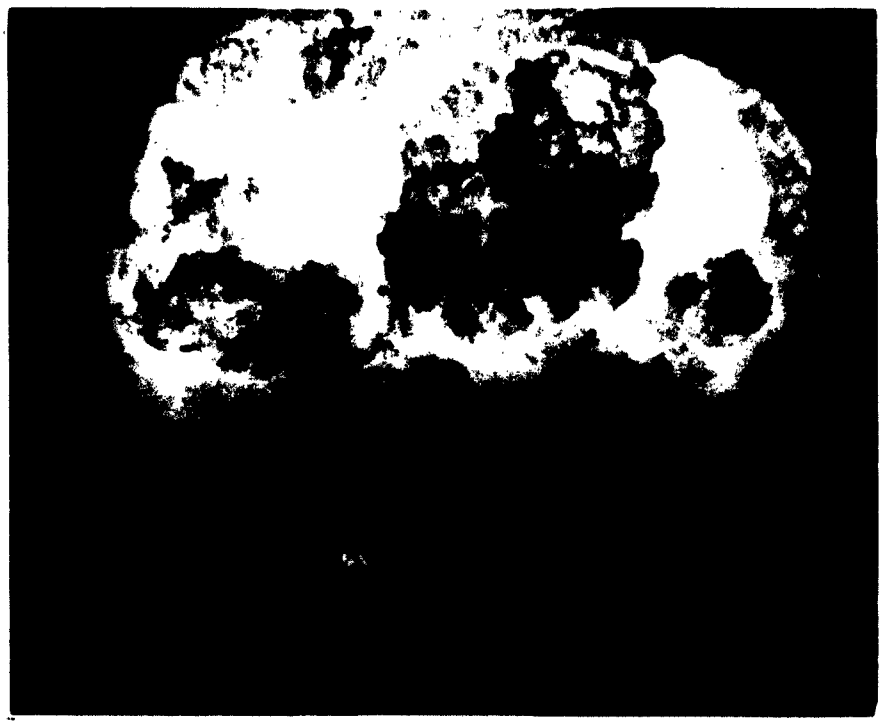

Frame 27

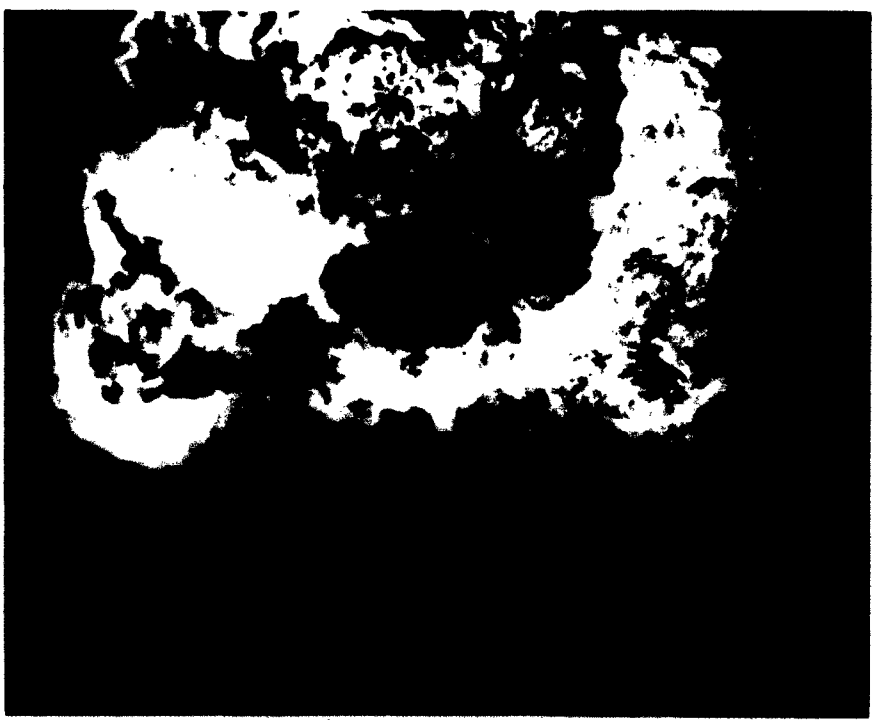

Frame 44

Figure 3.18 Shot 2, Film 311.

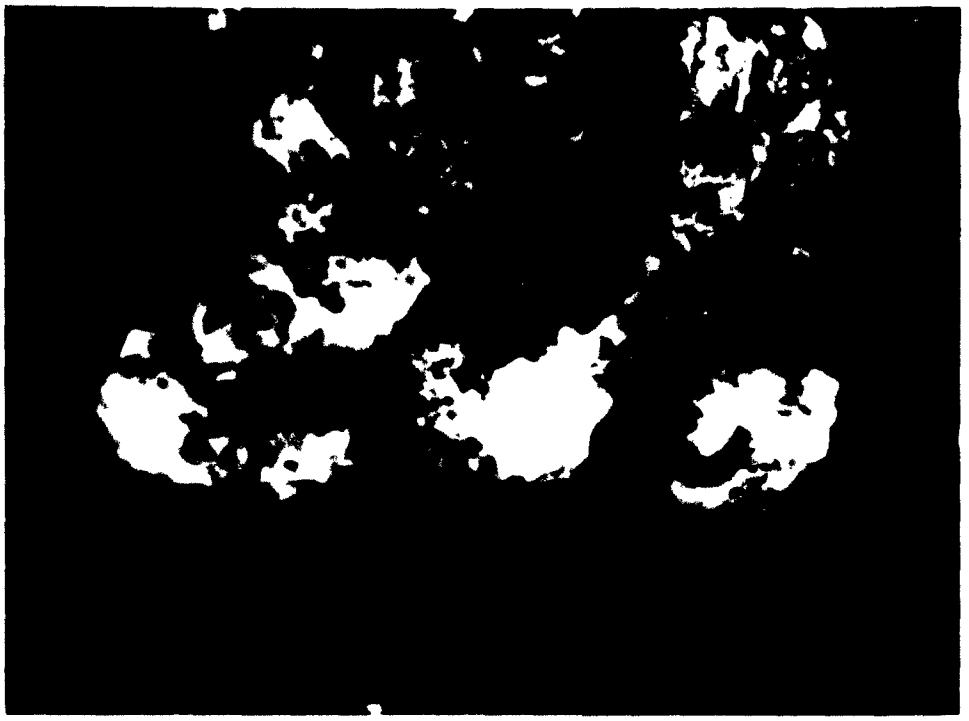

Frame 78

Figure 3.19 Shot 2, Film 311.

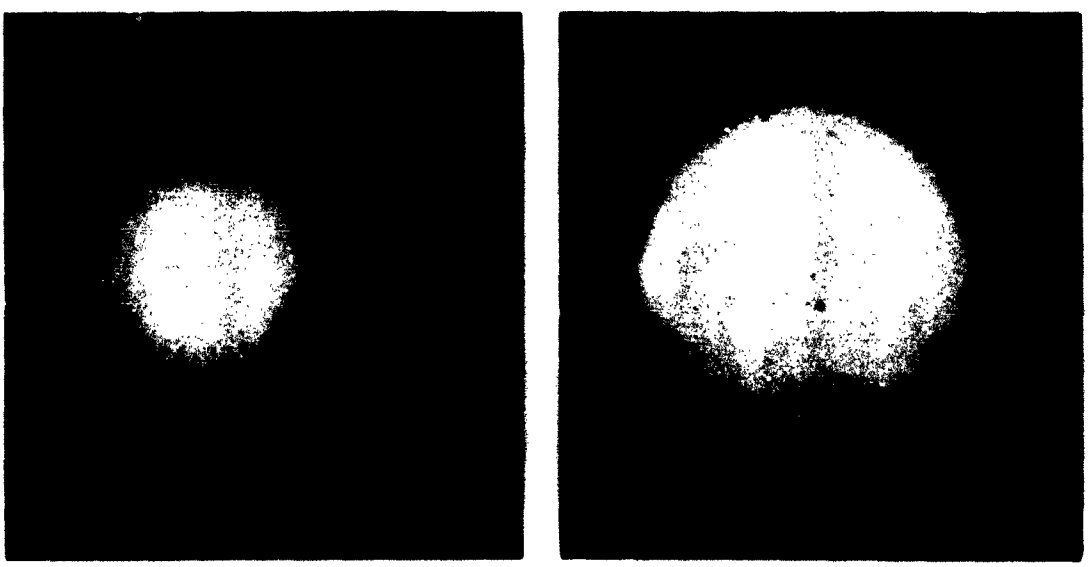

Frame 1 Frame 2

Figure 3.20 Shot 2, Film 313.

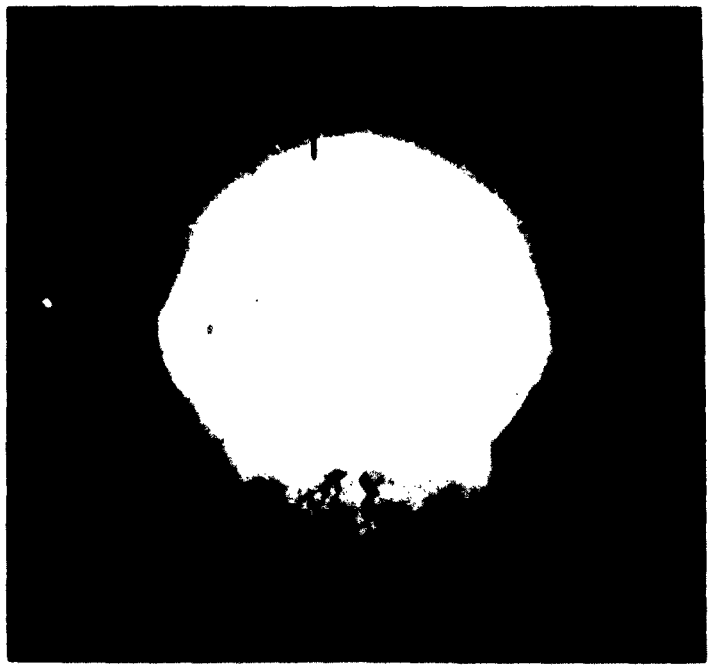

Frame 3

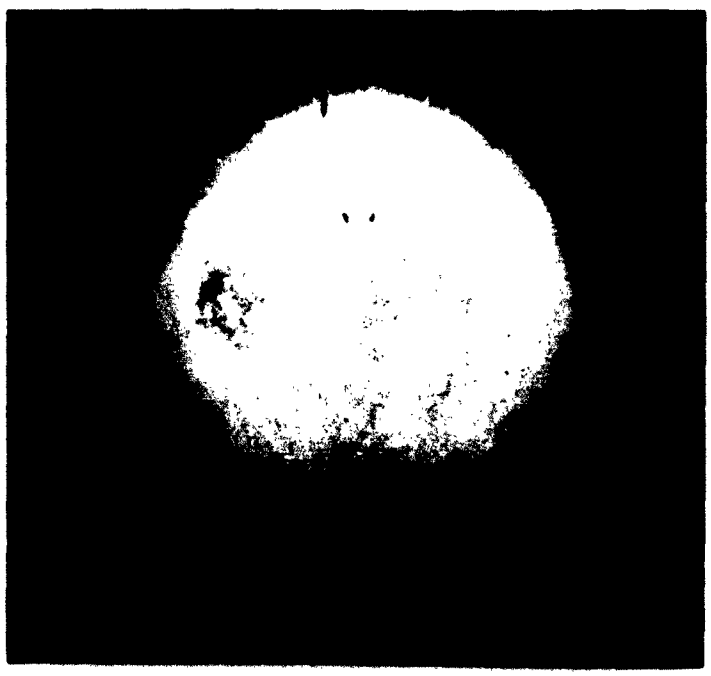

Frame 4

Figure 3.21 Shot 2, Film 313.

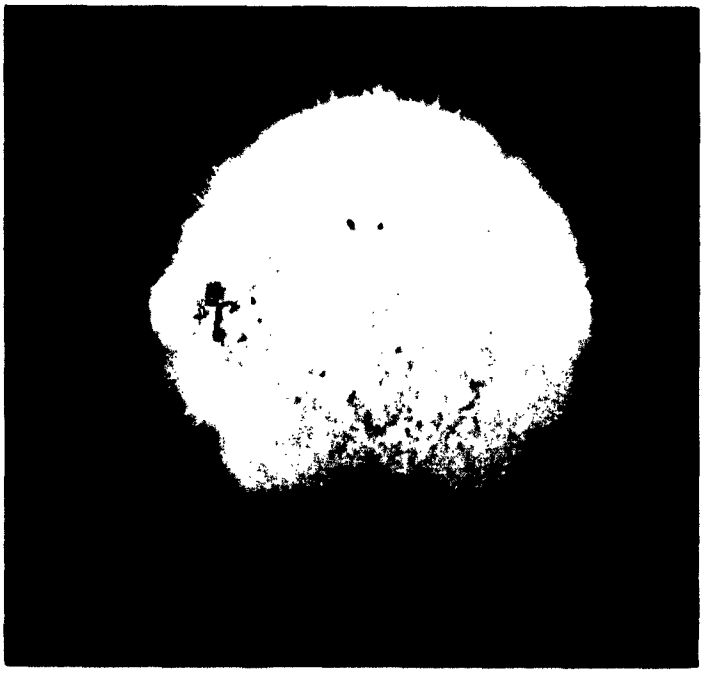

Frame 5

Frame 7

Figure 3.22 Shot 2, Film 313.

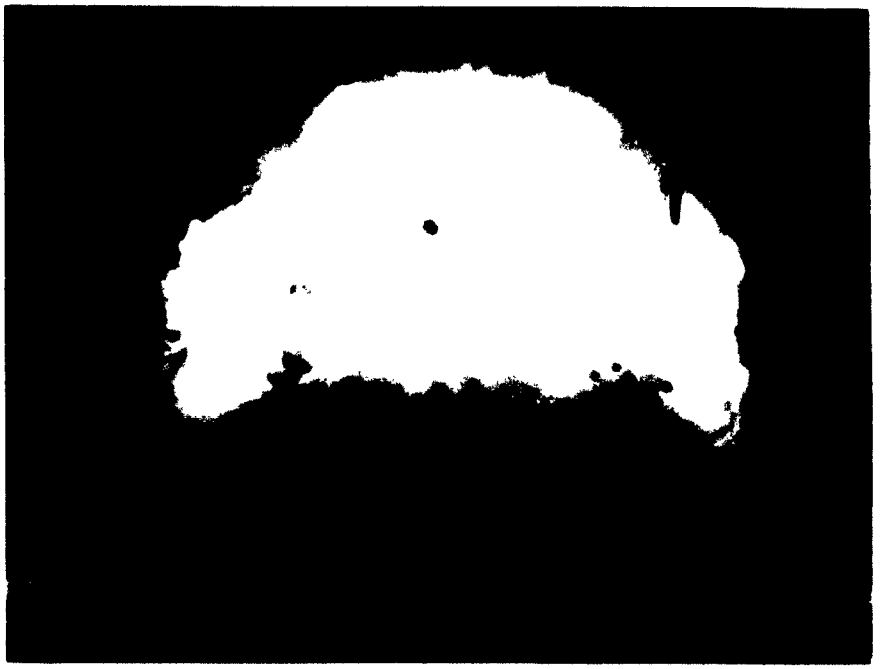

Frame 11

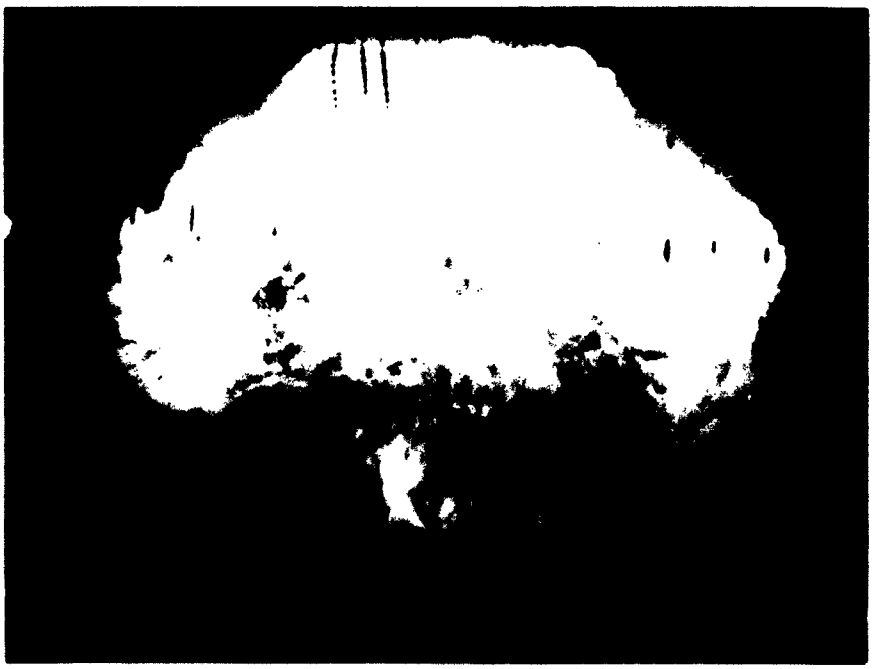

Frame 17

Figure 3.23 Shot 2, Film 313.

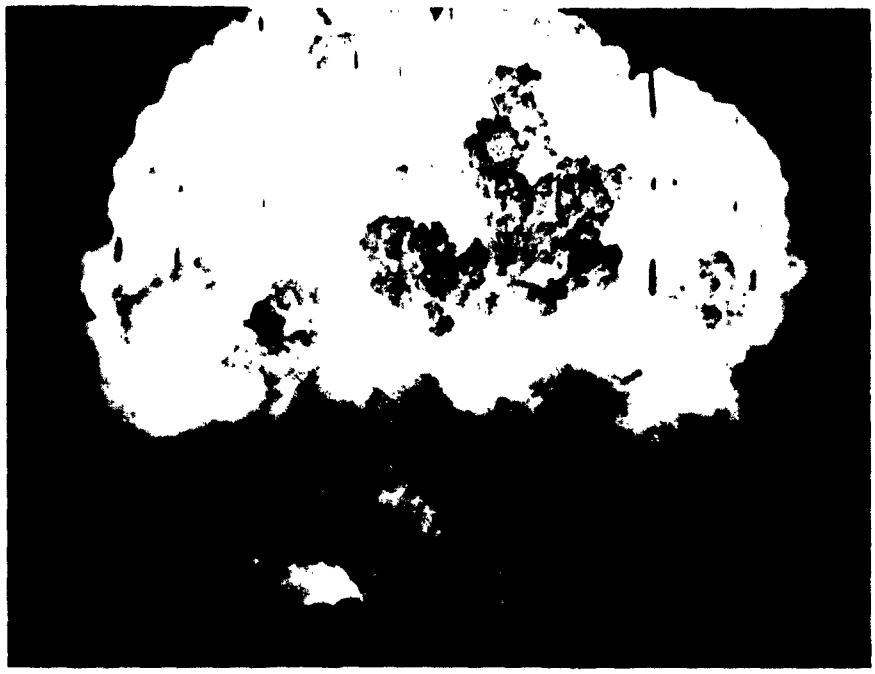

Frame 27

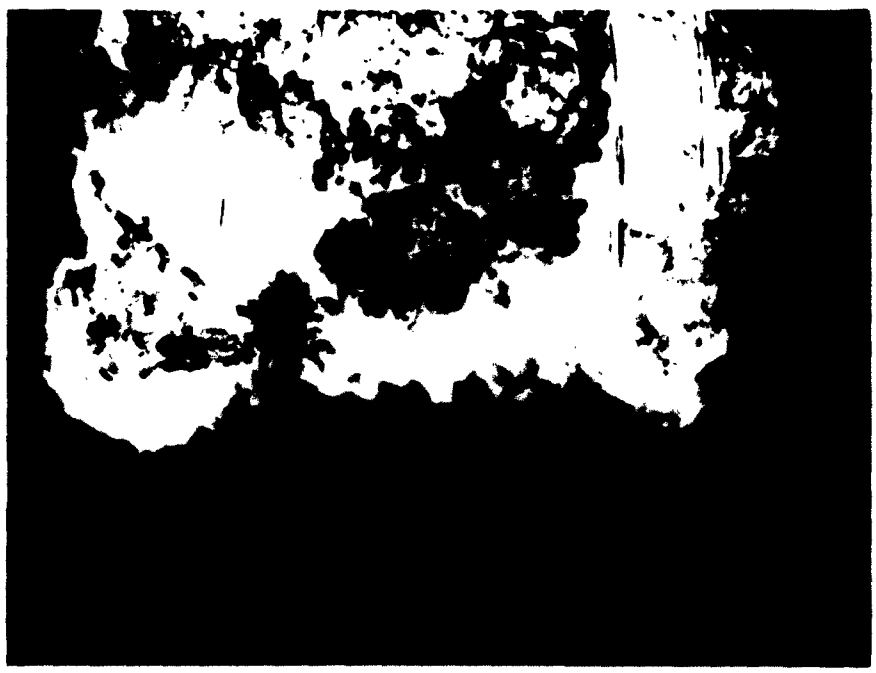

Frame 44

Figure 3.24 Shot 2, Film 313.

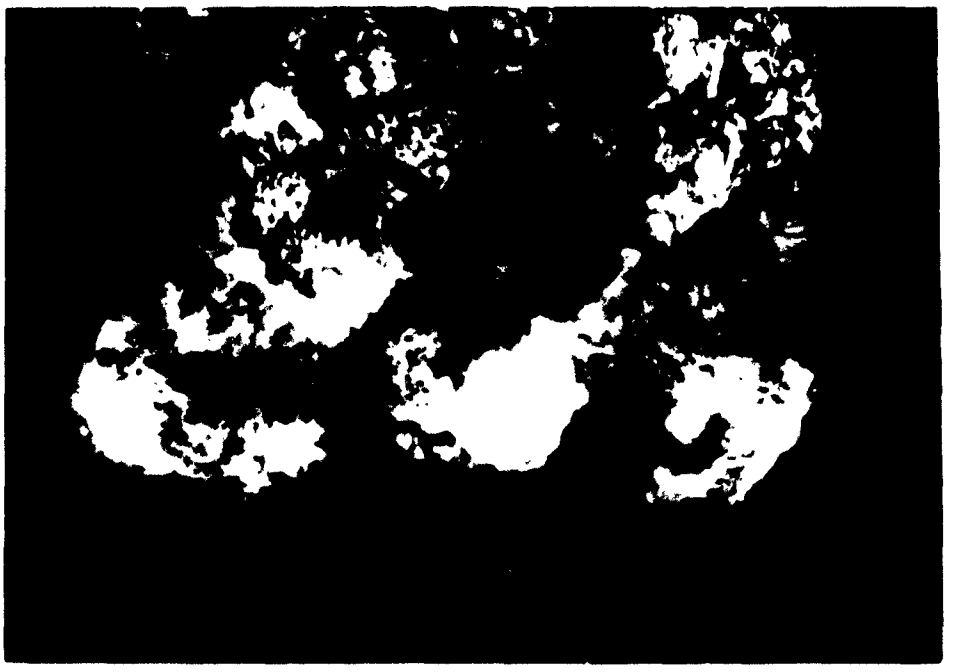

Frame 78

Figure 3.25 Shot 2, Film 313.

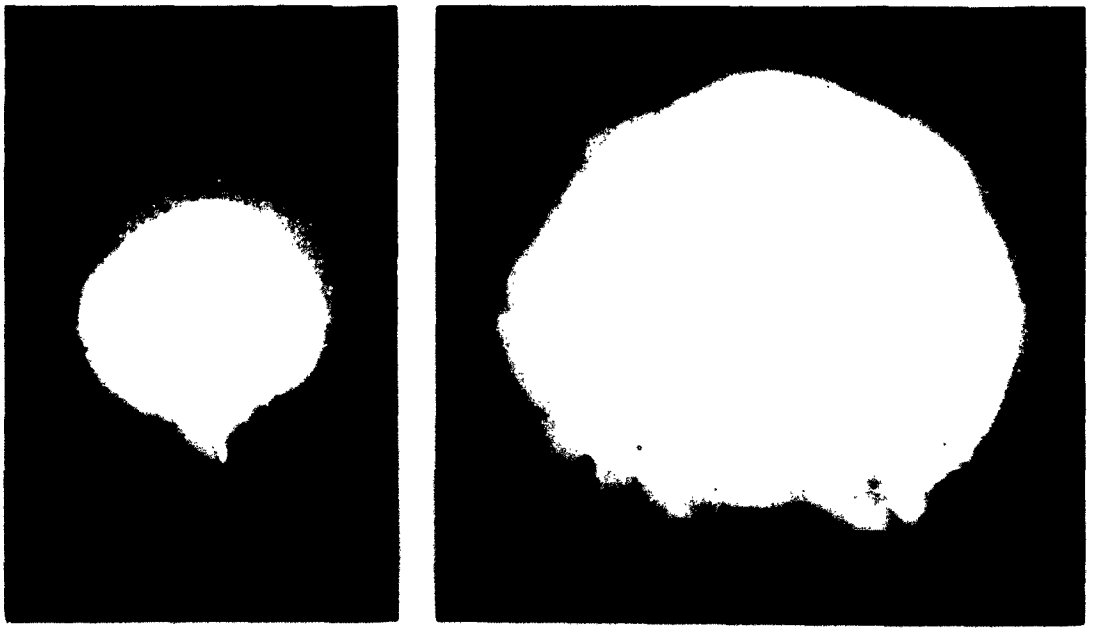

Frame 1 Frame 3

Figure 3.26 Shot 3, Film 322.

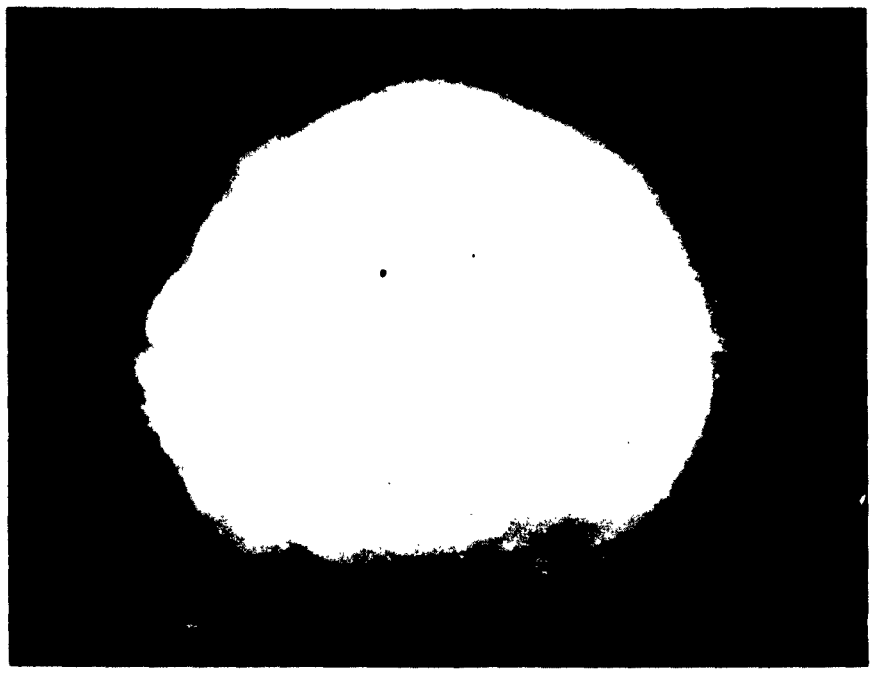

Frame 4

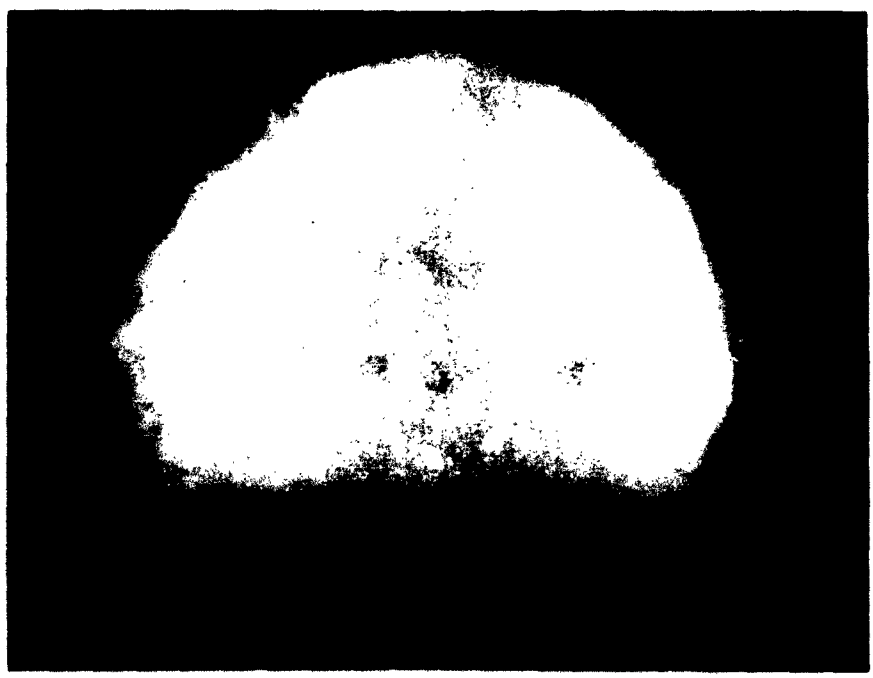

Frame 5

Figure 3.27 Shot 3, Film 322.

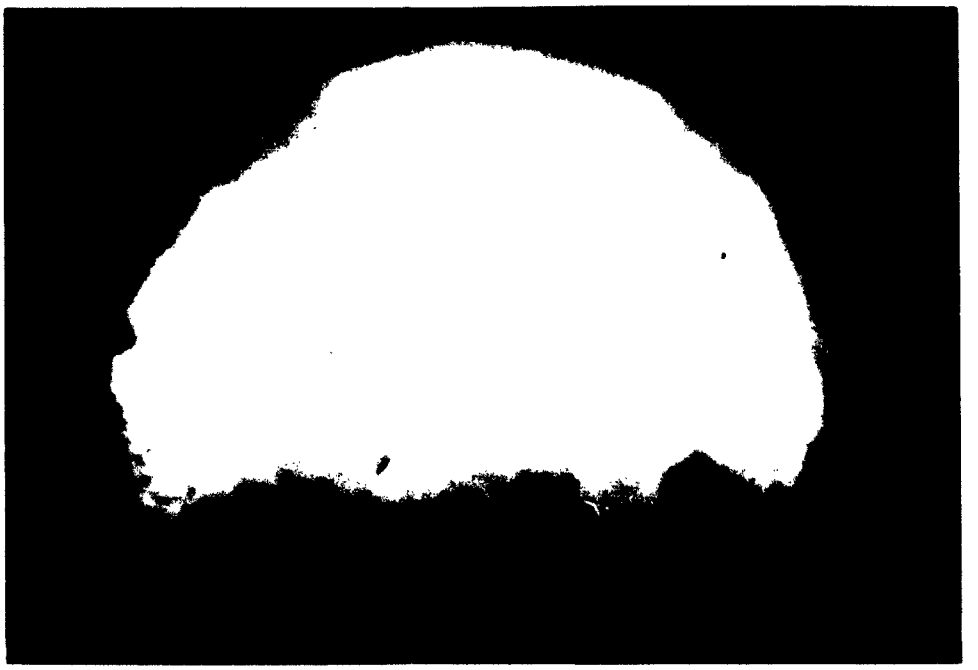

Frame 7

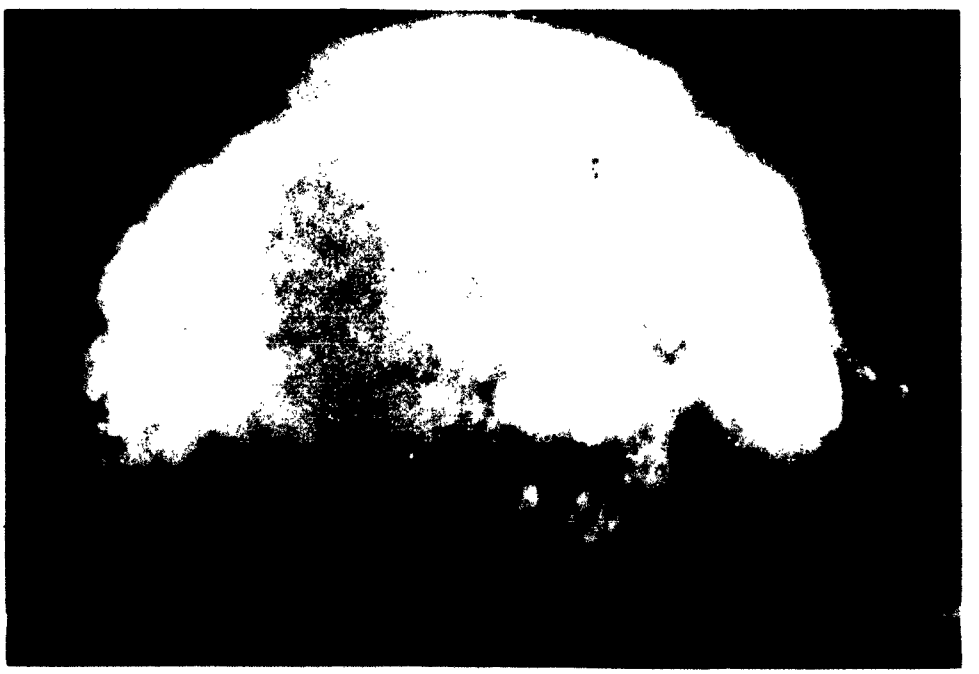

Frame 9

Figure 3.28 Shot 3, Film 322.

Frame 14

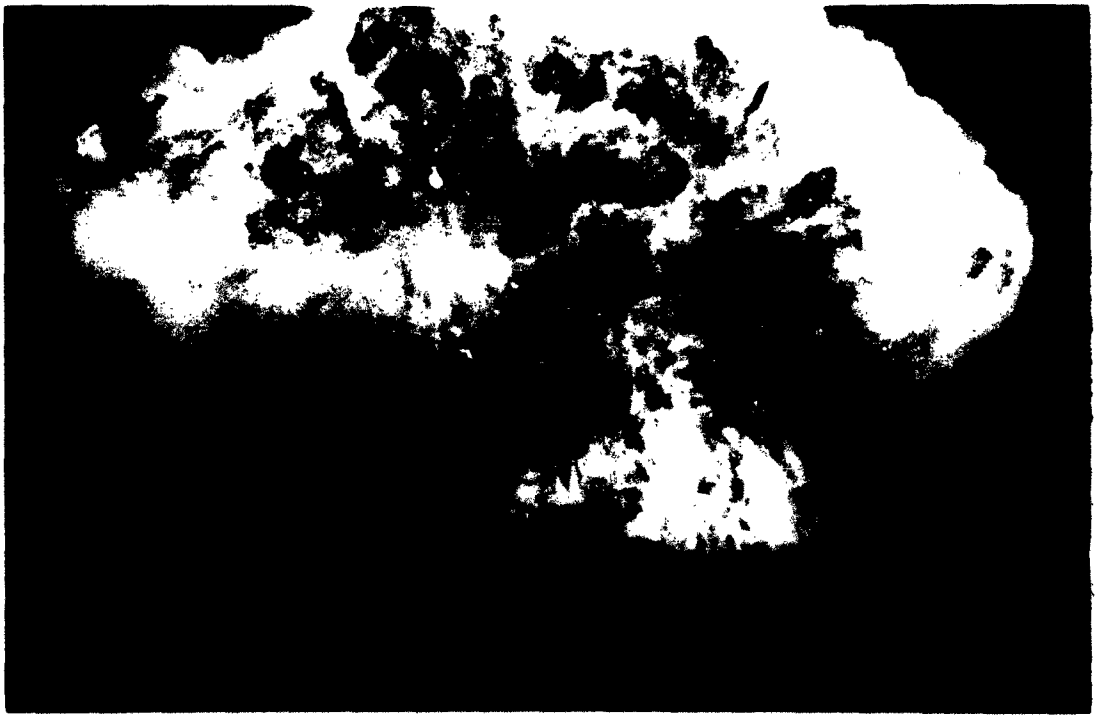

Frame 22

Figure 3.29 Shot 3, Film 322.

Frame 34

Frame 55

Figure 3.30 Shot 3, Film 322.

Frame 98

Figure 3.31 Shot 3, Film 322.

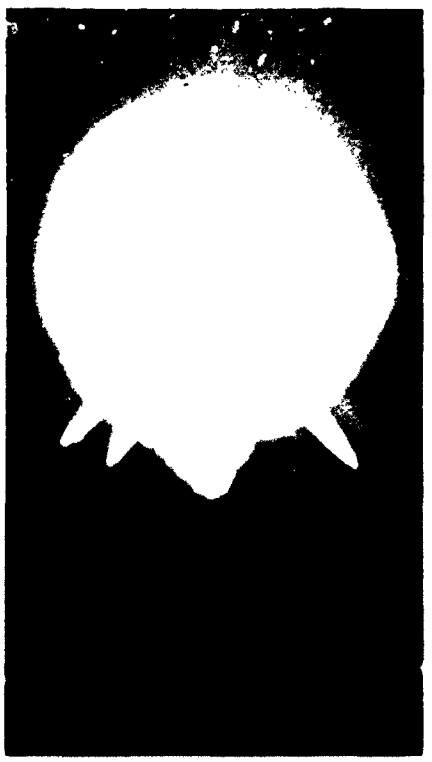

Frame 1

Frame 3

Figure 3.32 Shot 6, Film 392.

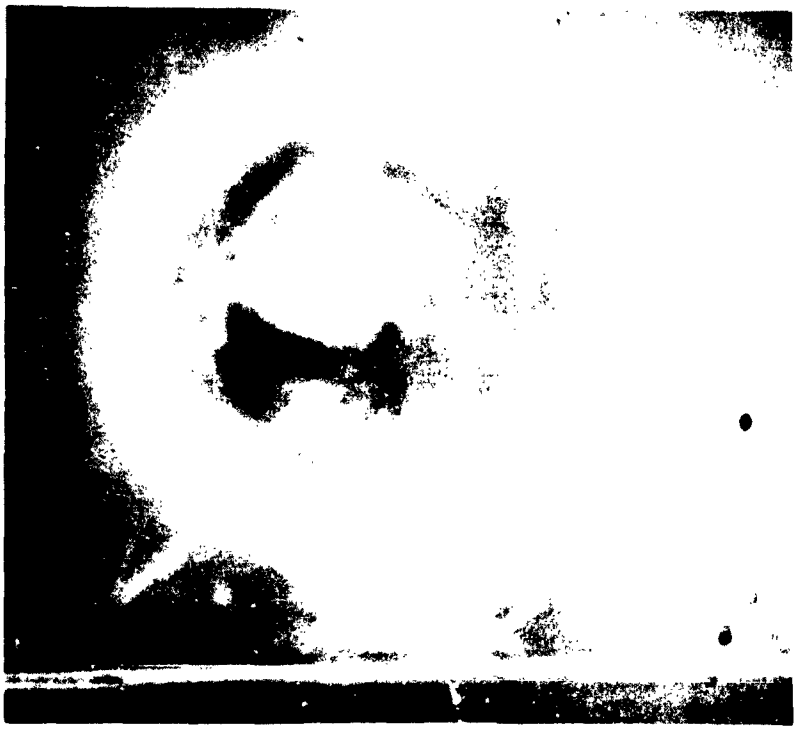

Frame 5

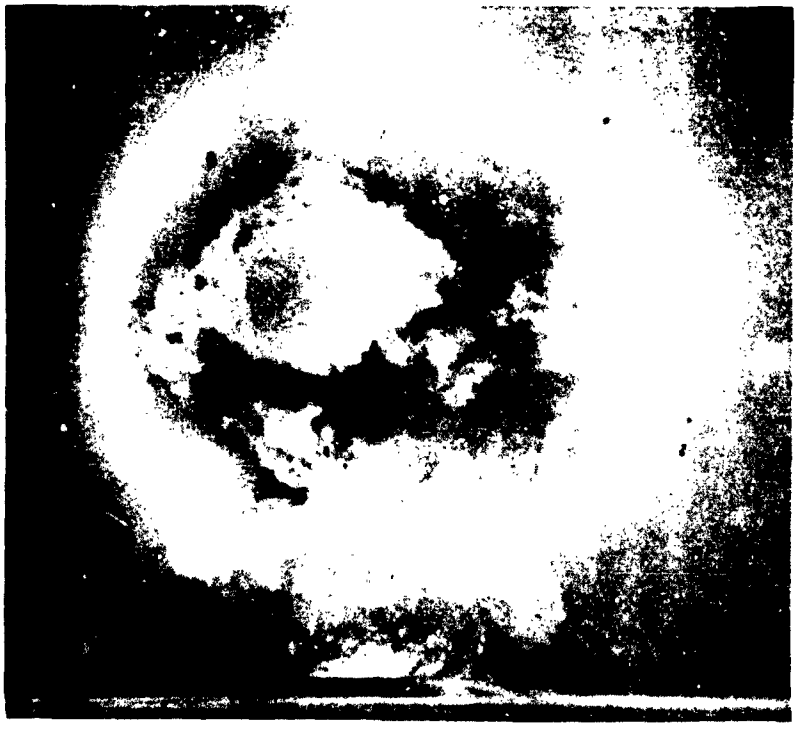

Frame 6

Figure 3.33 Shot 6, Film 392.

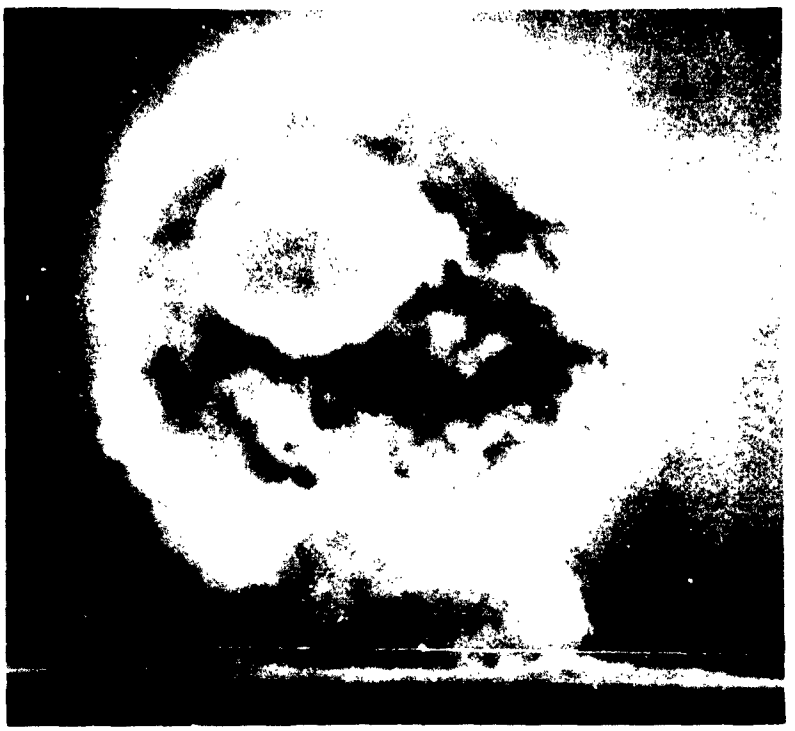

Frame 8

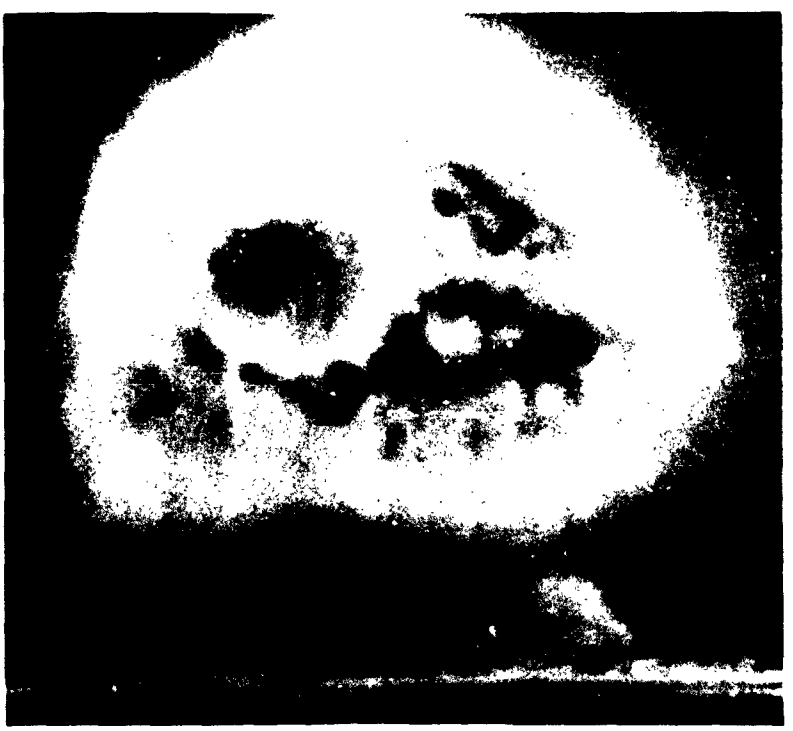

Frame 11

Figure 3.34 Shot 6, Film 392.

Frame 16

Frame 25

Figure 3.35 Shot 6, Film 392.

Frame 40

Frame 66

Figure 3.36 Shot 6, Film 392.

Frame 116

Figure 3.37 Shot 6, Film 392.

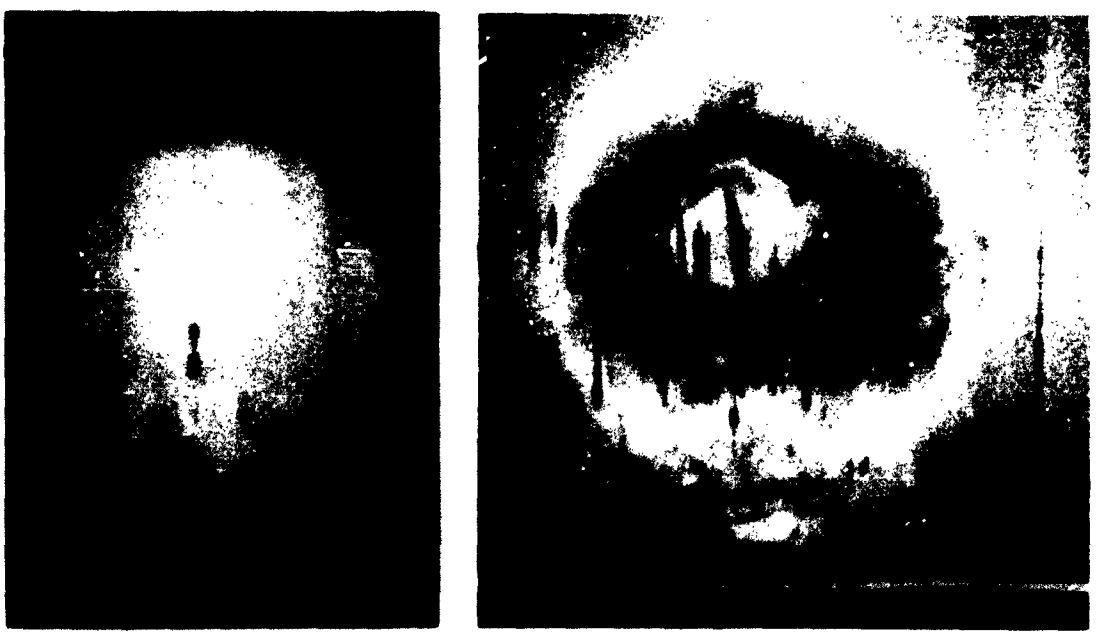

Frame 1 Frame 3

Figure 3.38 Shot 6, Film 393.

Frame 5

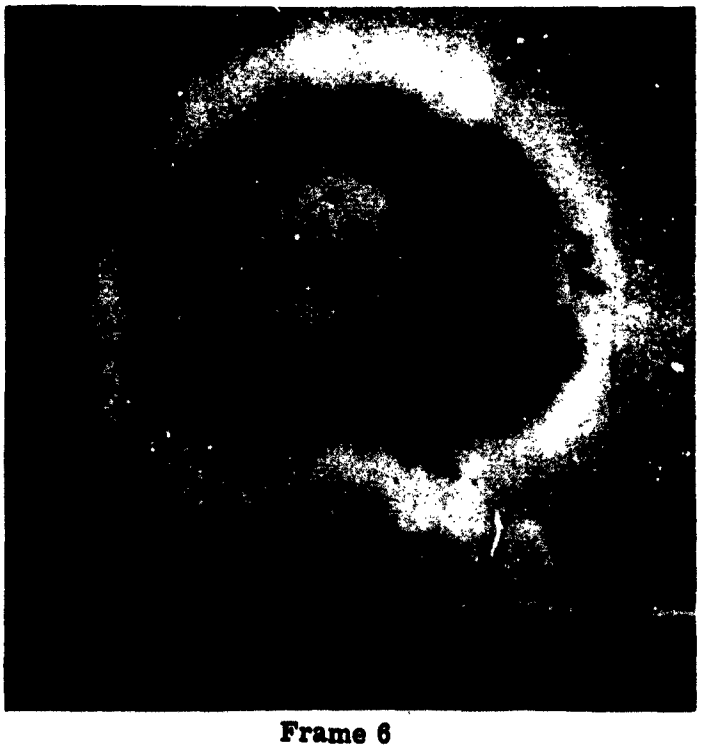

Frame 6

Figure 3.39 Shot 6, Film 393

Frame 8

Frame 11

Figure 3.40 Shot 6, Film 393.

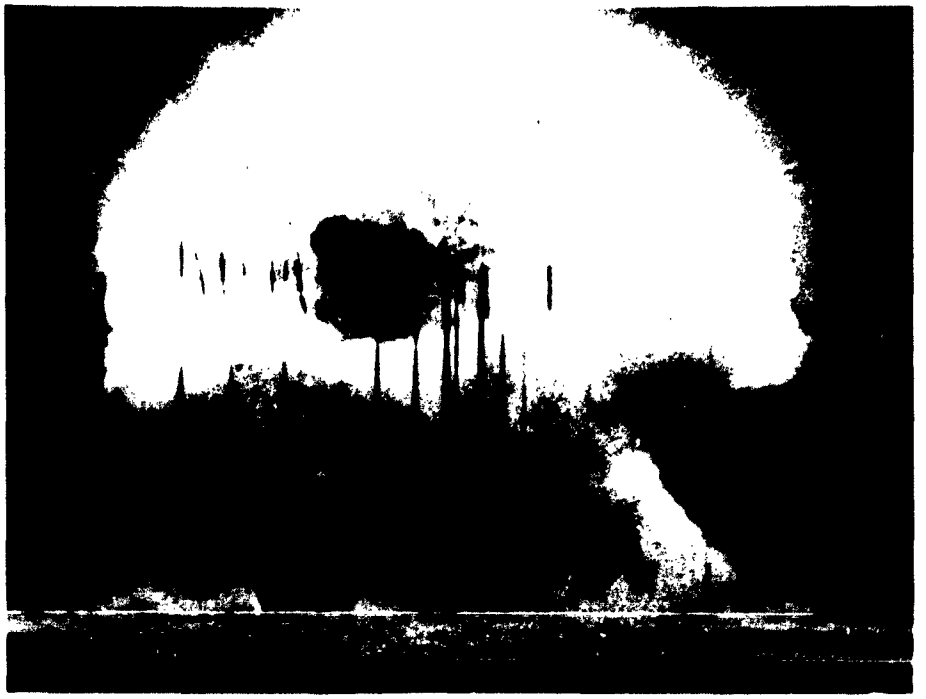

Frame 16

Frame 25

Figure 3.41 Shot 6, Film 393.

Frame 40

Frame 66

Figure 3.42 Shot 6, Film 393.

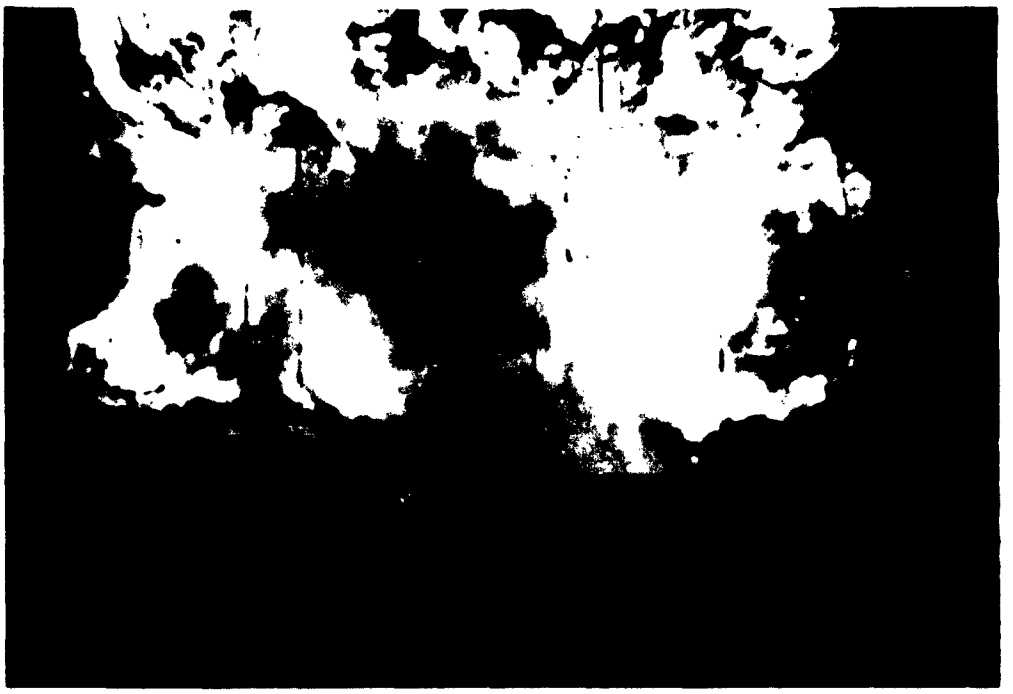

Frame 116

Figure 3.43 Shot 6, Film 393.

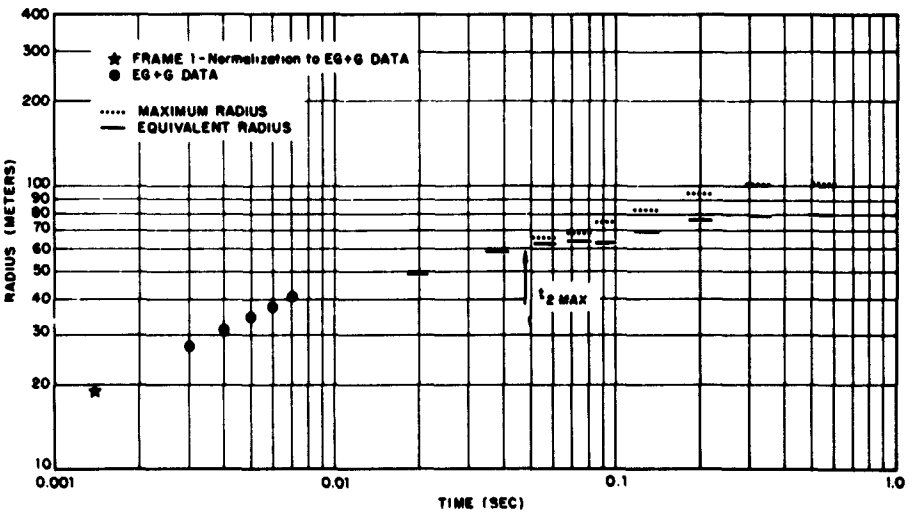

Figure 3.44 Fireball radius versus time, Shot 1.

SECRET

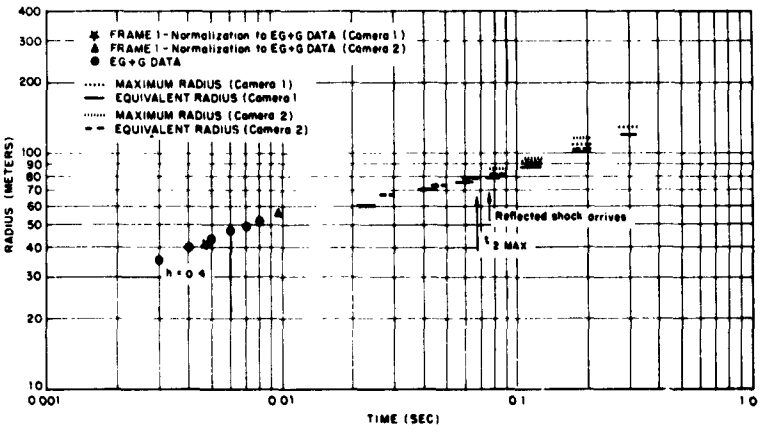

Figure 3.45 Fireball radius versus time, Shot 2.

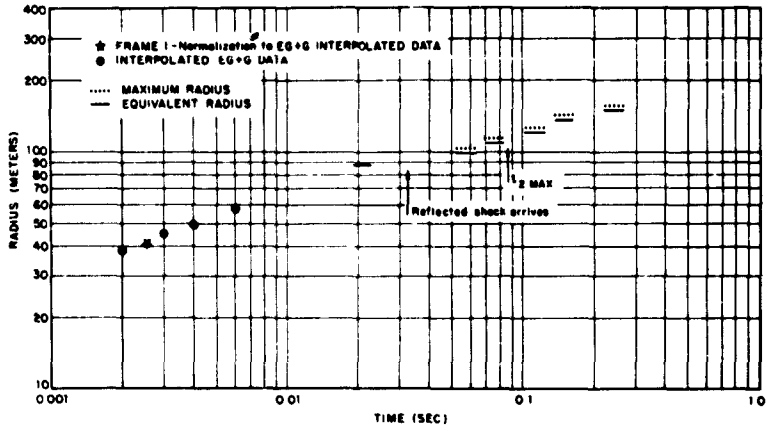

Figure 3.46 Fireball radius versus time, Shot 3.

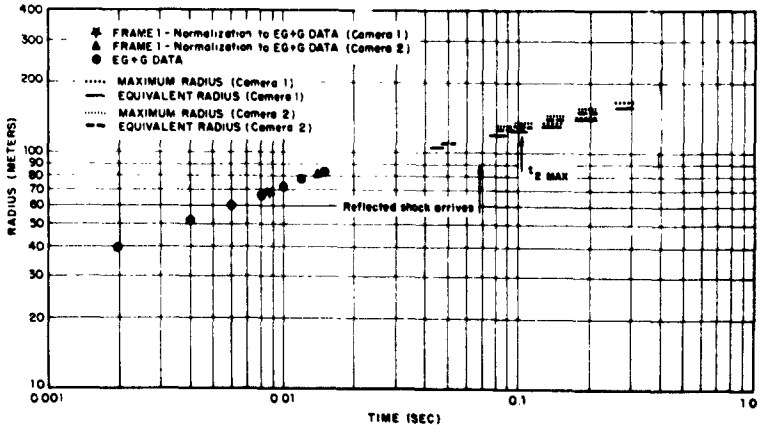

Figure 3.47 Fireball radius versus time, Shot 6.

that represents the average radius. This radius, and additional parameters, were used to determine the approximate surface or radiating area, and the approximate volume of hot material. The equivalent flat area refers to the estimated uniform cross-sectional source area of radiating source as estimated from the photographs with the aid of a planimeter. It allows for obscuration and asymmetry of the fireball. These estimates are generally not made when the areas of nonuniform radiating area exceed 20 percent of the total radiating area.

The degree of turbulence, extent of prominences, and surface details are, to some extent, a function of the photographic film, exposure, and processing. However, the values obtained are probably satisfactory to determine the gross characteristics and geometry of the fireball.

Chapter 4
DISCUSSION

The data obtained is sufficient to partially fulfill all of the objectives. The quantity and quality of data, however, is not sufficient to completely answer all the problems involved. Several trends, that seem to be apparent, cannot be definitely established on the basis of Teapot data alone, because the variation in yield of nuclear devices on which measurements were made is limited. These, and a few of the more general phenomena that can be established without doubt, will be treated later in this chapter.

The quality of data from Shot 1 is below that of the other detonations because of recorder noise. A new junction box, mounted on the recorder, had been utilized to make the field instrumentation simpler and more portable. In the rush of preparing for the field test, this new equipment was not thoroughly checked out. As a result, the records from the first shot show noise from the recorder motor. The difficulty was quite easily eliminated, once it had been discovered. The total energy data from Shot 1 was not affected, but the broad-band spectral data (which requires a high degree of precision) and the data for instruments of small fields of view (influenced by the large drop error) are of little value, since extremely accurate alignment is required.

For the air drops (Shots 1, 9, and 10) the drop error required at most 1 percent correction to the total-energy measurements and was ignored.

The data from Shots 2, 3, 5, 6, and 9 is generally very good, with a few possible exceptions caused by instrument malfunction or poor calibration. Some data was discarded when it was found to come from two particular calorimeters that gave results greatly different from several similar instruments under identical exposure conditions, the same difference being noted during several shots. In one such case, a post-mortem on the instrument revealed an intermittent connection, and in the other case the instrument failed completely during Operation Redwing.

A high percentage of the data was lost, due to failures in the recording systems for Shot 12. While it is true that difficulties were known to be of a great magnitude in using this particular type of recording system at close ranges, it was believed that these difficulties had been overcome. A trial station had been set up for Shot 4, and the system functioned perfectly at a closer distance to a higher-yield device than for Shot 12. Similarly, the measurements 1,048 feet from Shot 5 were executed without difficulty. The malfunctions on Shot 12 were of a type never before experienced and are not yet explained. For example, a particular recorder was activated properly at minus 5 seconds by the EG&G relay, that also activated two 1-minute time-delay switches (agastats) wired in parallel. The entire system was powered by two lead storage batteries, wired in parallel, the entire station being some 30 feet below the surface in a concrete shelter. The recorder ran perfectly and quit at exactly zero time. There was no visible or measurable damage to any part of the recording or timing system. Several theories involving the effects of nuclear radiation have been advanced. but none that bear repeating.

The measurements during Shot 5 under the smoke were made without difficulty, until the time of shock arrival. At least one of the calorimeter assemblies was demolished by a telephone pole that was blown outward from some location nearer to the burst. The attenuating

effects of the smoke were much in evidence and are reported in detail in Reference 6.

4.1 CALORIMETER DATA

Prior to Operation Teapot, calorimeter data had not been fully utilized and was known to contain errors in calibration and analysis that had not been rectified due to continuous utilization of available personnel in field test participation. An attempt was made during Teapot data analysis to correct the known errors and to report the data in such a manner that an attempt at theoretical calculations would be possible.

The calibration errors occurred because the instrumentation had been used under circumstances different from those for which it was designed. When thermal work began, there were no sources, measuring instruments, or standards suitable for the high irradiances and energies involved. Rather than await the outcome of a lengthy developmental program, instrumentation was developed that satisfactorily covered a narrow set of conditions, and all experiments were conducted within these limits. Laboratory and field experimentation, however, soon required the instrumentation to be used outside these limits.

Significant errors were ultimately detected, and it was found necessary to spend time studying the operation and calibration characteristics of the instrumentation in order to report data of value. This study has been completed for the Mark 6F calorimeter. An extensive investigation of the Minneapolis-Honeywell thermopile, the Mark 7F calorimeters, and Mark 6F radiometers has not been carried out, but it should be pointed out that the data taken in the field with these instruments are a matter of record and are, in themselves, relatively free from errors. The difficulties involved are in the reduction of the data and are of such a nature that they can be eliminated by laboratory investigations, and repetition of the field experiments should not be required. The methods used to obtain energy data from calorimeter records and calibration techniques are involved and are covered in detail in Reference 18.

The probable error in Teapot Mark 6F calorimeter measurements should be, in general, about ± 2 percent. But since budgets and manpower do not allow for adequate duplication of measurements, there is no sure way of assessing the actual error in an individual measurement. In addition, there are some notable exceptions and conditions to be observed. Certain of the calorimeters used during Operation Teapot were later destroyed in use during Operation Redwing or in other field uses. These instruments were calibrated prior to the instrumental study and improvement of the calibration techniques, and no method is available to obtain an accurate calibration. Measurements made with these instruments are indicated by parentheses around the type of measurement, e.g.(SP 052). The calibrations of these instruments can be deduced from cross calibration to within better than ± 10 percent. Thus, taking these exceptions into account, where data from one instrument on one shot indicate some trend different from what is observed on similar shots, this particular measurement may well be an experimental error. Where such a trend is consistently observed on several shots, it may then be worthy of notice.

Certain conditions must also be observed in applying the ± 2 percent probable error. This probable error is certainly not applicable to the total thermal energy delivered by the burst, nor for any measurements after arrival of the shock wave at the measurement station, nor when large amounts of dust have been raised between the burst point and the measurement station. Thermal measurements, integrated over the entire time of thermal emission of a burst, cannot generally be expected to have meaning, nor give consistent correlations from shot to shot. Late-time readings are also subject to greater error, since the correction for heat losses of the receiver increases with time. Errors in application of heat-loss corrections are usually negligible at times less than a second.

It is well known that many of the parameters, important in determining the characteristics of the thermal radiation from a detonation, vary considerably with time; for example, fireball size and temperatures vary over wide ranges during any particular shot. In order to specify the radiating characteristics, it is necessary to report data as a function of time, rather than the total radiation over all times. Since it would not be feasible to list values for every point

in time, some method of choosing times of interest was required. Interpolation could then be used to specify the characteristics at intermediate times. The method chosen takes into account the thermal characteristics of the detonation, the characteristics of the measuring instrumentation, the feasible means of data reduction, and the ultimate interpretation and application of the data.

Were the radiometer type of instrumentation further developed and more reliable, this technique could be applied readily. However, the integrating calorimeter type of instrumentation is further developed, and most of the available data have been taken with this type of instrumentation. The construction of the Mark 6F calorimeter, however, is such that its time response is fast enough so that differentiation of the curve of energy versus time yields the irradiance versus time. As a practical matter, the instantaneous slope of the curve for energy versus time cannot be determined, with sufficient accuracy, from the oscillographic records. Thus, a different technique was applied, yielding essentially the same results.

Instead of considering what obtains at a particular instant of time, we consider instead what obtains during each of a finite number of short, contiguous, time intervals. These intervals are chosen short enough so that the average radiating characteristics of the fireball, during any one interval, have meaning. The data-reduction problem is then to determine $\Delta Q/\Delta t$, rather than dQ/dt, which can be done with reasonable accuracy. This technique has the advantage that all of the radiation is used in arriving at the final data, rather than spaced points in time, and also that an error in reading a particular ΔQ from the oscillographic record is compensated for in the following ΔQ, since the two intervals have the same end point reading in common. Thus, for example, a low color temperature in one time interval, caused by a trace reading error, would be followed by a high color temperature in the following time interval. Smoothing of the final results then presents a consistent picture of the variation of color temperature with time.

Preliminary examination of the data, fireball photography, and the ultimate application of the data, suggested that time intervals be chosen in such a fashion that each contained 10 percent of the total energy as integrated over all time. Several difficulties immediately arose, however, because the characteristics of the fireball change many orders of magnitude during the delivery of the first few percent of the energy and because the boundary of the last time interval (t equals infinity) is difficult to locate. The intervals were then shifted to consider eleven intervals, the first and last containing 5 percent of the energy and all others containing 10 percent. This had the added feature that the time to second maximum, which occurs after delivery of about 20 percent of the energy, is now nicely bracketed by the 15-to-25 percent time interval, so that the characteristics at the second maximum may easily be deduced from the data.

Since radiation phenomena have been found to scale in terms of the time to second maximum, standard time intervals were chosen and expressed in terms of this time. This technique allows direct comparison between different detonations without extensive manipulation of the reported data. An additional adjustment of the time intervals was made to enable easier correlation of data for experimenters who have been using ten times the time to second maximum as a time limit to the second pulse.

The end points of the time intervals used in reporting the calorimeter data are given in Table 4.1 and Figure 4.1. These values were selected, in the manner prescribed above, from rough data from this and previous operations and then rounded to even numbers for convenience. The reported data for energy versus time is then given at each of these times in Tables 3.1 through 3.8. The data on Shot 10 are given for the scaled times of both Shots 9 and 10 in Table 3.9. The entries in Tables 3.1 through 3.8 are given to as much as four significant figures, even though the probable error does not seem to warrant this. This was done because most applications of the data require further calculations to be performed to obtain the final information. In all calculations based on this data, the final answer should be rounded to three significant figures. The probable error in the calorimeter data is ± 2 percent, except for the entries after shock arrival, or one trace reading unit, whichever is the larger. The magnitude of one reading unit (1 RU) is given below each column in Tables 3.1 through 3.8. The applicca-

TABLE 4.1 BOUNDARIES OF TIME INTERVALS USED IN REDUCTION OF CALORIMETER DATA

Interval	Time
	units of t_2 max
I	0 to 0.5
II	0.5 to 0.9
III	0.9 to 1.1
IV	1.1 to 1.4
V	1.4 to 1.8
VI	1.8 to 2.6
VII	2.6 to 4.0
VIII	4.0 to 6.0
IX	6.0 to 10.0
X	10.0 to 16.0
XI	16.0 to 30.0
XII	30.0 to ∞

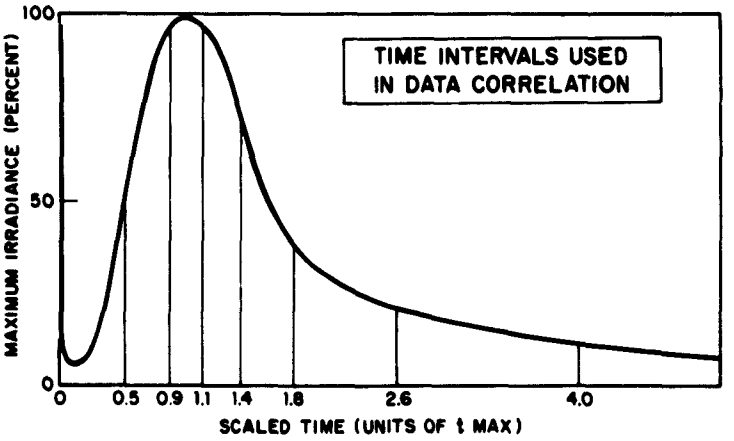

Figure 4.1 Time intervals used in data correlation.

tion of standard calorimeter data is discussed in the sections that follow, which include discussions of thermal yield, color and power temperatures, and atmospheric attenuation.

4.2 THERMAL YIELD

The calorimeter data, given in Chapter 3, can be used to give a fairly accurate estimate of the total amount of thermal energy radiated in each detonation. This computation has been performed in an approximate manner in previous reports (References 1 and 4) for the special case of the true air burst. The method that was used in these computations is not generally applicable to all bursts and contains errors that can become significant. While a precise determination of the total thermal radiant output is neither feasible nor possible, usable values may be obtained by making approximate corrections for such factors as asymmetrical geometry, atmospheric transmission, filter transmission, and obscuration. This process is discussed in detail in Reference 18.

The geometrical problem is essentially one of computing the total output of the fireball in all directions from a single measurement made from some distant point. Such a computation can be approximated as long as the fireball is well defined and the obscuration is held to within reasonable limits. When the fireball is well defined, the energy at any point on a sphere concentric with the fireball and including the measuring instrument in its surface can be assumed proportional to the projected area of the fireball as seen from that point. Integration over the sphere and normalization based on the single measured value yields the total energy that would arrive on the entire sphere were the fireball and the sphere isolated in a vacuum. By correcting the single measured value for atmospheric and filter transmission and obscuration, to obtain the energy that would be incident at the single point were it in a vacuum, the total thermal energy radiated, for one time, may be computed. This entire process must be carried out as a function of time, and the results summed to obtain a quantity called the calorimetric thermal yield.

The geometrical correction cannot be made for all times during which the bomb is radiating, i.e., it can only be made when the projected area of the fireball has been measured or can be computed for every point on the integrating sphere. Lacking complete photographic coverage, the correction can be made only when the fireball may be approximated by one, or a series, of regular geometrical figures. This can usually be done for up until the time that two thirds of the energy is radiated. At about that time, the fireball becomes turbulent and mixes with the surrounding air. When this happens, the geometrical correction can be made only to within limits of about ± 25 percent. But since only about a third of the energy is involved, the thermal yield can be computed to about ± 8 percent, which is adequate for most purposes.

The methods for handling atmospheric and filter corrections are straightforward, but also involve some approximations. Both of these corrections require the spectral distribution of the radiation to be known. If this is the case, the total transmission, ϕ, at any one time, can be computed based on the following type of formulation (Reference 18):

$$\phi = \frac{\int_\lambda J_\lambda F_\lambda f_\lambda \, d\lambda}{\int_\lambda J_\lambda \, d\lambda} \tag{4.1}$$

Where: J_λ = the spectral intensity of the source at wave length λ

F_λ = the transmission of the atmosphere at wave length λ (Section 4.6)

f_λ = the transmission of the filter at wave length λ (Figure 4.2)

If the spectral distribution is not known, the correction cannot be made with a workable degree of accuracy. For example, in a typical measurement of the energy incident at a station, a calorimeter having a quartz filter might measure 100 cal/cm^2. Of this energy, about 0.5 cal/cm^2 can be shown to be between 2,000 and 3,500 Å. The filter transmission is uniform

with wave length in this region and presents no problem. The atmospheric transmission in this spectral region can vary by a factor of ten or more with wave length, but more significant, it is nearly zero for the distance of interest. Thus in correcting the 0.5 cal/cm^2 to get the source intensity, a quantity that is difficult to determine accurately must be divided by a

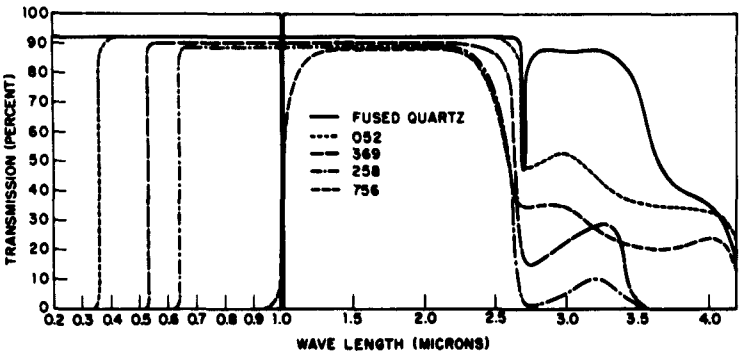

Figure 4.2 Transmission of filters.

number approaching zero. Very small errors in the measurement or correction can thus lead to enormous uncertainties in thermal yield.

Similar difficulties arise at other regions of the spectrum, if the spectral distribution of the source is not known, when atmospheric absorption bands or filter cutoffs make the transmission nonuniform with wave length. Thus, even if it were possible to determine the energy arriving at the station in broad bands by differencing the readings of the calorimeters having different color filters, these values could not be corrected to obtain the source output. This together with the geometrical corrections, are the heart of the data analysis problem and the reasons why other instrumentation has been recommended for any future thermal measurements that may be made at field tests.

To make the corrections for atmospheric and filter attenuations, it is necessary to assume a spectral distribution and test to see if it is capable of predicting all of the observed results, which are of many varieties and are measured under many differing conditions. In assuming a spectral distribution, we have placed the requirement that at least 80 percent of the radiated energy arrives at the detecting element of the calorimeter, so that the correction is then no more than 20 percent and the error in the corrected value considerably smaller.

The details of the selection of a spectral distribution are treated in Reference 18. The important point is that if any reasonable spectral distribution is assumed and if correction is made for atmospheric attenuation, the thermal-yield values obtained are significantly higher than those obtained in previous calculations (References 1 and 4). An indication of how this increase takes place is given in Section 4.5.

The correction for "obscuration" is more than a correction for opaque bodies absorbing radiation that would otherwise have arrived at the calorimeter. It includes correction for reflections from clouds, the earth's surface, etc. The correction is made by use of a photograph, representing the time of interest, taken by a camera immediately adjacent to the calorimeter and aimed in the same direction. The boundaries of the fireball are first sketched in and the total area of uniformly bright fireball area determined. Obscurations are then handled as perturbations by adding and subtracting areas weighted in accord with their apparent brightness on the photograph.

Were the film a nonselective receiver, it could be densitometered and an accurate correction obtained. Since this is not the case, we limit the cases that can be analyzed to those in which the total obscured area is 20 percent or less of the total fireball area. The error in the corrected value is then much smaller than 20 percent and gives a usable result. The hot stem on tower shots, for example, is treated as an obscuration. Sufficient pictorial data was included

in Chapter 3 so that the reader may verify the merits of this technique.

Thermal-yield data for Shots 1, 2, 3, 6, and 9 are given in Table 4.2. Shot 5 was excluded, because of lack of photographic data. Shot 9 was included, even without photographic data, since it was a true air burst for which the geometrical and obscuration considerations are less critical than for tower or surface bursts. Thermal-yield data for each shot were computed for each standard time interval.

Certain of the values listed in Table 4.2 are followed by footnotes. This indicates that the fireball geometry was not well defined during the time interval and that the geometrical correction is thus uncertain. This geometrical correction arises because the fireball may radiate more in some directions than in others. A sphere, for example, would tend to radiate uniformly in all directions, whereas a hemisphere of horizontal base would tend to radiate more toward the zenith than toward the horizontal. The most-extreme geometrical correction leads to an increase of about 50 percent in the total thermal energy, as compared with a spherical fireball. The correction approaches this magnitude for tower shots, measured from the plane of their

TABLE 4.2 THERMAL YIELD

Time Interval		Thermal Energy Radiated During Time Interval 10^{10} cal/cm^2						
Time Interval	Scaled Time	Shot 1 Station 220	Shot 2 Station 8.4b-1	Shot 3 Station 8.4b-2	Shot 6 Station 220	Shot 6 Station 221	Shot 9* Station 220	Shot 9* Station 221
I	0 to 0.5	1.11	3.54	7.53	7.31	7.56	3.90	3.98
II	0.5 to 0.9	4.86	7.11	15.6	21.7	20.9	15.6	16.0
III	0.9 to 1.1	4.18	4.45	9.61	14.7	14.3	10.1	10.5
IV	1.1 to 1.4	5.25	6.15	14.1	21.0	21.6	13.6	13.7
V	1.4 to 1.8	5.83	8.06	18.0	26.6	26.2	12.8	13.2
VI	1.8 to 2.6	6.14	13.2	31.0	36.2	36.5	12.1	12.6
VII	2.6 to 4.0	5.26	18.8	45.9	41.0	40.6	12.4	12.5
VIII	4.0 to 6.0	5.58†	12.4	26.5†	31.6†	32.3†	10.3†	10.3†
IX	6.0 to 10.0	5.26†	10.3†	28.0†	31.8†	34.3†	11.2†	11.5†
X	10.0 to 16.0	4.86†	7.24†	17.4†	27.2†	29.7†	9.66†	9.71†
XI	16.0 to 30.0	6.27†	6.25	13.8†	27.8†	29.5†	16.0†	15.4†
XII	30.0 to ∞	15.44†	6.94	20.2†	22.4†	24.9†	30.7†	31.4†
Total Thermal Yield, kt		0.70	1.04	2.50	3.09	3.18	1.58	1.61
Total Yield, kt		1.16	2.39	6.85	7.76	7.76	3.16	3.16
Thermal Partition, percent		60	44	36	40	41	50	51

* Spherical fireball shape assumed in the absence of photographic data.
† Indicates that fireball is no longer well-defined and that geometrical correction is thus uncertain. See text for further explanation.

of their horizontal base, where their fireballs become hemispherical due to the reflected shock wave. At very late times, where the convective pattern has been set up, the fireball tends to lose all definition and again approach a nondirectional radiating pattern, which requires no geometrical correction. Thus, for tower bursts, the correction is about 1.5 entering Time Interval VIII, and is about 1.0 at Time Interval XII. Rather than attempt an estimate of how this correction would vary with time, a standard geometrical correction of 1.25 was used on all tower bursts after the fireball became undefined. Since about a third of the energy is radiated during this time, and the correction uncertain by ± 20 percent, the net error due to geometrical corrections is probably less than ± 10 percent over the whole radiating life of the fireball.

For the small air bursts well away from the ground (Shots 1, 9, and 10), the distribution of radiated energy was assumed symmetrical. This assumption probably does not hold when the convective pattern has been established and the familiar doughnut shape is in evidence. Thus, the ± 10 percent uncertainty in geometrical correction can be applied to all shots.

Additional uncertainties arise in the processes of making transmission corrections, so that the values for total thermal yield and partition listed in Table 4.2 are probably uncertain by about ± 15 percent.

It will be noted that the thermal yields are significantly higher than previously quoted values

(References 1 and 4) and the W/3 scaling law. The general increase is primarily due to better techniques in handling atmospheric transmission and filter transmission. These corrections, however, if ignored, would still not allow the data to even approach the W/3 scaling law, since the uncorrected values for Shots 1 and 9 (and Tumbler-Snapper Shots 1 and 2) are above 40 percent. Further, if independent determinations of blast (27 percent) and nuclear (15 percent) partitions are considered, a thermal partition approaching 60 percent is not unreasonable for a 1-kt air burst.

The thermal yield for Shot 10 is discussed in Section 4.11.

4.3 BROAD-BAND SPECTRAL DISTRIBUTION

A subtractive technique may be applied to the data of Tables 3.1 through 3.8 in order to find an approximate spectral distribution of the energy arriving at the measuring station. For example, subtracting the readings for any time interval of calorimeters having Corning 3-69 and 2-58 filters would yield the approximate energy between 0.53 and 0.64 microns. This method is only approximate, since the filter transmissions differ in more than one region of the spectrum. In the example given, the difference in readings also includes about 15 percent of the energy between 2.7 and 3.4 microns. In practice, atmospheric transmission and probable spectral distribution considerations allow this subtractive technique to yield results that are satisfactory for most effects experiments. Corrections should also be applied for filter-reflectance losses, if absolute energies are desired.

The results obtained by this technique differ for each shot and each distance. A preferable description of the spectral distribution is given in Section 4.8 in terms of color temperature of the radiation at the source. Application of the atmospheric transmission techniques of Section 4.5 then allows computation of the spectral distribution for any desired location.

4.4 IRRADIANCE VERSUS TIME

Curves for irradiance versus time are given in Figures 3.1 through 3.6. The radiometers used are useful in determining the general shape of the pulse at each station. There are some uncertainties in calibration factors, time response, and late-time drift associated with these instruments that would require a fairly extensive theoretical and experimental study for their complete resolution. Corrections for filter transmission and atmospheric transmission would then have to be applied, as for the calorimeter data, in order to determine the output of the source. The final data so obtained would be little improved over the calorimeter data given below and thus does not merit the cost and manpower required. The radiometer pulse shapes given should be more than adequate for effects work.

The average total thermal emission of the fireball during each time interval may be obtained by dividing the corrected energy values of Table 4.2 by the length of the corresponding time intervals. The results of this calculation are given in Table 4.3. This data was in turn normalized to the total yield of each shot and is plotted in Figure 4.3 as a function of time interval. The values for interval I are considerably less accurate than those for the other intervals, because of the small amount of energy involved and the rapidly changing conditions of geometry and transmission. Three features can be noted from Figure 4.3. Firstly, the peak irradiance decreases as the yield increases. Secondly, the air-burst pulse shape is distinctly different from the tower-burst pulse shape, being much higher and sharper. And thirdly, the pulse shape of Shot 3, where lead and paraffin were employed and the scaled height was lower, is even lower and broader than the other tower shots. These same effects may also be observed by careful study of Figures 3.1 through 3.6.

An interesting feature, observed on all shots except Shot 3, is the time dependence of the amount of energy being lost by the fireball after about twice the time to second maximum. Extrapolation of this slope backwards in time to 3×10^{-7} seconds results in a peak temperature of between 10^6 and 10^7 K. It is also interesting to note that the rate of loss of energy by electromagnetic radiation following the time of this high temperature has nearly the same time

dependence as is here observed at extremely late times. This time dependence is not evident in late-time data that has not been corrected for atmospheric and filter transmissions, which have appreciable effects at these times.

4.5 ATMOSPHERIC ATTENUATION

The experiments conducted in connection with atmospheric attenuation were of two basic types: (1) scattered energy versus field of view and distance and (2) total energy versus wave length and distance.

The scattering experiments were designed to determine the scattered energy as a function

TABLE 4.3 AVERAGE TOTAL THERMAL EMISSION VERSUS TIME, kt/sec

Time Interval	Shot 1 Station 220*	Shot 2 Station 8.4b-1	Shot 3 Station 8.4b-2	Shot 6 Station 220	Shot 6 Station 221	Shot 9 Station 220	Shot 9 Station 221
I	0.46	1.04	1.75	1.43	1.48	1.05	1.07
II	2.56	2.63	4.58	5.43	5.22	5.39	5.51
III	4.18	3.18	5.65	7.36	7.14	7.24	7.50
IV	3.75	3.08	5.63	6.98	7.19	6.19	6.25
V	3.07	2.98	5.28	6.50	6.38	4.36	4.56
VI	1.57	2.40	4.55	4.47	4.50	2.05	2.08
VII	0.78	1.98	3.85	2.90	2.87	1.22	1.23
VIII	0.58	0.91	—	—	—	0.70	0.70
IX	0.27	—	—	—	—	0.38	0.39
X	0.17	—	—	—	—	0.22	0.22
XI	0.09	—	—	—	—	0.16	0.15
XII	—	—	—	—	—	—	—

* Station indicates origin of basic calorimeter data used in computation.

of the angle from the line of sight between the measuring instrument and the source by the use of calorimeters having successively larger fields of view. This type of experiment is not suited to bomb measurements, and the probability of success in Nevada is less than negligible for the following reasons:

1. The Nevada atmosphere is not highly scattering and requires a long path length to attain appreciable scattering. The calorimeters require a short path length to obtain measurable energy.
2. Nearly all the energy is in the direct beam, so that a measurement of the scattered energy requires instrumental precision not available with calorimetric techniques.
3. The majority of the energy is scattered at angles less than the angular width of the fireball. Thus scattered energy from one part of the source cannot be distinguished from direct energy from another part of the source.
4. The scattering is a function of the wave length of the radiation. The measured value would be the sum of the scattering contribution from all wave lengths, with the amount of energy at each wave length changing with time.
5. The sensitivity of the calorimeters decreases with increasing angle, becoming zero at 90 degrees off axis.

Thus, were the instrumental precision great enough to give reliable values, the problems of geometry, spectral distribution, and small amount of scattered energy would make analysis of the data next to impossible and the final results of little value.

The problems were further complicated by difficulties in the fabrication of quartz domes for the 180-degree-field-of-view instruments. Although the sample domes were of high quality, the production models had noticeable lens effects that negated the measurements. The difference in energy that would be seen by 90-degree and 180-degree instruments is only about

2 percent. The lens effect caused errors as high as 20 percent.

If we start with a theoretical approach, using the best approximation for spectral distribution, wave length dependence of scattering, angular scattering function, effect of finite size of source, atmospheric composition, angular sensitivity of instrumentation, lens effects of filters, and uncertainty in field-of-view discrimination, the measured results can be justified to within the magnitude to within the magnitude of the experimental error. The converse of this process is not true. It is thus recommended that field-of-view measurements by calorim-

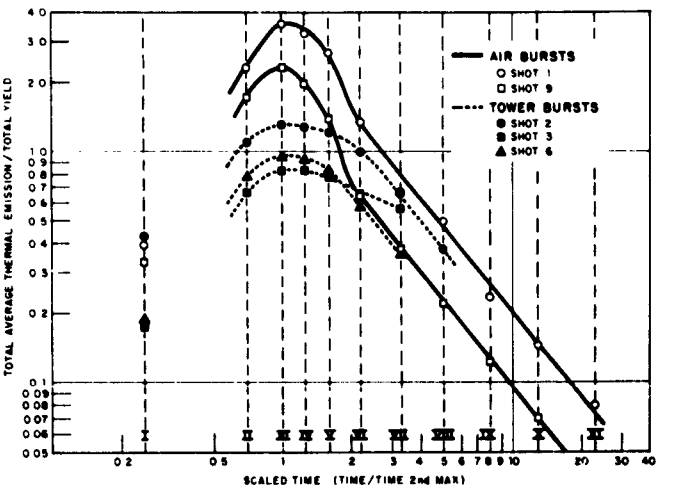

Figure 4.3 Normalized thermal emission versus scaled time.

eters not be attempted in future Nevada tests. The required scattering information can better be obtained using other instrumentation, such as a repeatable point source having a 4π distribution of radiation, wherein the experimental conditions can be better controlled and repetition of measurements is possible.

About all that can be shown from the present experiment is that the scattering behaves about as expected.

The second type of measurement, total energy versus wave length and distance, also suffers from data analysis problems in that the physics of the attenuation cannot be derived from the observed results. It is thus necessary to assume spectral distribution and attenuation properties of the atmosphere and try to predict the measured values.

It is first necessary to assume some type of a spectral distribution for the source. It is known that the source emits from below 3,500 to above 42,000 Å, and probably over a much wider range of wave lengths. It is also known that the source emits more or less continuously with wave length, but that line spectra are observed both in emission and in absorption. Certain gases, known to have continuous absorption, are also believed to be present at various times on various shots. The great uncertainty is as to what extent the line spectra and gas absorption would affect the spectral distribution of the energy received at a distance. For example, an absorption band 10 Å wide may have little effect on the energy received in a 1,000 Å band width at 1 mile.

As a starting point, a Planckian distribution of emissivity one was assumed, with provision for later consideration of differing emissivities varying with wave length. This assumption ultimately led to predictions in agreement with experiment for all but the small air bursts, where a phenomenon, different from that of other bursts, seems to be taking place. This effect can result in only about a 10-percent error in the corrected total energy. The Planckian distribution was thus used in the transmission corrections, since a better approximation was

lacking.

In formulating the effective atmospheric transmission, both theory and experiment were involved. In the case of a nearly symmetrical geometry, attenuation can be attributed to true absorption and differential scattering. In true absorption, the photon is captured by an air molecule, and the air molecule loses the energy of the photon by collision with other air molecule, and the air molecule loses the energy of the photon by collision with other air molecules before re-radiation takes place. The photon is then essentially lost as far as our total-energy measurement is concerned. Water vapor and carbon dioxide absorption were thus applied at each wave length, through use of the values given in References 15 and 16 and the observed humidities.

Differential scattering applies to scattering resulting in a net flow of energy in a nonradial direction; for example, net scattering into a less dense region of the atmosphere or net scattering into the ground. Mathematical formulation and solution is not possible, except for the simplest cases, and even then numerical integration is usually required. The method used in making this correction was to assume that the wave length dependence of the scattering was similar to the wave length dependence observed in References 13 and 14, and the total attenuation, including absorption, was adjusted to fit the observed results of total energy versus distance. It is interesting to note that the scattering coefficients so obtained agree closely in absolute magnitude with those measured by parallel-beam measurements for the prescribed atmospheric conditions.

In reality, the exact mechanism of this attenuation that we have attributed to differential scattering is not known, i.e., all or part of it may well be absorption. It is, however, known to behave exponentially with distance, and it has been treated in that manner.

The formula for atmospheric transmission is then:

$$T = \frac{\int_\lambda J_\lambda \tau_\lambda e^{-\sigma_\lambda D} \, d\lambda}{\int_\lambda J_\lambda \, d\lambda} \tag{4.2}$$

Where: J_λ = the spectral intensity of the source at wave length λ

τ_λ = the water vapor and CO_2 transmission at wave length λ

σ_λ = the differential scattering coefficient at wave length λ

D = the path length

Details regarding the selection of absorption and scattering coefficients are given in Reference 18.

A formulation similar to Equation 4.2 can be used to compute the energy arriving at a station if obscurations and geometry considerations are taken into account.

To compute the energy that would be measured by a calorimeter, the transmission of the filter as a function of wave length must also be included in the integral in the numerator.

In practice, it is not convenient to express filter transmissions and band absorption analytically. Thus, using a digital form, the correction which must be applied to each calorimeter result can be expressed as:

$$\phi = \frac{\sum_{\lambda=0.05_\mu}^{\lambda=10_\mu} J_\lambda \tau_\lambda e^{-\sigma_\lambda D} f_\lambda}{\sum_{\lambda=0.05_\mu}^{\lambda=10_\mu} J_\lambda} \tag{4.3}$$

Where: f_λ = the transmission of the calorimeter filter at wave length λ

It is of interest to consider the application of Equation 4.3 to a typical Nevada atmosphere under several circumstances and to compute the average transmission per mile. The results of such computations are given in Table 4.4. Typical Nevada atmospheres contain 1 to 3 mm of precipitable water vapor per mile of path. It can be readily seen that if one were to measure transmission over a 10-mile path using a tungsten light (about 3,000 K) and apply the result to a 1-mile path, considerable error would be encountered.

The required correction factor was computed for each time interval for each shot by use of the appropriate spectral distribution, relative humidities, and slant ranges, the summations being carried over as many as 115 individual wave lengths. It was not deemed feasible to pub-

TABLE 4.4 TYPICAL TRANSMISSION CALCULATIONS

Color Temperature of Source	Distance	Water Vapor	Total Transmission	Average Transmission per Mile
°K	mi	mm/mi		
3,000	10	1	0.558	0.94
3,000	10	3	0.506	0.93
3,000	1	1	0.819	0.82
3,000	1	3	0.758	0.76
6,000	1	1	0.888	0.89
6,000	1	3	0.867	0.87

lish the details of these calculations in this report. Typical calculations are shown in detail in Reference 18. It is well, however, to point out two significant factors which increase the transmission corrections over those used in previous reports. In the case of water-vapor absorption and deep ultraviolet scattering, most of the attenuation takes place in short path lengths and results in an attenuation that is high near the burst and becomes less important as distance increases, i.e., the attenuation is not a simple exponential process. Secondly, the transmission of a fused quartz filter is not independent of the spectral distribution of the burst. The net result of these effects is to raise the corrected energy values above those that would be obtained by using an atmospheric transmission of 95 percent/mile and a fixed filter transmission of 92 percent.

The present justification for these techniques of computing transmission lies only in their apparent success. Further investigation is indicated to see if the techniques are generally applicable.

4.6 COLOR TEMPERATURES

For the purposes of this report, "color temperature" is defined as the temperature of the Planckian radiator that most nearly matches the radiation from the source at all wave lengths. Using the technique described in Section 4.6 and Reference 18, the ratio energies that would be received at a distance, D, from a Planckian source of temperature, θ, by two calorimeters having color filters, n and m, can be calculated as a function of θ using Equation 4.4:

$$R(\theta)_{n/m} = \frac{\sum_{\lambda} J_{\lambda}(\theta)\, \tau_{\lambda}(D)\, e^{-\sigma_{\lambda} D} f_{\lambda, n}}{\sum_{\lambda} J_{\lambda}(\theta)\, \tau_{\lambda}(D) e^{-\sigma_{\lambda} D} f_{\lambda, m}} \qquad (4.4)$$

This computation, of course, must be carried out for each station on each shot and for each pair of filters used, and for all temperatures of interest. An example of the results of a typical

computation are plotted in Figure 4.4. The observed ratios were then taken from the calorimeter results in Chapter 3 and the color temperatures determined from the computed curves. The results so obtained are given in Figures 4.5 through 4.12. These results are displayed graphically because the process is not capable of great precision. Power temperatures are also indicated on these figures and are discussed in Section 4.8. Agreement between color temperatures, as determined from different pairs of filters, indicates the assumption of a gray-body spectral distribution was a good approximation. This type of agreement is seen on the tower bursts, but not on the air bursts. Lack of agreement can mean a difference in spectral distribution or an experimental error. Since the same instrumentation was used at Station 220

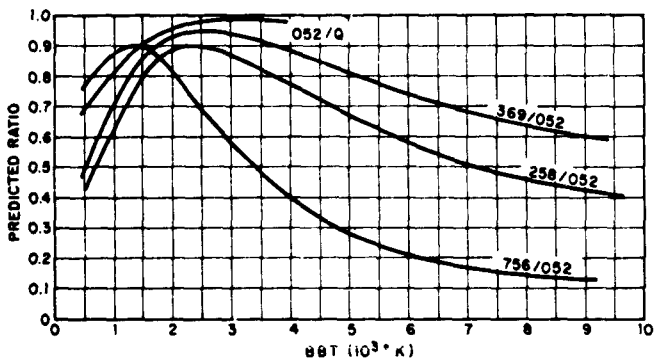

Figure 4.4 Predicted ratios of energies received from a Planckian adiator through various filters under a specific set of atmospheric conditions.

for Shots 1 and 9, this might tend to indicate instrumental difficulties. However, the same type of results were observed at Station 221 during Shot 9, which had independent instrumentation. In addition, the pulse shapes for the small air bursts indicate the phenomena to be real.

Although it is beyond the resolution of calorimetric instrumentation to determine the nature of this difference between tower and air bursts, it appears to be absorption phenomena in the spectral region between 6,400 and 9,500 Å, or excessive emission between 3,500 and 5,300 Å. Spectral measurements of higher-wave-length resolution are required if the phenomena are to be documented.

When the power temperature agrees with the color temperature, it implies that the source emissivity is unity. However, an emissivity of 0.5 results in only about a 20-percent decrease in temperature, so that the determination of emmissivities is beyond the limitations of the measurements. Thus, at the present time, temperature and emissivity cannot yield energy predictions any more accurately than they can be made empirically, but these considerations have explained the observed results.

4.7 SIZE AND GEOMETRY OF THE FIREBALL

The size and geometry of the fireball are of importance for scaling and data analysis. These parameters are determined from analysis of photographic data such as that given in Chapter 3.

The size of the fireball, as determined by the photographic process, is to some extent a function of photographic technique and spectral sensitivity of film. For example, in two photographs of the same shot, one may show a fireball with sharp boundaries and uniform brightness, and the other a diffuse boundary and variations in surface brightness. The size of the fireball is used primarily in power-temperature calculations and for scaling. For both purposes sufficiently accurate diameters can be determined in the region of the second maximum. The temperature calculations are insensitive to small errors in fireball size, because of the fourth root (Section 4.8). Scaling phenomena are generally considered over four or more orders of

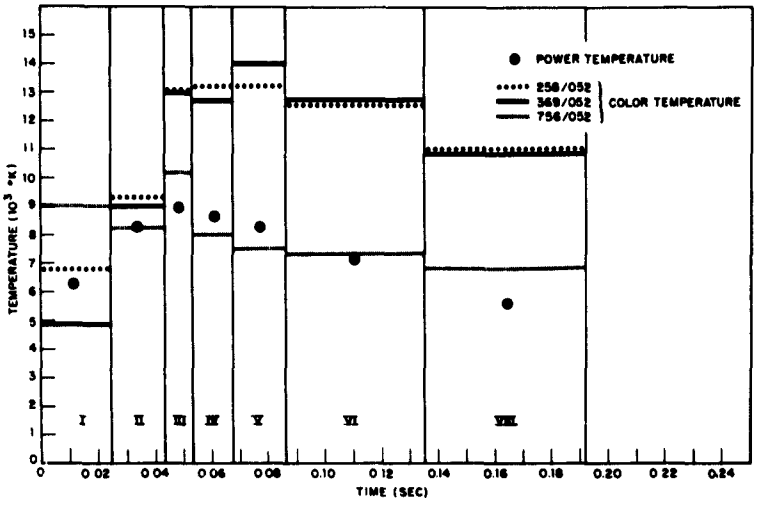

Figure 4.5 Temperature versus time, Shot 1.

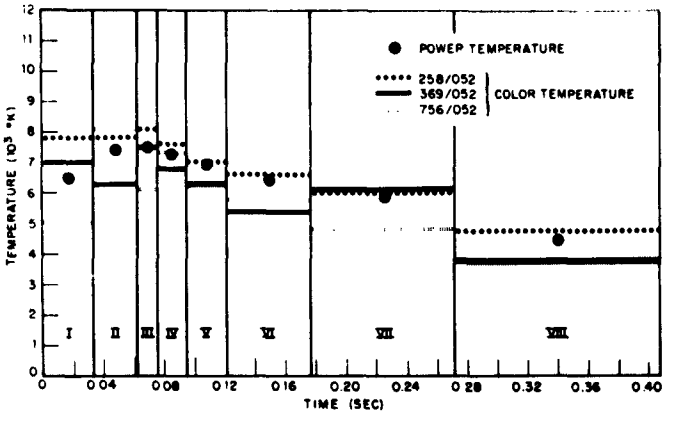

Figure 4.6 Temperature versus time, Shot 2.

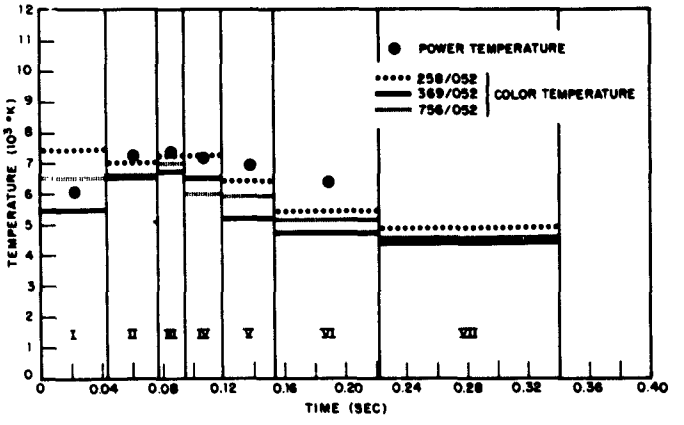

Figure 4.7 Temperature versus time, Shot 3.

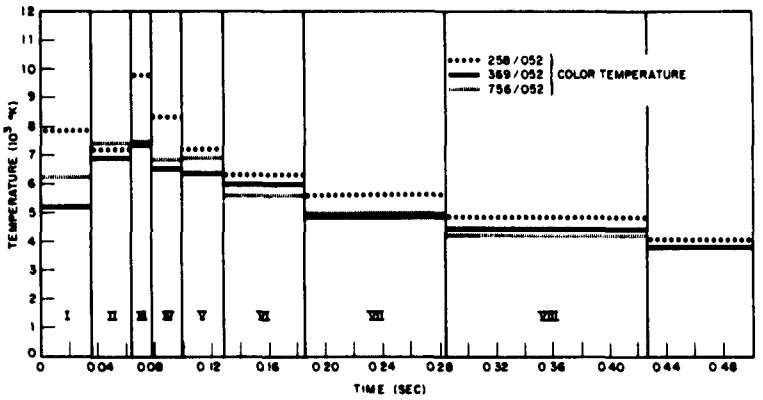

Figure 4.8 Temperature versus time, Shot 5.

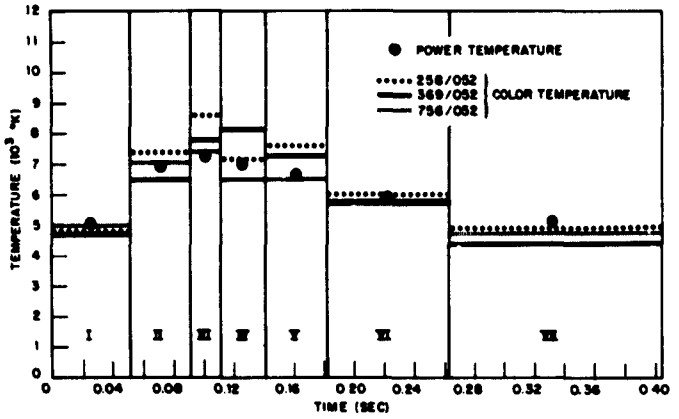

Figure 4.9 Temperature versus time, Shot 6 (Station 220).

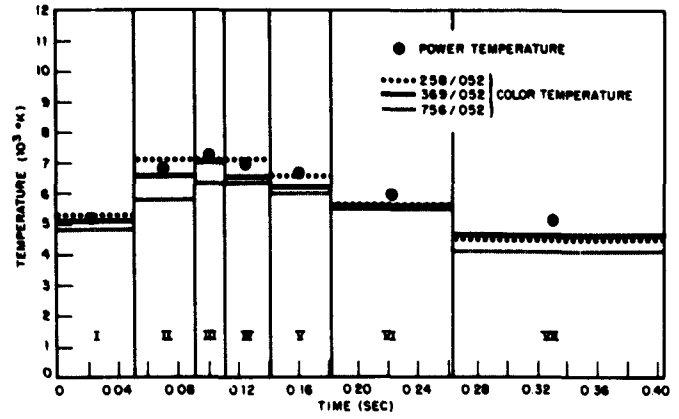

Figure 4.10 Temperature versus time, Shot 6 (Station 221).

magnitude in yield, so that small random errors become insignificant as long as a sufficiently large number of shots are considered.

Fireball sizes cannot be determined with precision at late times because of illumination, definition, and film sensitivity problems. Thus, fireball diameters are given in Figures 3.44 through 3.47 only when a relatively good photographic image was obtained.

The geometry of the fireball is important in correcting the calorimeter readings for asym-

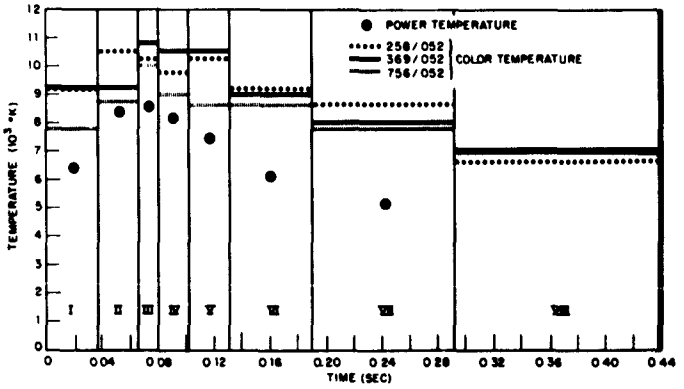

Figure 4.11 Temperature versus time, Shot 9 (Station 220).

metrical spatial distribution of thermal energy from the fireball. Absolute dimensions are not required for this purpose. In making geometrical corrections, the fireball is approximated by one or more regular geometrical figures, thus allowing the surface to be expressed analytically for integration purposes. Examples of this technique are given in Reference 18.

The geometrical corrections can be applied with sufficient accuracy only during the times

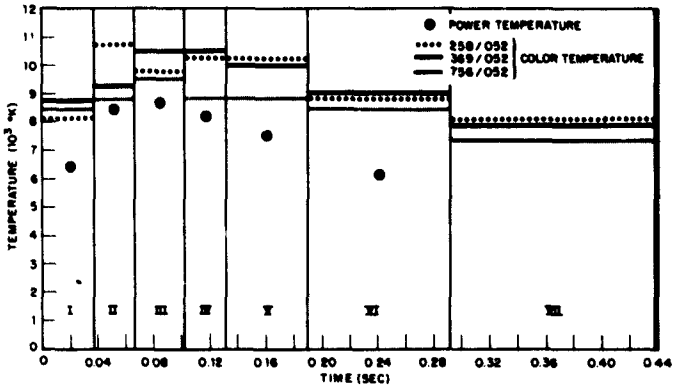

Figure 4.12 Temperature versus time, Shot 9 (Station 221).

when the fireball is well-defined. When this is not the case, an estimated correction must be made. The accuracy limitations involved are discussed in Section 4.2.

4.8 POWER TEMPERATURES

The measurements of total thermal energy versus time can be combined (Reference 18) with

the photographic measurements and geometry considerations to determine a power temperature from Stefan's law, yielding, for each time interval Δt:

$$\theta = \left(\frac{\pi D^2}{\sigma \epsilon A \phi} \frac{\Delta q}{\Delta t} \right)^{1/4} \tag{4.5}$$

Where: θ = the minimum power temperature (Kelvin)

σ = Stefan's constant (1.356×10^{-12} cal cm^{-2} deg^{-4} sec^{-1})

ϵ = the effective emmissivity

A = the flat area of the source; corrected for obscuration as determined by photography (cm^2)

ϕ = the total transmission to the calorimeter (Equation 4.3)

Δq = the energy measured by the calorimeter during the time interval Δt (cal cm^{-2} sec^{-1})

D = the slant range (cm)

The results are indeterminant, since ϵ is unknown. However, since ϵ can, by definition, vary only between 0 and 1, we can determine a minimum power temperature. The effect of an emissivity less than one is to raise the power temperature. However, the calculation is not sensitive to ϵ, since a factor of 2 change in ϵ changes the temperature less than 20 percent.

Power temperatures are shown as points (to distinguish them from color temperatures which are shown as lines) in Figures 4.5 through 4.12 for each station for which there was sufficient data. An emissivity of one was used in all cases, because of the resulting general agreement between color and power temperatures. Although this agreement is not present for the air bursts, it is not felt that the data is sufficiently accurate, nor the corrections well enough known, to determine actual values of emissivity by comparison of power and color temperatures.

In the case of Shots 9 and 10, fireball areas were scaled from other air-burst data, since photographic data was not available.

Although the minimum power temperature determination is not one of great precision, it is revealing. Knowing the approximate energy at a given distance and the approximate size of the fireball, a power temperature may be calculated. Corrections that are applied and the errors in measurement have relatively little effect on this value. Thus, if a minimum power temperature of 7,000 K is reported, it is likely that the fireball was at least that hot.

4.9 THERMAL MEASUREMENTS AT EXTREMELY CLOSE RANGES

More than half of the data from the extremely close stations on Shot 12 were lost due to instrumental difficulties and excessive electromagnetic pickup. These measurements were not required, but were undertaken because the recorders and instrument stations were required for other measurements and because there was a chance to get valuable data should the effort prove successful. The difficulties with electromagnetic pickup were not unexpected, and the probability of making successful measurements at close ranges were known in advance to be very low. The difficulties in the operation of the records are as yet unexplained.

The instrumentation layout for the close-range thermal measurements attempted during Shot 12 are given in Table 4.5. At all stations, with the exception of the 2,000-foot station on the asphalt line, two special Mark 8F calorimeters were mounted at an elevation of 12 feet and

aimed at air zero. In each case, one instrument had a 90-degree field of view and the second instrument a 180-degree field of view. The station at 2,000 feet over asphalt had only one instrument having a 180-degree field of view.

The data from the 2,500-foot station is in fair agreement with the predicted value; however, this measurement was not at a close range. The data from the 2,000-foot station over asphalt

TABLE 4.5 EXTREMELY CLOSE RANGE MEASUREMENTS

Surface Material	Ground Distance	Slant Range	Shock Arrival	Predicted Energy to Shock Arrival	Measured Energy to Shock Arrival
	ft	ft	sec	cal/cm^2	cal/cm^2
Desert*	2,500	2,532	1.01	92	85
Water	1,000	1,077	--	Data destroyed by pickup	—
Desert	2,000	2,040	—	Recorder failure	—
Desert	1,000	1,077	—	Partial recorder failure	—
Asphalt	2,000	2,040	0.22†	57	117
Asphalt	1,000	1,077	—	Recorder failure	—

* Near water line.

† Instruments at 12-foot elevation obscured at 0.22 seconds, energy predicted and measured up until this time. Shock arrival was 0.45 seconds.

only raises new questions rather than answering old ones. Thus, the close-range measurements cannot be termed completely successful.

4.10 THERMAL INPUT TO SHOT 12 MATERIAL PLOTS

As previously mentioned, a major portion of the Shot 12 results were negated by instrumental difficulties. The data given in Table 3.14 indicate the extremely short times and low energies required to cause obscuration of the surfaces of asphalt, concrete, and fir boughs. The reduction of total thermal energy received at the surface, prior to shock arrival, is also significant. The predicted unobscured value at 2,000 feet, up until shock arrival, would be approximately 120 cal/cm^2, as compared to the measured values of 6.1, 42, and 41 cal/cm^2 for the asphalt, concrete, and fir boughs, respectively. The implication that this difference in energy would go into heating the media above the plots would lead to appreciable changes in the composition and temperatures of the media.

4.11 EFFECTS OF BURST ALTITUDE

The total energy data for Shot 10 is summarized in Table 4.6. The energies given are not corrected for atmospheric attenuation and filter attenuation. The B-36 instrument station was located in the tail of the drop aircraft (Reference 12). The ground-zero station (8.4b-3) was about 2,000 feet east of ground zero. Station 410 was near the control point area (Appendix).

Estimated thermal yields, subject to the corrections and limitations discussed in Section 4.2 can be calculated from this data. Many additional problems arise, however. The scattering corrections, Section 4.5, were on the basis of losses seen by an observer in the same horizontal plane as the source and were attributed to scattering into the ground and toward less dense regions of the atmosphere. The paths for two of the stations on Shot 10 were essentially vertical, so this formulation is probably not applicable. Secondly, there are problems in calculating the quantity and transmission of water vapor over a vertical path, part of which is be-

low 0 C. Thirdly, observers report that the floor of Yucca Flat was covered with a layer of dust on the morning of Shot 10, so that transmission to the ground-zero station was probably affected, but not the 410 and B-36 stations. Finally, there is a problem in the selection of a spectral distribution for the source on which to base the atmospheric and filter corrections.

Solution of the scattering problem over a vertical path is beyond our present capability; so for the purposes of this analysis, we will use the same corrections as for a horizontal path, using an average atmospheric density over the actual path to compute the equivalent horizontal path. This procedure should tend to over-correct for transmission and raise the resultant thermal yield values.

The water-vapor transmission over the essentially vertical paths from the ground stations can be approximated with sufficient accuracy, since the first ½ mm of precipitable water accounts for most of the absorption. Both ground stations have at least this amount of water

TABLE 4.6 TOTAL ENERGY DATA, SHOT 10

Station	Slant Range	Total Energy Measured through Filter
	ft	cal/cm^2
B-36	21,500	0.156
Ground zero	32,565	0.0558
410	47,175	0.0260

vapor, at temperatures for which the transmission has been measured, at the station end of the optical path. Thus, the problems of handling absorption due to vapor below the ice point can largely be circumvented.

In the case of the B-36 station, it was assumed that there was no vapor absorption. If it had been assumed that the vapor attenuation was the same as for low altitudes, but scaled on a density basis, the final energy value would be increased about 3 percent. Thus, the errors due to vapor absorption corrections are probably negligible.

We have no means of correcting for the transmission of the dust layer covering the ground-zero station. All we can do in this case is to expect a somewhat-lower thermal-yield value from the measurements at this station.

Choosing a spectral distribution for Shot 10 is something of a problem. The results of the tower- and air-burst measurements at low altitudes show that the Planckian distribution is adequate for tower bursts, but that there is an increasing departure from this spectral distribution as the temperature is higher, as in the case near the second maximum of air bursts. The color temperature results for Shot 10 (Table 3.10) are not complete or accurate enough to give usable information other than to indicate the same type of difference between color and power temperatures as observed near the second maximum of Shots 1 and 9.

It is possible to make a rough approximation of the expected temperature at the second maximum of Shot 10 by using the ratio of peak irradiance to total energy. This ratio is not critically dependent upon temperature, the atmosphere and filter corrections tending to balance out. The explanation for this is rather complicated and extensive and is discussed in Reference 18. A preliminary inspection of the data shows the ratios of maximum irradiance to total energy are approximately 4.7 for Shot 9 and 12.5 for Shot 10, and the total energy of Shot 10 to be about three fourths that of Shot 9. From Reference 17, the radius of Shot 10 is seen to be about 1.23 times the radius of Shot 9. As a result, the peak power temperature for Shot 10 should be about 1.07 times the peak power temperature of Shot 9, or about 9,200 K. The measured power tem-

peratures for the ground-zero station are given in Table 4.7, the peak value being 8,800 K, within 4 percent of the predicted value.

Thus, the temperatures for Shot 10 are probably not much different than the temperatures on Shot 9. There still remains the problem, however, of choosing a suitable spectral distribution, or color temperature, for either Shot 9 or Shot 10. Since it is our purpose to compare the two events, we made the comparison for spectral distributions corresponding to peak temperatures of 9,000 K and 12,000 K, and using temperature versus time profiles typical of small air bursts, such as Shots 1, 9, and 10.

A summary of the thermal partitions on Shots 9 and 10 is given in Table 4.8. The three values listed for each station represent the corrected values based (as explained above) on a 9,000-K peak temperature, on a 12,000-K peak temperature, and by the previously used methods

TABLE 4.7 POWER TEMPERATURE VERSUS TIME, SHOT 10

Time Interval	Temperature
	°K
I	5,400
II	8,600
III	8,800
IV	8,600
V	8,200
VI	7,600
VII	6,600
VIII	5,500
IX	4,200
X	3,200
XI	2,000

(References 1 and 4) of assuming a transmission of 94.7 percent per horizontal surface mile, altitude scaling directly proportional to total air density, and a constant filter transmission of 92 percent.

To seek a conclusion regarding the thermal partition of Shot 10 as compared with that of Shot 9, we have only to examine the results of any of the three methods to conclude that Shot 10 had a lower thermal partition. However, it must be remembered that there are many factors involved in the comparison which involves assumptions that have not been fully tested. Thus, a more conservative conclusion would be that there was no drastic change in the amount of total thermal energy emitted over the range of altitudes involved in this experiment.

Because the yield of Shot 10 was larger than anticipated in preoperational planning, all of the instruments at the ground zero station gave a fairly reliable measurement of the energy in the "first" pulse. These instruments were integrating instruments, but their time response was sufficiently fast to indicate a small plateau on the recorder records at about 0.005 second. This plateau is not completely flat, but its elevation may be determined to about ± 20 percent, yielding an energy value of 0.00055 cal/cm^2. This indicates that about 0.9 percent of the total thermal energy was delivered in the first pulse. It is unfortunate that the same high sensitivity instruments were not used at a similar distance to Shot 9 so as to give directly comparable data for the "first" pulse of that shot.

Figures 3.6 and 3.7 show the irradiance-time curves for Shots 9 and 10. A significant dif-

ference in the time scaling is obvious, Shot 9 having a time to second maximum of almost twice that of Shot 10. If we were to assume that the effective time over which radiation is emitted in proportion to the time to second maximum, the temperatures, radii, and thermal yields reported herein are consistent. Thus, a higher-altitude shot radiates less total energy, has a

TABLE 4.8 THERMAL PARTITION FOR SHOTS 9 AND 10

Shot and Station	9,000 Peak Temperature Approximation	12,000 Peak Temperature Approximation	Previously Used Method*
	°K	°K	
Shot 9, Station 220	0.50	0.54	0.41
Shot 9, Station 221	0.51	0.55	0.40
Shot 10, B-36 Station	0.35	0.40	0.29
Shot 10, Ground Zero Station	0.38	0.46	0.27
Shot 10, 410 Station	0.41	0.52	0.29

* See text.

shorter time scale, a larger fireball, a higher peak irradiance, and about the same temperatures as a lower-altitude burst.

4.12 SCALING LAWS

The scaling laws for thermal yields of air bursts cannot be intelligently discussed until the newer methods of making atmospheric and filter corrections, which are used herein on the small-yield Teapot shots, are applied to the data from Operations Upshot-Knothole and Castle. However, if the older methods of correction are used, the thermal yield (E), in kilotons, fits very closely the relationship $E = 0.41\ W^{0.97}$, where W is the total yield in kilotons. The newer methods will probably make this more nearly $E = 0.52\ W^{1.00}$, but this should be considered as preliminary information and subject to later change. In any event, W/3 scaling does not work for air bursts.

Scaling of thermal yields on tower bursts appears to involve the tower, tower height, device mass, and other variables. The only conclusion that can be drawn at present is that the more the mass of material in the fireball, the lower the observed thermal yield. There are presently too many variables and not enough data to formulate any general scaling relationship.

While the instrumentation used to measure thermal radiant power versus time at close distances does not have sufficient time response to adequately resolve the first maximum, the time to second maximum (as indicated by these instruments) can be related to the yield of the device. Table 4.9 lists the times to second maximum, as measured with radiometers at close range, as the total yield, for all shots for which this information is available. The Castle data were taken from Reference 19, the Tumbler-Snapper data from Reference 1, the Upshot-Knothole data from Reference 4, and the Teapot yields from Reference 17.

The data of Table 4.9 are plotted on a log-log plot in Figure 4.13. It is evident from these data that a straight line will give as good a fit as any simple curve, and would thus suggest a scaling relationship of the form:

$$W = A(t_m)^p \qquad (4.6)$$

Where: W = total yield in megatons

A = numerical constant, approximately equal to 1

t_m = time to second maximum in seconds

p = an exponent, approximately equal to 2

If A is taken as equal to 0.95 and p equal to 2.06, the relationship, as represented by the solid line in Figure 4.13 gives a reasonably good fit. However, since both in practice and in theory, any individual device may show considerable deviation from any curve fitted through

TABLE 4.9 TIMES TO SECOND MAXIMUM VERSUS YIELD

Shot	Total Yield	Time to Second Maximum
		sec
Castle 1	15 Mt	3.85
Castle 2	11 Mt	3.29
Ivy Mike	10.5 Mt	3.10
Castle 4	7 Mt	2.42
Castle 6	1.7 Mt	1.35
Ivy King	540 kt	0.85
Upshot-Knothole 11	60.8 kt	0.25
Tumbler-Snapper 3	30 kt	0.18
Upshot-Knothole 9	26 kt	0.175
Tumbler-Snapper 4	19.6 kt	0.16
Upshot-Knothole 10	14.9 kt	0.13
Upshot-Knothole 4	11.0 kt	0.114
Teapot 6	8.1 kt	0.103
Teapot 3	7.0 kt	0.087
Teapot 5	3.6 kt	0.067
Teapot 9	3.1 kt	0.072
Teapot 10	3.1 kt	0.045
Teapot 2	2.5 kt	0.068
Teapot 1	1.2 kt	0.048
Tumbler-Snapper 2	1.15 kt	0.110
Tumbler-Snapper 1	1.05 kt	0.100
Upshot-Knothole 3	0.2 kt	0.015

the empirical data, it is suggested that A be taken equal to 1, and p be taken equal to 2, as an approximate relationship, because of the obvious ease in calculation and application. The fit of this relationship is shown as a dotted line in Figure 4.13.

Scaling relationships for other parameters are discussed in Reference 18.

4.13 EVALUATION OF THE DIFFERENCE BETWEEN TOWER AND AIR BURSTS

The data obtained herein shows appreciable differences in the thermal properties of tower and air bursts. The tower bursts have lower thermal yields and lower peak temperatures. The air bursts have higher peak temperatures and much sharper second thermal maxima.

Although these changes appear to correlate with the quantity of material, other than air, that is involved in the formation of the fireball, the correlation does not appear to be one that can be explained simply in terms of mass and heat capacities of the constituents. From an examination of the thermal yield data and the corrected irradiance curves (Figure 4.3) it appears that the actual mechanism of fireball formation is modified by the presence of significant quantities

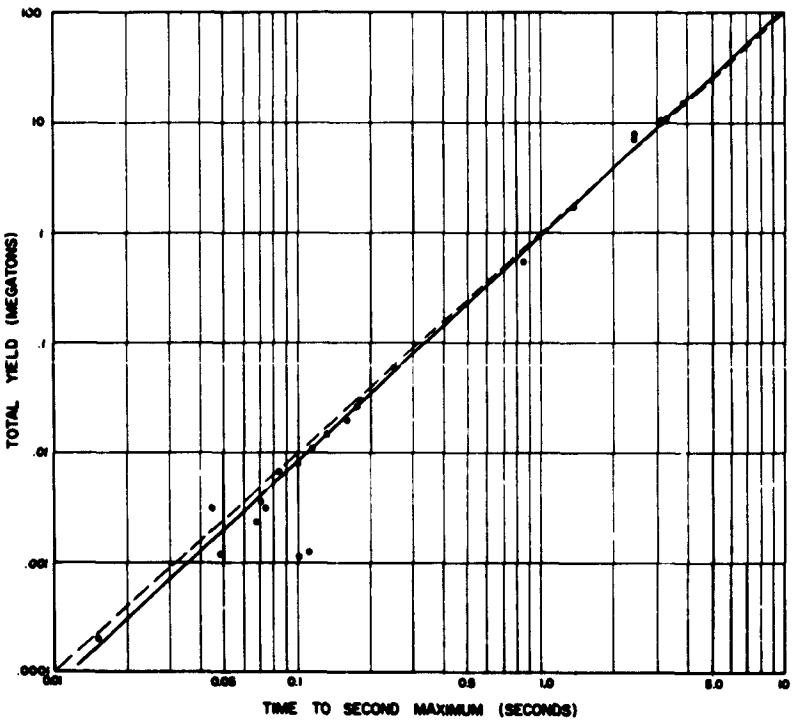

Figure 4.13 Plot of total yield of a number of shots as a function of time to second maximum.

of material other than air. This is largely speculative, however, since there are again more variables and unknowns than we have measurements to evaluate.

4.14 EFFECTS OF DEVICE TYPE ON THERMAL CHARACTERISTICS

The lead and paraffin loading on Shot 3 appears to have had an effect on the pulse shape (Figure 4.3) and thermal yield. This shot was of approximately the same yield as Shot 6 and should have had about the same thermal characteristics. The time to second maximum was also much shorter than scaling would predict. However, Shot 3 was a large-yield detonation on a short tower, so this difference cannot be definitely attributed to the weapon design on the basis of one observed result.

4.15 TESTS OF NEW INSTRUMENTATION

The new instrumentation used by this project performed as expected and gave good results. Details of this instrumentation can be found in Chapter 2.

The Mark 7F instrumentation, designed for low levels of thermal energy, gives satisfactory results; but since it has a fairly high rate of heat loss, it should be used only with considerable care on large shots where delivery times are very long, as the corrections become very large.

The heat-flow problems in the commercially available instruments, used on Shot 10, make data reduction prohibitive, if accuracy is desired. These instruments should be used only in emergencies.

Chapter 5
CONCLUSIONS and RECOMMENDATIONS

5.1 CONCLUSIONS

Basic thermal data, such as thermal yield, pulse, shape, and temperature versus time, for small air and tower bursts, has been adequately documented for effects purposes.

The thermal data available for small tower and air bursts, of yields from 1 to 10 kt, are adequate for effects scaling laws.

The mass of material, other than air, involved in the formation of the fireball, has a significant effect on the radiating characteristics of the fireball. This material, together with the action of the reflected shock wave, effect the shape of the second thermal pulse, the time to second maximum, and the spectral distribution and quantity of the radiated energy. In general, greater mass of tower and nuclear device and lower burst height result in lower temperatures and less thermal energy. A general theory describing these correlations has not been advanced, because of the lack of sufficient data to define the large number of variables.

A correlation between thermal characteristics and device assembly appears to exist on Shot 3, but cannot be established with certainty due to the unknown influence of other parameters.

A change in ambient air density (burst altitude) causes changes in thermal characteristics. The high-altitude burst, Shot 10, appears to have radiated less total thermal energy and had about the same temperature at time to second maximum, a larger fireball, and a shorter time scale.

A method of formulating the effective atmospheric transmission has been developed and appears to give consistent results. The attenuation does not follow a simple exponential relationship with distance, the departure being more significant to close ranges. The corrections result in significantly higher thermal yields in all cases.

The spectral distribution of the radiated energy is much like that of a Planckian radiator, except near the second maxima of small air bursts.

The power and color temperatures of the fireball as a function of time appear to be in agreement, except near the second maxima of small air bursts. These temperatures are useful tools in making corrections to thermal data from field tests and in making thermal energy predictions.

5.2 RECOMMENDATIONS

The methods of analysis applied in this report, and described in detail in Reference 18, show great promise of establishing a correlation between source parameters (yield, burst conditions, atmospheric conditions, geometrical conditions) and the characteristics of the thermal radiation received at a distance. This is in distinction to the large quantity of empirical data currently available, applicable only to specific test conditions. It is recommended that these methods be applied to data operations and to past operations where possible in order to better determine the quantity and type of thermal measurements required at future tests.

Broad-band spectral measurements and air scattering measurements made with calorimeters should be discontinued because of difficulties in measurement and data interpretation. Spectral distribution should be determined at field tests with other instrumentation, such as a very-low-wave-length-resolution, slow-speed scanning spectrometer, covering a wide region

of the spectrum. Air scattering data can be determined with a source other than the nuclear device.

Calorimeter measurements on a megaton-range air burst, under clear atmospheric conditions, on a 1-to-10-kt surface burst, and on fractional-kiloton bursts, together with adequate spectral measurements on at least one shot, are needed to complete the scaling of thermal characteristics for effects purposes.

REFERENCES

1. A. Broido and others; "Thermal Radiation from a Nuclear Detonation"; Project 8.3, Operation Tumbler-Snapper, WT-543; Naval Radiological Defense Laboratory, San Francisco, California; Secret Restricted Data.

2. L.B. Streets; "Basic Characteristics of Thermal Radiation for an Atomic Detonation"; AFSWP-503, December 1953; Secret Restricted Data.

3. A Broido and others; "The Effects of Thermal Radiation on Material"; Project 6.2, Operation Greenhouse, WT-70; Naval Radiological Defense Laboratory, San Francisco, California; Unclassified.

4. A Guthrie and R.W. Hillendahl; "Physical Characteristics of Thermal Radiation from an Atomic Bomb Detonation"; Project 8.10, Operation Upshot-Knothole, WT-773; Naval Radiological Defense Laboratory, San Francisco, California; Secret Restricted Data.

5. G.M. Sleipevich and others; "Attenuation of Thermal Radiation by a Dispersion of Oil Particles"; AFSWP-749; Confidential.

6. E.H. Engquist and J.J. Mahoney; "Protection Afforded by Operational Smoke Screens against Thermal Radiation"; Project 8.3, Operation Teapot, WT-1144; Chemical and Radiological Laboratories, Army Chemical Center, Maryland; Secret Restricted Data.

7. T.R. Broida, A. Broido, and A.B. Willoughby; "Air Temperatures in the Vicinity of a Nuclear Detonation"; Project 8.2, Operation Tumbler-Snapper, WT-542; Naval Radiological Defense Laboratory, San Francisco, California; Secret Restricted Data.

8. R.C. McLoughlin and F.C. Foushee; "Sound Velocities Near the Ground in the Vicinity of an Atomic Explosion"; Project 8.12a, Operation Upshot-Knothole, WT-776; Navy Electronics Laboratory, San Diego, California; Confidential Restricted Data.

9. E.C.Y. Inn; "Air Temperature Measurements over Several Surfaces"; Project 8.4e, Operation Teapot, WT-1149; Naval Radiological Defense Laboratory, San Francisco, California; Confidential Formerly Restricted Data.

10. T.R. Harrison and W.H. Wannamaker; "An Improved Radiation Pyrometer, Temperature, Its Measurement and Control in Science and Industry"; Page 1,206; Unclassified.

11. "Glass Color Filters"; published by Corning Glass Works, Corning, New York, June 11, 1956; Unclassified.

12. R.P. Day and Andrew Guthrie; "Thermal Measurements from Aircraft in Flight"; Project 8.4a, Operation Teapot, WT-1145; Naval Radiological Defense Laboratory, San Francisco, California; Secret Formerly Restricted Data.

13. J.A. Curcio and others; "An Experimental Study of Atmospheric Transmission"; Journal of Scientific American, 43, No. 2, February 1953, Page 97; Unclassified.

14. L. Dunhelman; "Horizontal Attenuation of Ultraviolet and Visible Light by the Lower Atmosphere"; NRL-4031, September 1952; Unclassified.

15. H. A. Gebbie and others; "Atmospheric Transmission in the 1 - 14 micron Region"; Proc Roy Soc, 206, Page 87, March 1951; Unclassified.

16. J. N. Howard, D. L. Burch, and D. Williams; "Near-Infrared Transmission through Synthetic Atmospheres"; Goephysical Res Papers No. 40, AFCRC-TR-55-213, November 1955; Unclassified.

17. H. K. Gilbert and E. B. Doll; "Summary Report of the Technical Director, Programs 1 - 9"; Operation Teapot, WT-1153; Secret Restricted Data.

18. R. W. Hillendahl; "Characteristics of the Thermal Radiations from Nuclear Weapons"; Report in preparation; Secret Restricted Data.

19. R. P. Day and A. Guthrie; "Airborne Thermal Radiation Measurements at Operation Castle"; USNRDL-TR-87, May 1956; Secret Restricted Data.

Appendix
STATION and BURST COORDINATES

Coordinates in feet using the Nevada State Grid System; E = East; N = North; A = Altitude, msl

Ground Zero Shot 1 (T-7-4):	E = 688,074.34 N = 851,123.89 A = 4,195.00	Shot 10:	E = 677,318 N = 829,951 A = 36,620
Shot 1:	E = 687,684 N = 851,159 A = 4,921	Shot 12:	E = 716,000.29 N = 746,249.98 A = 3,477.50
Shot 2:	E = 688,416.41 N = 837,026.05 A = 4,326.00	Station 410:	E = 678,853.33 N = 795,759.48 A = 4,144.25
Shot 3:	E = 680,506.00 N = 865,221.00 A = 4,321.00	Station 220:	E = 688,340.61 N = 848,961.62 A = 4,100
Shot 5:	E = 687,164.39 N = 834,310.10 A = 4,306.50	Station 221:	E = 688,088.22 N = 847,483.00 A = 4,100
Shot 6:	E = 687,502.18 N = 854,123.94 A = 4,745.00	Station 8.4b-1	E = 683,420.00 N = 837,026.05 A = 4,096.00
Ground Zero Shot 9:	E = 688,074.34 N = 851,123.89 A = 4,195	Station 8.4b-2	E = 680,506 N = 870,171 A = 4,200
Shot 9:	E = 688,012 N = 851,218 A = 4,934	Station 8.4b-3 (near Shot 10 Ground Zero)	E = 679,714.65 N = 829,987.41 A = 4,037
Ground Zero Shot 10:	E = 677,714.65 N = 829,987.41 A = 4,037.74		

DISTRIBUTION

Military Distribution Category 82

ARMY ACTIVITIES

1 Deputy Chief of Staff for Military Operations, D/A, Washington 25, D.C. ATTN: Dir. of SW&R
2 Chief of Research and Development, D/A, Washington 25, D.C. ATTN: Atomic Div.
3 Assistant Chief of Staff, Intelligence, D/A, Washington 25, D.C.
4- 5 Chief Chemical Officer, D/A, Washington 25, D.C.
6 Chief of Engineers, D/A, Washington 25, D.C. ATTN: ENNB
7 Chief of Engineers, D/A, Washington 25, D.C. ATTN: ENOTB
8- 9 Office, Chief of Ordnance, D/A, Washington 25, D.C. ATTN: ORDTB
10 Chief Signal Officer, D/A, Comb. Dev. and Ops. Div., Washington 25, D.C. ATTN: SIOCO-4
11 The Surgeon General, D/A, Washington 25, D.C. ATTN: MEDNE
12- 14 Commanding General, U.S. Continental Army Command, Ft. Monroe, Va.
15 Director of Special Weapons Development Office, Headquarters COMARC, Ft. Bliss, Tex. ATTN: Capt. Chester I. Peterson
16 President, U.S. Army Artillery Board, U.S. Continental Army Command, Ft. Sill, Okla.
17 President, U.S. Army Infantry Board, Ft. Benning, Ga.
18 President, U.S. Army Air Defense Board, U.S. Continental Army Command, Ft. Bliss, Tex.
19 President, U.S. Army Aviation Board, Ft. Rucker, Ala. ATTN: ATBG-DG
20 Commandant, U.S. Army Command & General Staff College, Ft. Leavenworth, Kansas. ATTN: ARCHIVES
21 Commandant, U.S. Army Air Defense School, Ft. Bliss, Tex. ATTN: Dept. of Tactics and Combined Arms
22 Commandant, U.S. Army Armored School, Ft. Knox, Ky.
23 Commandant, U.S. Army Artillery and Missile School, Ft. Sill, Okla. ATTN: Combat Development Department
24 Commandant, U.S. Army Aviation School, Ft. Rucker, Ala.
25 Commandant, U.S. Army Infantry School, Ft. Benning, Ga. ATTN: C.D.S.
26 The Superintendent, U.S. Military Academy, West Point, N.Y. ATTN: Prof. of Ordnance
27 Commandant, The Quartermaster School, U.S. Army, Ft. Lee, Va. ATTN: Chief, QM Library
28 Commandant, U.S. Army Ordnance School, Aberdeen Proving Ground, Md.
29 Commandant, U.S. Army Ordnance and Guided Missile School, Redstone Arsenal, Ala.
30 Commanding General, Chemical Corps Training Comd., Ft. McClellan, Ala.
31 Commandant, USA Signal School, Ft. Monmouth, N.J.
32 Commanding General, The Engineer Center, Ft. Belvoir, Va. ATTN: Asst. Cmdt, Engr. School
33 Commanding General, Army Medical Service School, Brooke Army Medical Center, Ft. Sam Houston, Tex.
34 Director, Armed Forces Institute of Pathology, Walter Reed Army Med. Center, 625 16th St., NW, Washington 25, D.C.
35 Commanding Officer, Army Medical Research Lab., Ft. Knox, Ky.
36 Commandant, Walter Reed Army Inst. of Res., Walter Reed Army Medical Center, Washington 25, D.C.
37- 39 Commanding General, QM R&D Comd., QM R&D Cntr., Natick, Mass. ATTN: CBR Liaison Officer
40- 41 Commanding General, U.S. Army Chemical Corps, Research and Development Comd., Washington 25, D.C.
42- 43 Commanding Officer, Chemical Warfare Lab., Army Chemical Center, Md. ATTN: Tech. Library
44 Commanding General, Engineer Research and Dev. Lab., Ft. Belvoir, Va. ATTN: Chief, Tech. Support Branch
45 Director, Waterways Experiment Station, P.O. Box 631, Vicksburg, Miss. ATTN: Library
46 Commanding Officer, Diamond Ord. Fuze Labs., Washington 25, D.C. ATTN: Chief, Nuclear Vulnerability Br. (230)
47- 48 Commanding General, Aberdeen Proving Grounds, Md. ATTN: Director, Ballistics Research Laboratory
49 Commanding General, U.S. Army Electronic Proving Ground, Ft. Huachuca, Ariz. ATTN: Tech. Library
50 Commanding Officer, USA Signal R&D Laboratory, Ft. Monmouth, N.J. ATTN: Tech. Doc. Ctr., Evans Area
51 Director, Operations Research Office, Johns Hopkins University, 6935 Arlington Rd., Bethesda 14, Md.
52 Commander-in-Chief, U.S. Army Europe, APO 403, New York, N.Y. ATTN: Opot. Div., Weapons Br.
53 Commanding Officer, 9th Hospital Center, APO 180, New York, N.Y. ATTN: CO, US Army Nuclear Medicine Research Detachment, Europe

NAVY ACTIVITIES

54 Chief of Naval Operations, D/N, Washington 25, D.C. ATTN: OP-03EG
55 Chief of Naval Operations, D/N, Washington 25, D.C. ATTN: OP-36
56- 57 Chief of Naval Research, D/N, Washington 25, D.C. ATTN: Code 811
58- 59 Chief, Bureau of Aeronautics, D/N, Washington 25, D.C.
60- 64 Chief, Bureau of Aeronautics, D/N, Washington 25, D.C. ATTN: AER-AD-41/20
65 Chief, Bureau of Medicine and Surgery, D/N, Washington 25, D.C. ATTN: Special Wpns. Def. Div.
66 Chief, Bureau of Ordnance, D/N, Washington 25, D.C.
67 Chief, Bureau of Ordnance, D/N, Washington 25, D.C. ATTN: S.P.
68 Chief, Bureau of Ships, D/N, Washington 25, D.C. ATTN: Code 423
69 Chief, Bureau of Yards and Docks, D/N, Washington 25, D.C. ATTN: D-440
70 Director, U.S. Naval Research Laboratory, Washington 25, D.C. ATTN: Mrs. Katherine H. Case
71- 72 Commander, U.S. Naval Ordnance Laboratory, White Oak, Silver Spring 19, Md.
73- 74 Director, Material Lab. (Code 900), New York Naval Shipyard, Brooklyn 1, N.Y.
75 Commanding Officer and Director, Navy Electronics Laboratory, San Diego 52, Calif.
76- 79 Commanding Officer, U.S. Naval Radiological Defense Laboratory, San Francisco, Calif. ATTN: Tech. Info. Div.
80 Officer-in-Charge, U.S. Naval Civil Engineering R&E Lab., U.S. Naval Construction Bn. Center, Port Hueneme, Calif. ATTN: Code 753
81 Commanding Officer, U.S. Naval Schools Command, U.S. Naval Station, Treasure Island, San Francisco, Calif.
82 Superintendent, U.S. Naval Postgraduate School, Monterey, Calif.
83 Officer-in-Charge, U.S. Naval School, CEC Officers, U.S. Naval Construction Bn. Center, Port Hueneme, Calif.
84 Commanding Officer, Nuclear Weapons Training Center, Atlantic, U.S. Naval Base, Norfolk 11, Va. ATTN: Nuclear Warfare Dept.
85 Commanding Officer, Nuclear Weapons Training Center, Pacific, Naval Station, San Diego, Calif.
86 Commanding Officer, U.S. Naval Damage Control Tng. Center, Naval Base, Philadelphia 12, Pa. ATTN: ABC Defense Course
87 Commanding Officer, Air Development Squadron 5, VX-5, China Lake, Calif.
88 Director, Naval Air Experiment Station, Air Material Center, U.S. Naval Base, Philadelphia, Pa.
89 Commander, Officer U.S. Naval Air Development Center, Johnsville, Pa. ATTN: NAS, Librarian

90 Commanding Officer, U.S. Naval Medical Research Institute, National Naval Medical Center, Bethesda, Md.
91 Officer-in-Charge, U.S. Naval Supply Research and Development Facility, Naval Supply Depot, Bayonne, N.J.
92- 95 Commandant, U.S. Marine Corps, Washington 25, D.C. ATTN: Code A03H
96 Commanding Officer, U.S. Naval CIC School, U.S. Naval Air Station, Glynco, Brunswick, Ga.

AIR FORCE ACTIVITIES

97 Assistant for Atomic Energy, HQ, USAF, Washington 25, D.C. ATTN: DCS/O
98 Deputy Chief of Staff, Operations HQ. USAF, Washington 25, D.C. ATTN: Operations Analysis
99-100 Assistant Chief of Staff, Intelligence, HQ. USAF, Washington 25, D.C. ATTN: AFCIN-3B
101 Director of Research and Development, DCS/D, HQ. USAF, Washington 25, D.C. ATTN: Guidance and Weapons Div.
102 The Surgeon General, HQ. USAF, Washington 25, D.C. ATTN: Bio.-Def. Pre. Med. Division
103 Commander-in-Chief, Strategic Air Command, Offutt AFB, Neb. ATTN: OAWS
104 Commander, Tactical Air Command, Langley AFB, Va. ATTN: Doc. Security Branch
105 Commander, Air Defense Command, Ent AFB, Colorado. ATTN: Atomic Energy Div., ADIAN-A
106 Commander, Air Force Ballistic Missile Div. HQ. ARDC, Air Force Unit Post Office, Los Angeles 45, Calif. ATTN; WDSOT
107 Commander, Hq. Air Research and Development Command, Andrews AFB, Washington 25, D.C. ATTN: RDRWA
108-109 Commander, AF Cambridge Research Center, L. G. Hanscom Field, Bedford, Mass. ATTN: CRQST-2
110-114 Commander, Air Force Special Weapons Center, Kirtland AFB, Albuquerque, N. Mex. ATTN: Tech. Info. & Intel. Div.
115-116 Director, Air University Library, Maxwell AFB, Ala.
117 Commander, Lowry AFB, Denver, Colorado. ATTN: Dept. of Sp. Wpns. Tng.
118 Commandant, School of Aviation Medicine, USAF, Randolph AFB, Tex. ATTN: Research Secretariat
119 Commander, 1009th Sp. Wpns. Squadron, HQ. USAF, Washington 25, D.C.
120-122 Commander, Wright Air Development Center, Wright-Patterson AFB, Dayton, Ohio. ATTN: WCOSI
123-124 Director, USAF Project RAND, VIA: USAF Liaison Office, The RAND Corp., 1700 Main St., Santa Monica, Calif.
125 Commander, Air Defense Systems Integration Div., L. G. Hanscom Field, Bedford, Mass. ATTN: SIDE-S
126 Commander, Air Technical Intelligence Center, USAF, Wright-Patterson AFB, Ohio. ATTN: AFCIN-4Bla, Library
127 Assistant Chief of Staff, Intelligence, HQ. USAFE, APO 633, New York, N.Y. ATTN: Directorate of Air Targets
128 Commander-in-Chief, Pacific Air Forces, APO 953, San Francisco, Calif. ATTN: PFCIE-MB, Base Recovery

OTHER DEPARTMENT OF DEFENSE ACTIVITIES

129 Director of Defense Research and Engineering, Washington 25, D.C. ATTN: Tech. Library
130 Director, Weapons Systems Evaluation Group, Room 1E880, The Pentagon, Washington 25, D.C.
131-138 Chief, Defense Atomic Support Agency, Washington 25, D.C.
139 Commander, Field Command, DASA, Sandia Base, Albuquerque, N. Mex.
140 Commander, Field Command, DASA, Sandia Base, Albuquerque, N. Mex. ATTN: FCTG
141-145 Commander, Field Command, DASA, Sandia Base, Albuquerque, N. Mex. ATTN: FCWT
146 Commander, JTF-7, Arlington Hall Station, Arlington 12, Va.
147 Administrator, National Aeronautics and Space Administration, 1520 "H" St., N.W., Washington 25, D.C. ATTN: Mr. R. V. Rhode
148 U.S. Documents Officer, Office of the United States National Military Representative - SHAPE, APO 55, New York, N.Y.

ATOMIC ENERGY COMMISSION ACTIVITIES

149-151 U.S. Atomic Energy Commission, Technical Library, Washington 25, D.C. ATTN: For DMA
152-153 Los Alamos Scientific Laboratory, Report Library, P.O. Box 1663, Los Alamos, N. Mex. ATTN: Helen Redman
154-158 Sandia Corporation, Classified Document Division, Sandia Base, Albuquerque, N. Mex. ATTN: H. J. Smyth, Jr.
159-161 University of California Lawrence Radiation Laboratory, P.O. Box 808, Livermore, Calif. ATTN: Clovis G. Craig
162 Weapon Data Section, Technical Information Service Extension, Oak Ridge, Tenn.
163-195 Technical Information Service Extension, Oak Ridge, Tenn. (Surplus)